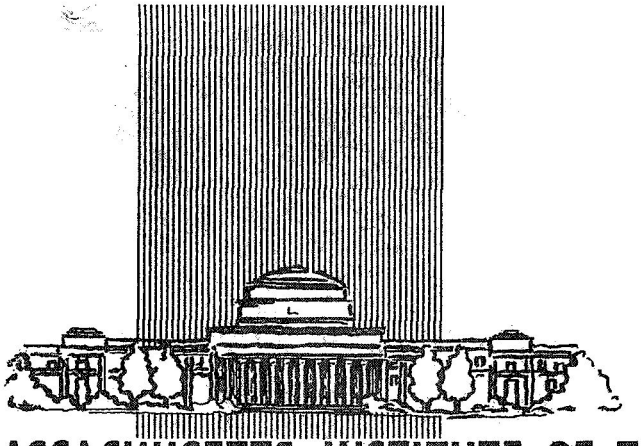

MASSACHUSETTS INSTITUTE OF TECHNOLOGY

TE-24

A MOLECULAR BEAM PRIMARY REFERENCE FOR LONG-TERM FREQUENCY STABILIZATION

SHAOUL EZEKIEL

MEASUREMENT SYSTEMS LABORATORY

MASSACHUSETTS INSTITUTE OF TECHNOLOGY
CAMBRIDGE 39, MASSACHUSETTS

TE-24

A MOLECULAR BEAM PRIMARY REFERENCE FOR LONG-TERM FREQUENCY STABILIZATION

BY

SHAOUL EZEKIEL

APRIL 1968

APPROVED: W. Markey

DIRECTOR
MEASUREMENT SYSTEMS LABORATORY

TE-24

A MOLECULAR BEAM PRIMARY REFERENCE FOR LONG-TERM LASER FREQUENCY STABILIZATION

by

Shaoul Ezekiel

B.Sc., Imperial College, London 1957
S.M., Massachusetts Institute of Technology 1964

Submitted in Partial Fulfillment
of the Requirements for the
Degree of Doctor of Science
in Instrumentation

at the

MASSACHUSETTS INSTITUTE OF TECHNOLOGY

April, 1968

Signature of Author _____
Department of Aeronautics and Astronautics

Certified by _____
Thesis Supervisor

Certified by _____
Thesis Supervisor

Certified by _____
Thesis Supervisor

Certified by _____
Thesis Supervisor

Accepted by _____
Chairman, Departmental Graduate Committee

A MOLECULAR BEAM PRIMARY REFERENCE FOR LONG TERM-LASER FREQUENCY STABILIZATION

by

Shaoul Ezekiel

Submitted to the Department of Aeronautics and Astronautics on 30 April 1968 in partial fulfillment of the requirements for the degree of Doctor of Science in Instrumentation.

ABSTRACT

The principal objective of the thesis is to find an atomic or molecular resonance, that can be excited by a laser in a molecular beam, to serve as a highly stable frequency reference in the feedback stabilization of the laser frequency. The result of the search is the observation, for the first time, of a laser induced transition in a molecular beam.

It has been demonstrated that a single longitudinal mode 5145 A argon ion laser induces resonance fluorescence of iodine in a molecular beam. The fluorescence first appears when the laser frequency is 600 MHz above the center of the laser gain curve and extends over a range of approximately 1300 MHz. The transitions excited in I_2 are between the $X'\Sigma_{0^+_g}$ electronic ground state and the $B^3\Pi_{0^+_u}$ electronic state, but the assignment of the vibration and rotation levels is by no means clear. The dipole moment matrix element for the transition is found to be 1.0×10^{-19} e.s.u. and the fraction of molecules in the beam that take part in the observed spectrum is estimated to be 2×10^{-3} based on molecular beam and absorption cell data. The structure of the resonances has been attributed partly to nuclear electric quadrupole splittings. The ultimate width of the iodine resonance lines observed is inferred to be 50 kHz from a lifetime measurement of the excited state in the beam.

The significance of the experiments performed lies in the possibility of using one of the I_2 resonances as an external frequency reference in the feedback stabilization of the argon laser. Based on the narrow width of such a reference, the fact that its center frequency is not Stark shifted by collisions in the molecular beam, and the large signal-to-noise ratio in the fluorescence yield, a high frequency stability and resettability of the order of several parts in 10^{13} is anticipated.

Thesis Supervisors:

Walter Wrigley, Sc.D.
Title: Professor of Instrumentation and Aeronautics

Rainer Weiss, Ph.D.
Title: Associate Professor of Physics

Ali Javan, Ph.D.
Title: Professor of Physics

John Hovorka, Sc.D.
Title: Staff Physicist, Experimental Astronomy Laboratory

ACKNOWLEDGEMENTS

I wish to thank my inter-departmental committee: Professor Wrigley, Professor Weiss, Professor Javan and Dr. Hovorka for their encouragement and helpful criticism. In particular, I would like to express deep gratitude to Professor Weiss for his guidance, keen interest and close cooperation and for exposing me to a wealth of techniques in experimental physics.

Thanks are also due to C. L. Summers, W. F. Doucette and R. Jankins for valuable technical assistance and to Irene Baumann for typing the early draft of the manuscript.

The Experimental Astronomy Laboratory under the direction of Professor Markey has provided support and a stimulating environment and this is greatly appreciated.

I would also like to thank the Research Laboratory of Electronics for use of its facilities and for providing most of the hardware.

Finally, I wish to express my thanks to my wife for her patience, understanding and encouragement.

The research was sponsored in part by the National Aeronautics and Space Administration under Grant No. ~~NsG 254-62~~ NGL-22-009-010 and in part by the Joint Services Electronics Program.

CONTENTS

Chapter		Page
1	INTRODUCTION	1
2	FREQUENCY STABILITY OF LASERS	4
	2.1 General	4
	2.2 Frequency Stability of Gas Lasers	4
	2.3 Schemes for Laser Frequency Stabilization	8
	2.3.1 Frequency Stabilization Schemes Using Inherent Properties of the Laser	8
	2.3.2 Frequency Stabilization Schemes Using an External Reference	10
	2.4 Need for a Primary Frequency Standard as an External Reference	12
3	MOLECULAR BEAM AS A FREQUENCY REFERENCE	14
	3.1 Why Molecular Beams	14
	3.2 Application of Molecular Beams to Laser Frequency Stabilization	16
	3.2.1 Molecular Beam Laser	16
	3.2.2 Molecular Beam as External Reference Using Atoms (or Molecules) Identical with the Lasing Atoms (or Molecules)	18

CONTENTS (CONTINUED)

Chapter		Page
	3.2.3 Molecular Beam External Reference Using Atoms (or Molecules) Different from the Lasing Atoms (or Molecules)	20
	3.3 Search for a Molecular Beam Reference---First Attempt	21
	3.4 Iodine-Argon Ion Laser Scheme	25
4	THE IODINE MOLECULE AND ITS INTERACTION WITH 5145 Å LASER LIGHT	27
	4.1 General	27
	4.2 The Iodine Molecule and its Interaction with 5145 Å Laser Light	27
5	THE APPARATUS	38
	5.1 General	38
	5.2 The Molecular Beam Apparatus	40
	5.3 Argon Ion Laser	47
	5.3.1 Argon Ion Discharge Tube	48
	5.3.2 Single Longitudinal Mode Cavity	51
	5.3.3 Design of the Single Longitudinal Mode Cavity	58

CONTENTS (CONTINUED)

Chapter		Page
	5.3.4 Alignment of Coupled Cavities	61
	5.3.5 Continuous Scanning of the Frequency of a Single Longitudinal Mode Laser	64
	5.3.6 Measurement of Laser Spectral Width	67
6	EXPERIMENTS PERFORMED AND RESULTS	78
	6.1 Measurement of Absorption of 5145 Å Laser Light in an I_2 Gas Cell	78
	6.2 Observation of Laser induced Resonance Fluorescence in a Molecular Beam of Iodine	83
	6.3 Lifetime Measurement of the Excited State of I_2 in the Beam	92
7	DATA ANALYSIS	100
	7.1 General	100
	7.2 Dipole Moment Matrix Element from Saturation Data	100
	7.3 Dipole Moment Matrix Element from Lifetime Data	102

CONTENTS (CONTINUED)

Chapter		Page
	7.4 Fraction of Molecules Taking Part in Transition from Absorption Cell Data	104
	7.5 Fraction of Molecules Taking Part in Transition from Molecular Beam Data	107
8	INTERPRETATION OF OBSERVED I_2 SPECTRUM	112
	8.1 General	112
	8.2 Calculation of I_2 Spectrum Using Available Molecular Constants	112
	8.3 Estimation of the Hyperfine Structure in the I_2 Molecule	115
	8.3.1 Nuclear Spin-Spin Interaction	115
	8.3.2 Nuclear Spin-Molecular Rotation Interaction	116
	8.3.3 Nuclear Electric Quadrupole Interaction	118
	8.4 External Field Dependence of I_2 Transitions	124
	8.5 Interpretation of Observed Spectrum	128
9	PROPOSED STABILIZATION OF 5145 Å ARGON LASER	133
	9.1 General	133
	9.2 Outline of Proposed Stabilization Scheme	133

CONTENTS (CONTINUED)

Chapter		Page
	9.3 Discussion on the Short Term Frequency Stability of the Free Running Argon Ion Laser	144
	9.3.1 Sources of Laser Frequency Fluctuations	145
	9.3.2 Fundamental Noise Sources in a Free Running Laser	149
	9.4 Discussion on the Use of I_2 Molecular Beam as a Long Term Reference	151
	9.4.1 Determination of the Resonance Peak	152
	9.4.2 The Effective Width of the I_2 Resonance in the Molecular Beam	154
	9.4.3 Frequency Shifts of the I_2 Resonance in the Beam	156
	9.5 Applications of Long Term Stable Lasers	161
10	SUMMARY AND DIRECTIONS FOR FUTURE WORK	164
	10.1 Summary of Work Accomplished	164
	10.2 Directions for Future Work	167
Appendix		
A	DETERMINATION OF TRANSITION PROBABILITY IN A TWO-LEVEL SYSTEM	169

CONTENTS (CONTINUED)

Appendix		Page
B	COMPUTED I_2 TRANSITIONS USING AVAILABLE MOLECULAR CONSTANTS	173
REFERENCES		188
BIOGRAPHICAL SKETCH		194

LIST OF FIGURES

Figure		Page
2.2-1	Fabry-Perot Cavity Selection of Laser Frequency	5
3.1-1	Classical Molecular Beam Apparatus	15
3.2.1-1	Molecular Beam Laser	17
3.3-1	Apparatus for Rubidium - 4965 Å Argon Laser Scheme	23
4.2-1	Potential Energy Curves for $X'\Sigma_{+}^{og}$ and $B^{3}\Pi_{+}^{ou}$ States of I_2	29
4.2-2	Potential Energy Curves and Examples of Wavefunctions	33
4.2-3	Vector Diagrams for (a) Hund's Case "c" - General (b) Hund's Case "c" - Applicable to $X'\Sigma_{+}^{og}$ and $B^{3}\Pi_{+}^{ou}$ States in I_2	35
5.2-1	Iodine Molecular Beam Apparatus (Not To Scale)	39
5.2-2	Photograph of Beam Apparatus	45
5.2-3	Photograph of some Construction Details of Beam Apparatus	46
5.3.1-1	Argon Ion Laser Discharge Tube	49
5.3.2-1	Michelson-Type Single Longitudinal Mode Cavity	53
5.3.2-2	General Properties of a Two Mirror Resonator	55
5.3.2-3	Mode Matching in a General Three Mirror Single Longitudinal Mode Cavity	56
5.3.3-1	Single Longitudinal Mode Cavity	59
5.3.3-2	Lasing Threshold Current vs. Argon Pressure	62

Figure		Page
5.3.3-3	Photograph of Single Longitudinal Mode Argon Ion Laser	63
5.3.5-1	Single Longitudinal Mode Scannable Laser (Spectral Width 2-17 MHz)	65
5.3.6-1	(a) Measurement of Laser Spectral Width Using a Fabry-Perot Interferometer (b) Mode Patterns of Fabry-Perot Cavity (Cylindrical Symmetry)	70
5.3.6-2	Spherical Fabry-Perot Cavity	72
5.3.6-3	Transmission Through Fabry-Perot as a Function of Pressure Using Stabilized 6328 A He-Ne Laser	74
5.3.6-4	Transmission Through Fabry-Perot as Single Mode Laser is Scanned in Frequency	76
5.3.6-5	Transmission Through Fabry-Perot as Single Mode Laser is Scanned in Frequency (Servo On) Integration Time 0.1 Second	77
6.1-1	Set-Up for Absorption Cell Experiments	79
6.1-2	Simultaneous Recording of (A) Direct Laser Power, and (B) Laser Power After Passing Through Absorption Cell, As the Laser Frequency is Scanned Over 3800 MHz.	81
6.1-3	Absorption Coefficient vs. Frequency	84
6.2-1	Experimental Set-Up for Observation of Laser Induced Resonance Fluorescence in a Molecular Beam of Iodine	86
6.2-2	Simultaneous Recording of CW Laser Power and Resonance Fluorescence Signal as the Laser Frequency is Scanned Over 3400 MHz. (Laser Spectral Width 100 MHz; Integration Time 0.03 Seconds)	87
6.2-3	Simultaneous Recording of CW Laser Power and Resonance Fluorescence Signal as the Laser Frequency is Scanned Over 3400 MHz. (Laser Spectral Width 2-17 MHz; Integration Time 0.03 Seconds)	88

Figure		Page
6.2-4	Total Fluorescence Yield vs. Peak Laser Power	91
6.2-5	Fluorescence Signal With High Current Quasi-CW Laser Operation	93
6.3-1	Set-Up for Lifetime Measurement	95
6.3-2	Sampling Data Obtained with Pulsed Laser Light. (A) Photomultiplier Output Attributable to Laser Light Scattered in the Apparatus vs. Time With Molecular Beam off (B) Photomultiplier Output with Molecular Beam on, Showing the Decay of the Resonance Fluorescence Signal	98
7.5-1	Geometry of the Interaction Area and Beam Detector	110
8.3.3-1	A Plot of $\frac{eqQ(MOLEC)}{eqQ(ATOM)}$ vs. Electro-Negativity Difference	121
8.3.3-2	Typical Calculated Quadrupole Splittings	125
8.5-1	Calculated I_2 Spectrum Near 5145 Å Argon Laser	131
9.2-1	Block Diagram of Stabilization Scheme	134
9.2-2	Schematic Diagram of Stabilization Scheme	137
9.2-3	Simplified Loop Diagram of Servo	142

LIST OF TABLES

Table		Page
6.2-1	Relevant Experimental Data Associated With Fig. 6.2-3	90
8.3.3-1	Allowed Transitions	123

CHAPTER 1

INTRODUCTION

The interest in laser frequency stabilization has been motivated by the need for precision long-term measurement of length, i.e length standards; for example, in very low frequency or d.c. earth strain seismometry, where changes in length of one part in 10^{-10} or less per year have to be measured.[1]

Of the many types of lasers that now exist, gas lasers are the most promising from the point of view of frequency stability. The short term stability of the Helium-Neon laser, in particular, has been studied by many workers in the field and stabilities of the order of one part in 10^{13} have been achieved for a period of a second.[2] The long term stability has not been so impressive. The stabilization of the laser frequency has been a tremendous challenge and several methods have been suggested and tried.[4] The majority of the stabilization schemes use a frequency reference element with which the laser frequency is compared. The laser frequency is locked to the reference by means of a feedback servo scheme. However, it is the lack of a suitable, highly stable optical frequency reference that has been the major drawback in achieving long term stability better than one part in 10^{8}.

At microwave frequencies, about 10,000 MHz, long term stability of a crystal oscillator has been achieved by comparing a harmonic of the oscillator frequency with an atomic resonance line excited in a molecular beam. The Cesium atomic beam frequency standard employs a magnetic-field-insensitive hyperfine transition in the ground state of the Cesium atom as the reference element. Long term stability of about one part in 10^{12} has been obtained.(3)

At microwave frequencies, the design criterion is the suitability of the molecular beam transition as regards to perturbation by external fields and ease of detection. The local oscillators offer no problems since they have a large tuning bandwidth.

The situation is very different at optical frequencies since the local oscillators, i.e., the lasers, have a limited tunability range which can vary from several parts in 10^6 to one part in 10^5, depending on the spectral width of the laser gain medium. At optical frequencies, therefore, the molecular beam transition has to match the laser. The application of molecular beams to laser frequency stabilization has been suggested by Professor Rainer Weiss of the M.I.T. Department of Physics.

This thesis is concerned with finding an atomic or molecular resonance line that can be excited by a laser in a molecular beam. This resonance line can then serve as a

primary frequency reference in the feedback stabilization of the laser.

So far as is known, there has been no report of a laser induced resonance transition in either an atomic or a molecular beam.

CHAPTER 2

FREQUENCY STABILITY OF LASERS

2.1 General

Fundamentally, the laser should be a very stable oscillator with an extremely narrow spectral width. In practice, however, the laser is far from ideal due mainly to external causes. This chapter discusses some of the external causes that are responsible for the frequency instability of the laser and the merits of the schemes that have been devised to reduce frequency instability.

2.2 Frequency Stability of Gas Lasers

The laser shown in Figure 2.2-1 consists of a gain medium, e.g. a He-Ne discharge tube, placed inside a short Fabry-Perot cavity. The frequency range of the gain medium above threshold extends from ν_1 to ν_2. The length of the cavity is chosen so that only one cavity mode falls within the bandwidth of the gain medium at any one time. The laser oscillates at a frequency ν_L determined approximately by the position of the cavity mode within the gain curve and is given by

$$\nu_L = N\frac{c}{2L_{opt}}$$

where N is an integer and is the number of half wavelengths

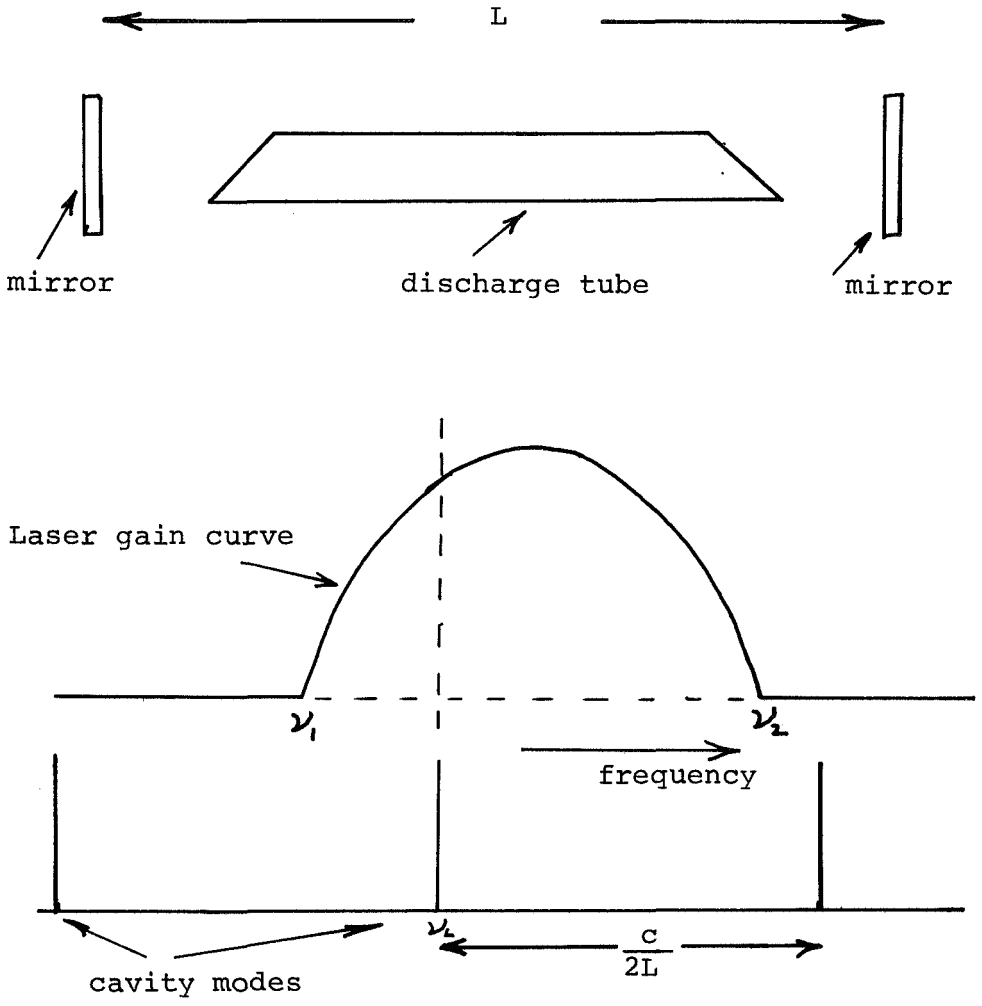

Figure 2.2-1 Fabry-Perot Cavity Selection of Laser Frequency

within the cavity; L_{opt} is the optical length of the cavity and c is the velocity of light. The laser frequency ν_L is therefore determined by L_{opt}.

The change in the laser frequency due to a change in L_{opt} is given by

$$\frac{\Delta\nu_L}{\nu_L} = - \frac{\Delta L_{opt}}{L_{opt}}$$

The value of L_{opt} is not a fixed quantity but is subject to a variety of disturbances, for example, fluctuations of the physical length of the cavity due to thermal, vibrational or acoustical effects; fluctuations of the refractive index of the laser medium caused by changes in the inverted population, electron density and gas pressure and by plasma oscillations.

The output of the laser oscillation is expected to have a narrow spectral width with some amplitude and frequency fluctuations. The amplitude and frequency fluctuations are not completely independent. A change in frequency moves the point of oscillation over the laser gain curve and this gives rise to a change in amplitude. Similarly, a change in amplitude, due to an increase in the excitation of the medium, changes the refractive index of the medium and hence the laser frequency. This latter effect is absent if the oscillation frequency is at the exact center of the gain curve.

The laser frequency instability may be characterized as follows:

(a) Short term fluctuations---these are fast changes in the laser frequency which are responsible for the laser spectral width observed during short time intervals e.g. less than 10^{-2} seconds.

(b) Short term drift---this corresponds to the wandering of the laser frequency during short time intervals in the range 10^{-2} -10 seconds.

(c) Long term drift---this is drift of the laser frequency during long periods of time e.g. minutes, days and even years.

Frequency resettability is a measure of the precision with which the laser frequency can be reproduced.

The experiments of Jaseja, Javan and Townes[2] have shown that, for a carefully designed 1.15 μ He-Ne laser in a well isolated environment, (a) the laser spectral width is about 8 parts in 10^{14} of the laser frequency for short periods of time (less than a second) and (b) the short term wandering of the laser frequency is about one part in 10^{13} per second.

These significant data support the theory that the fundamental spectral width of the laser is very narrow[2]. The data also show that the laser frequency does drift even under the closely controlled conditions of the experiment.

The wandering of the laser frequency is not surprising even if we consider a cavity made out of quartz with $\frac{\Delta L}{L} \sim 10^{-6}/°C$. In order to hold the laser frequency to $\frac{\Delta \nu}{\nu} = 10^{-13}$, the temperature has to be controlled to $\frac{\Delta T}{T} = 10^{-7}°C$.

To achieve long term stability, therefore, some form of

frequency stabilization has to be introduced.

2.3 Schemes for Laser Frequency Stabilization

Several approaches have been attempted for the stabilization of the frequency of the gas laser. Generally, the schemes fall into two groups. One group uses a property inherent to the laser as a frequency reference and the other group uses an external frequency reference.

All stabilization schemes are bandwidth limited and, therefore, cannot compensate for very fast fluctuations in the laser frequency. The laser itself has to be carefully designed to minimize fast frequency fluctuations as has been demonstrated by Jaseja et al.[2]

2.3.1 Frequency Stabilization Schemes Using Inherent Properties of the Laser

An obvious frequency reference inherent to the laser is the peak at the center of the gain curve. The width of the gain curve depends on the laser medium used and on the frequency of the transition. For example, the width of the gain curve is about 1000 MHz for the 6328 Å line in He-Ne, 50 MHz for the 10.6 micron line in CO_2, while that of the 4880 Å line in singly ionized argon is 10,000 MHz.

Shimoda and Javan[5] carried out an extensive program to stabilize a He-Ne 1.15 micron laser to the center of the gain curve. They achieved a stability of $\frac{\Delta\nu}{\nu} \sim 10^{-10}$ for periods

of hours.

Bennett, et al,[6] have exploited the fact that the anomalous dispersion of the laser medium as a function of frequency goes through zero at the exact center of the atomic transition. On either side of line center, the anomalous dispersion has a different sign and its magnitude depends on the inverted population. Frequency stability of about one part in 10^9 for a period of a few hours was achieved with a He-Ne laser oscillating at 3.39 microns.

Another scheme has been proposed by Tobias et al,[7] which is based on the fact that for a single mode laser operation subjected to a small axial magnetic field, the right and left circularly polarized Zeeman components of the light have different intensities. The intensities, however, become equal only if the frequencies are symmetrically disposed about the line center.

All the above schemes have a common drawback. The achievable frequency stability can be no better than the stability of the reference used, i.e., the stability of the center frequency of the gain curve.

A study of the frequency shifts of the center of the gain curve in a 6328 Å He-Ne laser has been made recently by Bloom and Wright[8] and by White.[9] Bloom and Wright found that shifts due to variation in pressure (i.e. the quadratic Stark effect due to collisions) of the gas mixture was about -20 MHz/mm Hg in the range of 2-4 mm Hg. They conclude that

for He-Ne lasers stabilized to the Lamb dip at the center of the gain curve, the frequency stability and reproducibility can be no better than a few parts in 10^8. In addition to pressure shifts, White[9] has shown that shifts exist due to variation in the discharge current. The magnitude of these shifts were about 2 MHz per mA at a discharge current of 19 mA.

2.3.2 Frequency Stabilization Schemes Using an External Reference

Several stabilization schemes have been investigated that use an external reference as a frequency discriminator. No attempt will be made to discuss them all; however, the salient features and limitations of several different approaches will be given.[4]

One approach uses the transmission characteristics of a high Q external Fabry-Perot interferometer as a frequency discriminator. The passive external cavity can be designed to have a high Q, high stability and can be isolated from thermal and acoustical disturbances. Cavity width of less than 10 MHz can be achieved.[10] The laser frequency is locked to one of the Fabry-Perot cavity resonances by means of a feedback loop. The limitation in this method is the variation of the length of the cavity with temperature. For $|\frac{\Delta\nu}{\nu}| = |\frac{\Delta L}{L}| = 10^{-10}$, a temperature tolerance better than 10^{-4}°C is required for a quartz cavity. The resettability of the laser frequency depends on knowledge of the exact length of the Fabry-Perot cavity which is difficult to measure. Material

creep and thermal drifts make the scheme unsuitable as a long term frequency reference. However, for short-term operation the external cavity is very useful because of the narrow discriminator width and the high signal to noise ratio it can provide. Lipsett and Lee[11] achieved short term stability of $\frac{\Delta\nu}{\nu} = 2 \times 10^{-10}$ for several hours.

Another approach is the use of an absorption cell which can be placed either outside or inside the laser cavity. White, Gordon and Labuda[12] have used an external absorption cell, containing a Ne discharge to generate some population at the laser lower level. The amount of absorption of the laser light, after passing through the Neon cell, is measured and the drift of the laser frequency with respect to the center of the Neon line is detected by a novel technique that does not require modulation of the laser frequency. The laser light is first converted alternately into left circularly polarized and right circularly polarized light. The absorption cell is subjected to an axial Zeeman field which splits the atomic line for different polarization of the incident light. The difference in absorption for light of each polarization determined the displacement of the laser frequency from the center of the atomic line. Although the pressure shifts in a pure isotopically enriched Neon may be predicted from experimental measurements[69], this scheme is still not suitable as a long term reference. In addition, shifts do exist

due to variations in the discharge current.[9] The broad doppler width of the Neon resonance in the discharge cell requires long integration times to determine the center of the resonance with great accuracy. A stability of 10^{-10} for a period of 1000 seconds was achieved using this scheme in conjunction with an external Fabry-Perot cavity for short term frequency stabilization.[10]

Recently, a novel scheme has been proposed by Lee and Skolnick[13] who performed an experiment with a Neon discharge cell placed inside the laser cavity. As the laser frequency was scanned across the gain curve, a pronounced peak appeared in the output power caused by an inverted Lamb dip effect.[13] The peak is due to the drop in absorption at saturation by atoms having zero doppler shift in the velocity distribution. The width of the peak was 30 MHz which provides a more sensitive discriminator than the Ne cell placed outside the laser cavity. However, this scheme also suffers from pressure and discharge current shifts. This saturated reference is at present being investigated for the stabilization of the He-Ne laser.[14]

2.4 Need for a Primary Frequency Standard as an External Reference

So far, none of the frequency stabilization schemes discussed offers a long term stability and resettability better than perhaps one part in 10^8, even though excellent short term stabilities have been measured. As already

mentioned, the stability of the laser can be no better than that of the reference.

A long term stable reference with a narrow resonance is therefore needed. This is the subject of Chapter 3.

CHAPTER 3

MOLECULAR BEAM AS A FREQUENCY REFERENCE

3.1 Why Molecular Beams

The interest in an atomic (or molecular) resonance as a frequency reference stems from the strong confidence in the quantum theory of atomic structure, the stability of atomic systems and the fact that particles of the same type are indistinguishable and have identical properties.

Molecular beam techniques provide a means for observing isolated particles where collisions are virtually absent. The effective doppler width is very much reduced if the beam is well collimated and the particles are observed at right angles to their motion. For example, the effective doppler width is 50 kHz for a beam angular width of 10 seconds of arc and a particle velocity of 10^4 cm/second, as will be discussed in Chapter 9. This width is equivalent to the doppler width of a a gas at a temperature of about 10^{-5}°K. The width of a transition observed in a molecular beam can, in principle, approach the inherent or natural width of the transition.

A classical molecular beam apparatus is shown in Figure 3.1-1. The source chamber or oven contains a gas at a pressure P_s. The aperture S_1 in a thin wall between the oven and the middle chamber has a dimension which is of the order of the mean free path in the oven. Particles effuse from the source slit and thereafter travel along straight paths until they

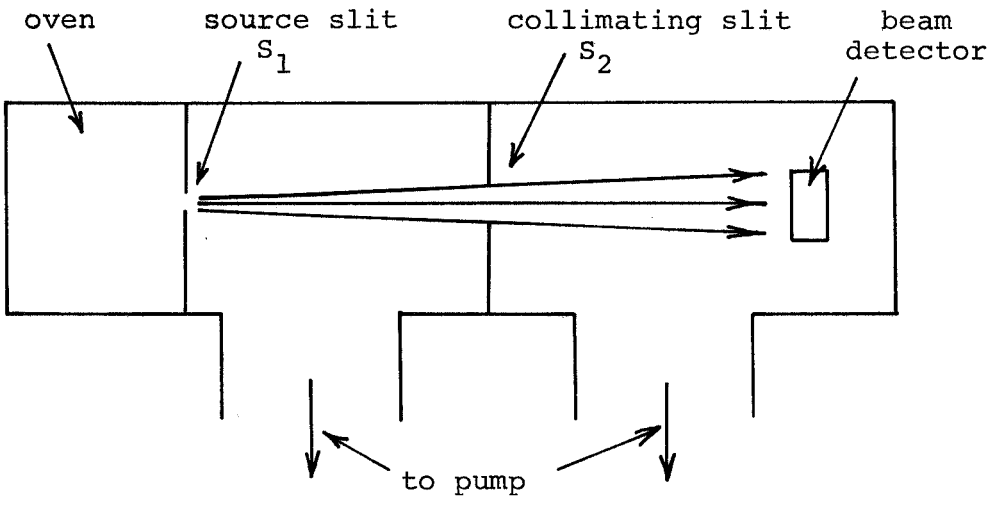

Figure 3.1-1 Classical Molecular Beam Apparatus

collide with a wall. The particles emerging from S_1 fill a solid angle of 2π. Another slit S_2 is used as a collimator and the angular width of the beam is defined by the geometry of the two slits.

The design of a molecular beam apparatus for various precision measurements of atomic, molecular and nuclear properties is found in reference (15).

3.2 Applications of Molecular Beams to Laser Frequency Stabilization

There are several ways in which the properties of molecular beams may be exploited to achieve a frequency stable laser. The various possibilities may be grouped under (a) a molecular beam laser, (b) a laser with a molecular beam external frequency reference that employs an atom identical with the lasing atom, and (c) a laser with a molecular beam external reference that employs an atom that is different from the lasing atom.

3.2.1 Molecular Beam Laser

Several major problems that contribute to laser frequency instability may be solved by the use of a molecular beam as the gain medium. Since the beam can be placed orthogonal to the cavity axis, as shown in Figure 3.2.1-1, the width of the gain curve is then limited by either the natural width or, if the lifetime is long, by the observation width i.e. the

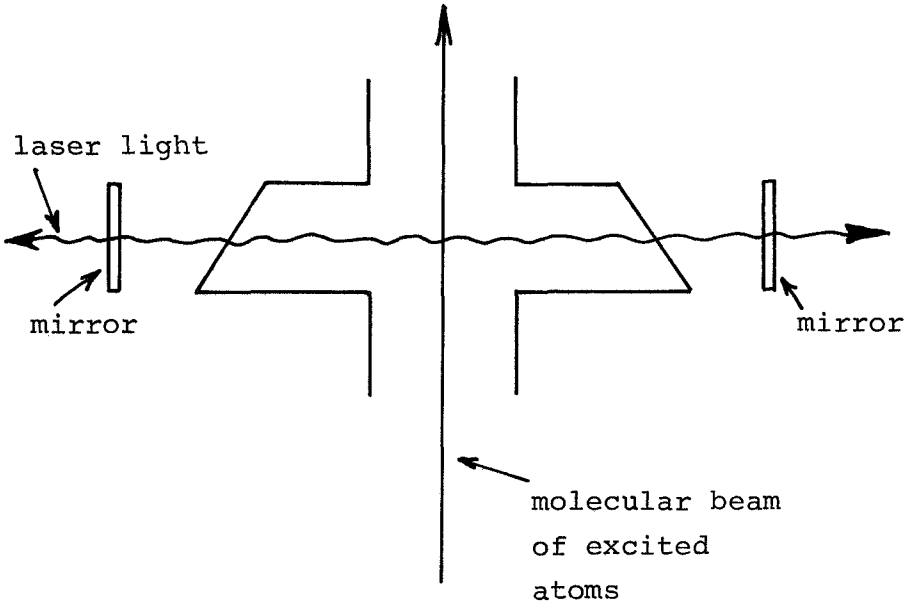

Figure 3.2.1-1 Molecular Beam Laser

width determined by the time the beam spends in the cavity. Either of these widths can be much narrower than the doppler width in the gas discharge. In addition, the resonance frequency of the transition is not shifted by Stark effects in gas collisions.

The molecular beam gain medium, however, introduces new difficulties. One, it requires that the atoms in the upper laser level have a sufficiently long lifetime, longer than 10^{-3} seconds, to be formed into a beam and, two, a sufficient density of atoms is needed to overcome cavity losses. The choice of cavity Q is influenced by two mutually incompatible conditions; to reduce cavity losses, in order to achieve oscillation, a high Q cavity is required, while to achieve frequency stability the atomic resonance must be much narrower than the cavity width which implies a low Q cavity.

Basov and Letokhov[16] have been investigating such possibilities. A recent paper[17] on the progress of this research indicates that a feasible scheme has not yet been found.

3.2.2 Molecular Beam as External Reference Using Atoms (or Molecules) Identical with the Lasing Atoms (or Molecules)

This approach exploits the properties of a molecular beam in the capacity of an external frequency reference.[18] The scheme consists of a laser inducing a transition in a molecular beam of atoms that are identical with the lasing

atoms and moving at right angles to the laser beam. The interaction between the laser and the beam atoms is detected and used, in a feedback scheme, to hold the laser frequency to the atomic resonance.

For an interaction to take place, the atoms in the beam must be in the lower level of the lasing transition at the interaction region. Generally, the lifetime of the laser lower level is short, about 10^{-8} seconds. Since thermal velocities are typically 10^{4} cm/sec, an atom will only remain in the laser lower level for a distance of 10^{-4}cm, so that the preparation of this level must be carried out at the interaction region. Excitation by electron bombardment introduces recoil shifts in the frequency of the absorption line, given by

$$\left(\frac{\Delta\nu}{\nu}\right)_{\text{electron}} = \frac{h\nu_0}{Mc^2}\left[\frac{2m_e c^2}{h\nu_0}\right]^{1/2}$$

where m_e is the mass of the electron, M is the mass of the atom and $h\nu_0$ is the minimum electron energy needed to excite an energy level $h\nu_0$ in the atom. This shift is about one part in 10^{7} for the Neon atom. Optical excitation does not introduce as much recoil shift and is given by

$$\left(\frac{\Delta\nu}{\nu}\right)_{\text{Photon}} = \frac{h\nu_0}{Mc^2}$$

The detection of the interaction between the molecular beam and the laser depends on the particular atom used and may involve (a) observation of the light re-radiated by the atom

after excitation by the laser, or, (b) detection of a change of state e.g. magnetic sub-state, in the atoms themselves after undergoing a transition. The detection of the laser light absorbed by the molecular beam is not suitable because of the low density of atoms in the molecular beam.

Finally, the width of such a reference depends on the lifetime of the upper and lower levels of the transition in the beam. In the case of the 6328 Å laser line in Neon, the natural width of the transition is about 30 MHz. One may do better by finding a match with a transition in another system in which the lifetimes are long.

3.2.3 Molecular Beam External Reference Using Atoms (or Molecules) Different from the Lasing Atoms (or Molecules)

The approach, in this case, is similar to that in section 3.2.2, except that the beam atom is different from the lasing atom.[18] The problems in generating the laser lower level are avoided if a ground state transition is found in an atom (or molecule) that closely matches the laser line to about 1 part in 10^6. In addition to matches with ground state transitions, one may examine matching transitions from metastable or long-lived states whose lifetime is at least 10^{-3} seconds.

The width of the absorption line depends on the properties of the chosen atom, if there is a choice, and may be narrower than the natural width of the lasing transition itself.

Detection schemes are similar to those discussed in the previous section. In addition, if the beam consists of metastable atoms (or molecules) which decay to the ground state after excitation, then one may detect a change in the metastable population arriving at the detector as a measure of the excitation. Certain atoms in metastable states can be detected by electron ejection from a surface that has a work function lower than the excitation energy of the metastable atom.[70]

3.3 Search for a Molecular Beam Reference---First Attempt

Since it became clear, after a thorough search, that no match existed between a known atomic ground state transition and any one of the 2000 reported laser frequencies, a systematic search for a match was carried out.

A computation was made of all ground state transitions in atoms, listed in Moore's Tables,[19] without regard to selection rules, in the range 3000 A - 10.1 microns. In addition, transitions from easily identifiable metastable states were also computed. The purpose of this computation was to help find a close match, to one part in 10^5, between an existing laser line and a ground (or metastable) state transition in atoms.

The computed transitions revealed over one hundred close matches,[20] none of which involved an allowed ground state electric dipole transition. One of the matches uncovered was

between the 4965 Å cw argon ion laser and the 5s-6s transition in Rubidium. The match[21] is within 1.5 cm^{-1} and seemed a desirable one since atomic beam techniques for alkalis are relatively easy and also that laser power on the order of 1 watt can be obtained at 4965 Å. Another attractive feature is the 5×10^{-8} second lifetime[22] of the 6s state which meant that the linewidth for the transition would be 3 MHz.

The 5s-6s transition in a free Rb atom, as also the 1s-2s transition in a free Hydrogen atom, is forbidden in a single quantum transition. The electric dipole matrix element is zero because of the parity of the levels and magnetic dipole transitions are forbidden in the Pauli approximation, since the spatial radial wavefunctions of the 5s and 6s levels are rigourously orthogonal. However, a magnetic dipole matrix element of order $(Z\alpha)^6$, where Z is the effective charge number and α is the fine structure constant, relative to an allowed electric dipole matrix element is predicted.[23] For Rubidium in the 5s state, $Z_{effective} \sim 9$ if calculated from the Fermi-Sergre formula for the hyperfine structure, so that $(Z\alpha)^6 \sim 10^{-7}$. However, since there is doubtless state mixing in the Rb atom, this is a lower estimate.

An attempt to observe the excitation of Rb by a 4965 Å argon laser in a molecular beam was made. The experimental arrangement is shown in Figure 3.3-1 and is, fundamentally, a standard Rabi-type atomic beam magnetic resonance apparatus[71]

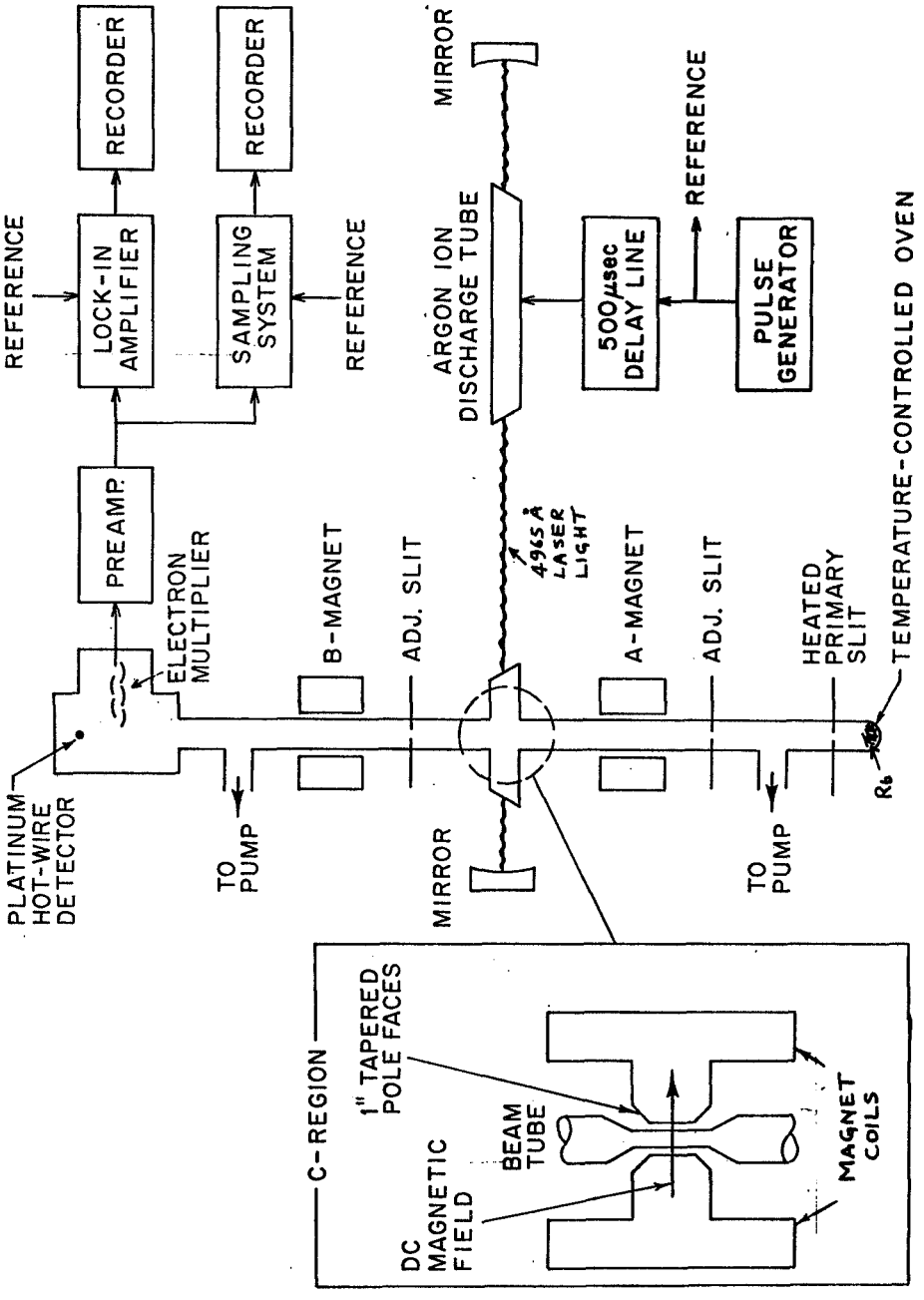

Figure 3.3-1 Apparatus for Rubidium - 4965 Å Argon Laser Scheme

except for the interaction or C-region. In the C-region, light from an argon ion laser oscillating at 4965 Å is incident at right angles to the state selected Rb beam. The interaction between the laser light and the Rb atoms takes place in a homogeneous d.c. magnetic field which, by the Zeeman effect, brings the atomic line into coincidence with the laser line. The laser induces a magnetic dipole transition in which $\Delta m_J = +1$ between the $(5s, m_J = -1/2)$ and $(6s, m_J = +1/2)$ states of the Rb atom. The laser magnetic field is set perpendicular to the homogeneous d.c. field. If an atom undergoes this transition, it decays back to the 5s state by a cascade of electric dipole transitions $6s \rightarrow 5p \rightarrow 5s$ and can end up in the $m_J = +1/2$ state. These atoms are focussed by an inhomogeneous magnetic field onto the hot wire detector, where they are ionized and the ions are accelerated to an electron multiplier. The output signal of the electron multiplier is electronically processed using a lock-in amplifier.

The C-region is made out of quartz and is located inside the laser cavity so as to achieve greater energy density at the interaction region. The C-region windows are optical flats placed at Brewster's angle. The Zeeman field in the C-region is provided by a 4" Varian electromagnet with 1" tapered pole faces. The gap between the pole faces is 1/4" so that a field of 29 kgauss can be obtained.

The laser consists of a water cooled argon ion discharge

tube, 3 mm I.D. and 30 cm long, with a coaxial anode and an off axis cathode. Narrow band high reflectivity mirrors are used to select the 4965 Å argon ion line which is ten times weaker than either the 4880 Å or the 5145 Å line. The laser is operated quasi-cw with a pulse duration of 500 microseconds and a repetition rate of 100 pulses per second. This enabled 80 A discharge currents to be achieved without damage to the discharge tube. Peak multimode laser power at the interaction region was 200 watts/cm^2 and the power spectral density was 0.02 watt/MHz/cm^2.

The data, or lack of it, indicated that the 5s-6s transition in Rubidium is weaker than an allowed electric dipole by a factor of at least 10^{-6}.

The experiment will be continued at some future date with a single longitudinal mode laser which is frequency locked to an external Fabry-Perot. The power spectral density is expected to increase by 10^4 which would enable transitions to be observed that are 10^{-10} of an allowed electric dipole.

3.4 Iodine - Argon Ion Laser Scheme

A progress report,[24] by Prof. J. I. Steinfield of the M.I.T. Department of Chemistry, concerned with the study of energy transfer mechanisms by excited molecules in a molecular iodine gas, indicated the observation of fluorescence in an I_2 gas cell after excitation by 5145 Å light from an

argon ion laser. This was further investigated in a gas cell as well as in a molecular beam and is the subject of the rest of this thesis.

Although transitions in molecules have been investigated and, in fact, computed for such molecules as N_2, Br_2, I_2, Na_2, K_2, Co, there was little confidence in the frequencies of the calculated lines because the available molecular constants were not precise enough to predict matches within 1 part in 10^5 - 10^6. The quickest method of establishing a match is perhaps to try different lasers with various molecules which are known to have absorption in the frequency range of the lasers.

CHAPTER 4

THE IODINE MOLECULE AND ITS INTERACTION WITH 5145 A LASER LIGHT

4.1 General

A brief discussion is given in this chapter on the iodine molecule and its properties that are involved in the interaction with 5145 Å laser light. This should provide some background for the chapters to follow, especially, in connection with the analysis of the data.

4.2 The Iodine Molecule and Its Interaction with 5145 Å Laser Light

The absorption of the iodine molecule in the visible[25] is known to take place between the ground electronic state $X^1\Sigma^+_{\sigma g}$ and the excited electronic state $B^3\pi^+_{\sigma u}$. The existence of a match between a ground state transition in I_2 and 5145 Å laser light has been demonstrated, as will be shown in chapter 6. The available molecular constants[26,27], however, are not sufficiently accurate to establish the vibrational and rotational quantum numbers of the levels involved in the transition, as will be shown in Chapter 8.

The potential energy curves for the two electronic levels in I_2 as a function of inter-nuclear separation[28] are shown in Figure 4.2-1. The vibration energy levels are indicated by horizontal lines. The rotational levels, which are closely

spaced energy levels associated with each vibration level, are not shown.

A transition between a vibration level v" in the ground state to a vibrational level v' in the upper electronic state is indicated by a vertical line as shown in the Figure. The length of this line corresponds to the energy in wavenumbers of the transition. Primed (') quantities refer to the upper level and double primed (") quantities refer to the lower level.

In I_2, the spacing between the lower vibrational levels in the ground electronic state is 214 cm^{-1} and the dissociation energy of the $B^3\pi_{+}_{ou}$ state is about 20,072 cm^{-1}. The energy in wavenumbers of the 5145 Å argon ion laser line is 19,429.7 cm^{-1}. This implies that ground state transitions induced by the laser are only possible from the three lowest vibrational levels in the ground state, i.e. v" = 0, 1, 2. A transition of 19,429.2 cm^{-1} from v" = 3 ends up above the 20,072 cm^{-1} dissociation limit of the $B^3\pi_{+}_{ou}$ state.

The interaction between the iodine molecule and the 5145 Å laser light depends on the transition probability between the states in I_2 that are involved in the transition. From Appendix A, the probability of a transition from a lower state 1 to an upper state 2 is $P_{(1\rightarrow 2)}$ where

$$P_{(1\rightarrow 2)} = \frac{8\pi^3}{3h^2c} \mu_{12}^2 I(\nu)t \quad \ldots\ldots\ldots 4.2\text{-}1$$

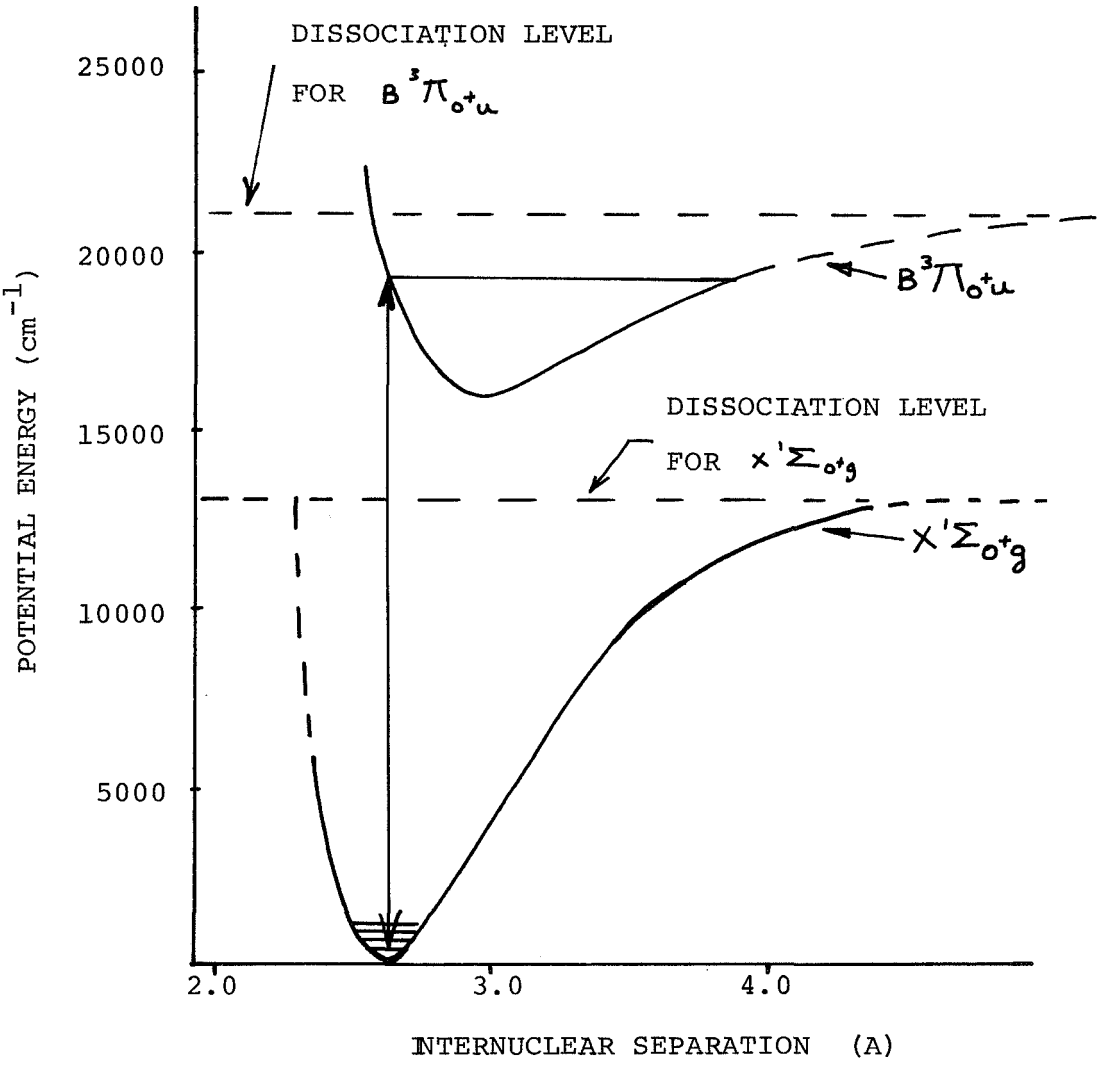

FIGURE 4.2-1 POTENTIAL ENERGY CURVES FOR $X\,^1\Sigma_{o^+g}$ AND $B\,^3\Pi_{o^+u}$ STATES OF I_2 (AFTER MATHIESON AND REES, J. CHEM. PHYSICS, 25, 753, (1956))

where μ_{12} is the off-diagonal matrix element of the electric dipole moment connecting state 1 and 2; $I(\nu)$ is the power spectral density of the radiation; t is the interaction time --- time molecule is exposed to exciting field; h is Planck's constant; c is the velocity of light.

The rate of spontaneous decay of an excited state is A_{21}, the Einstein A coefficient, and is given by

$$A_{21} = \frac{64\pi^4}{3hc^3} \nu_{21}^3 \mu_{21}^2 \quad \ldots\ldots\ldots\ldots\ldots 4.2\text{-}2$$

where μ_{21} is the frequency of the transition and $\mu_{21} = \mu_{12}$.

If the excited state can decay to more than one level, then the rate of spontaneous decay is increased and given by

$$\sum_i A_{2i} = \frac{64\pi^4}{3hc^3} \sum_j \nu_{2j}^3 \mu_{2j}^2 \quad \ldots\ldots\ldots\ldots\ldots 4.2\text{-}3$$

The effective lifetime of the excited state is τ_2 where

$$\tau_2 = \frac{1}{\sum_i A_{2i}} = \frac{3hc^3}{64\pi^4} \frac{1}{\sum_j \nu_{2j}^3 \mu_{2j}^2} \quad \ldots\ldots\ldots\ldots\ldots 4.2\text{-}4$$

It is evident that μ_{12} plays a dominant role in the excitation and the decay of the states in the molecule, so that a brief discussion on μ_{12} is perhaps worthwhile.

The total wavefunction Ψ of a given molecular state may be replaced, to a first approximation, by a product of three independent eigenfunctions[29], so that

$$\psi = \psi_e \cdot \psi_v \cdot \psi_r \quad \ldots\ldots\ldots \quad 4.2\text{-}5$$

where ψ_e is the electronic eigenfunction and ψ_v, ψ_r are the vibrational and rotational eigenfunctions associated with the nuclear motion. The matrix element of the dipole moment between two electronic states ψ' and ψ'' is

$$\mu = \int \psi'^* |M| \psi'' \, d\tau \quad \ldots\ldots\ldots \quad 4.2\text{-}6$$

where $\vec{M} = \sum_i e_i \vec{\rho}_i$ is the sum of the components of the electric dipole moment of the system, e_i is a charge element, ρ_i is its distance from the origin, $d\tau$ is a volume element and the integral is over all space. Substituting Equation 4.2-5 into Equation 4.2-6, we get

$$\mu = \int \psi_e'^* \, \psi_v'^* \, \psi_r'^* \, |M| \, \psi_e'' \, \psi_v'' \, \psi_r'' \, d\tau \quad \ldots \quad 4.2\text{-}7$$

M may be resolved into two components, one that depends on the electron coordinates, M_e, and the other on the nuclear coordinates, M_n, so that

$$M = M_e + M_n \quad 4.2\text{-}8$$

Substituting the above expression into Equation 4.27 we get

$$\mu = \int \psi_v^{*\prime} \, \psi_r'^* \, |M_n| \, \psi_v'' \, \psi_r'' \, d\tau_n \int \psi_e'^* \, \psi_e''^* \, d\tau_e$$

$$+ \int \psi_v'^* \, \psi_r'^* \, \psi_v'' \, \psi_r'' \int \psi_e'^* \, |M_e| \, \psi_e'' \, d\tau_e \quad 4.2\text{-}9$$

where $d\tau_n$, $d\tau_e$ are elements of volume of the space of the nuclear and electronic coordinates, respectively.

For transitions within the same electronic state, i.e. $\psi_e' \equiv \psi_e''$, so that $\int \psi_e''^* \, \psi_e'' \, d\tau_e = 1$ and $\int \psi_e''^* \, |M_e| \, \psi_e'' \, d\tau_e = 0$ then

$$\mu\Big|_{\substack{\psi' \\ e}}^{\substack{\psi'' \\ e}} = \int \psi'^{*}_{v}\, \psi'^{*}_{r}\, |M_n|\, \psi''_{v}\, \psi''_{r}\, d\tau_n$$

In a homonuclear diatomic molecule, such as I_2, $M_n = 0$ because of charge symmetry, so that $\mu = 0$ for transitions within the same electronic state. A vibrational spectrum and a pure rotational spectrum are therefore absent in homonuclear diatomic molecules.

For transitions between different electronic states, $\int \psi'^{*}_{e}\, \psi''_{e}\, d\tau_e = 0$, since ψ'_e and ψ''_e are orthogonal eigenfunctions. If we neglect the rotation of the molecule[29] we get

$$\mu\Big|_{\substack{\psi' \\ e}}^{\substack{\psi'' \\ e}} = \int \psi^{*}_{v}{}'\, \psi''_{v}\, d\tau_n \int \psi'^{*}_{e}\, |M_e|\, \psi''_{e}\, d\tau_e$$

Since the second integral is independent, to a first approximation, of the vibrational levels between the states, we can then write

$$\mu = \bar{\mu}_e \int \psi'_{v}\, \psi''_{v}\, dr$$

where $\bar{\mu}_e = \overline{\int \psi'^{*}_{e}\, |M_e|\, \psi''_{e}\, d\tau_e}$; $d\tau_n \equiv dr$; r is the internuclear separation and $\psi'^{*}_{v} = \psi'_{v}$ since ψ_v is real.

The probability of a transition depends on μ^2 and therefore on the square of the integral $\int \psi'_{v}\, \psi''_{v}\, dr$ which is referred to as the "overlap" integral or the "Franck-Condon factor". Figure 4.2-2 shows ψ'_v and ψ''_v for low values of v.

The pertinent angular momenta that are coupled in the molecule are electron orbital angular momentum, electron spin

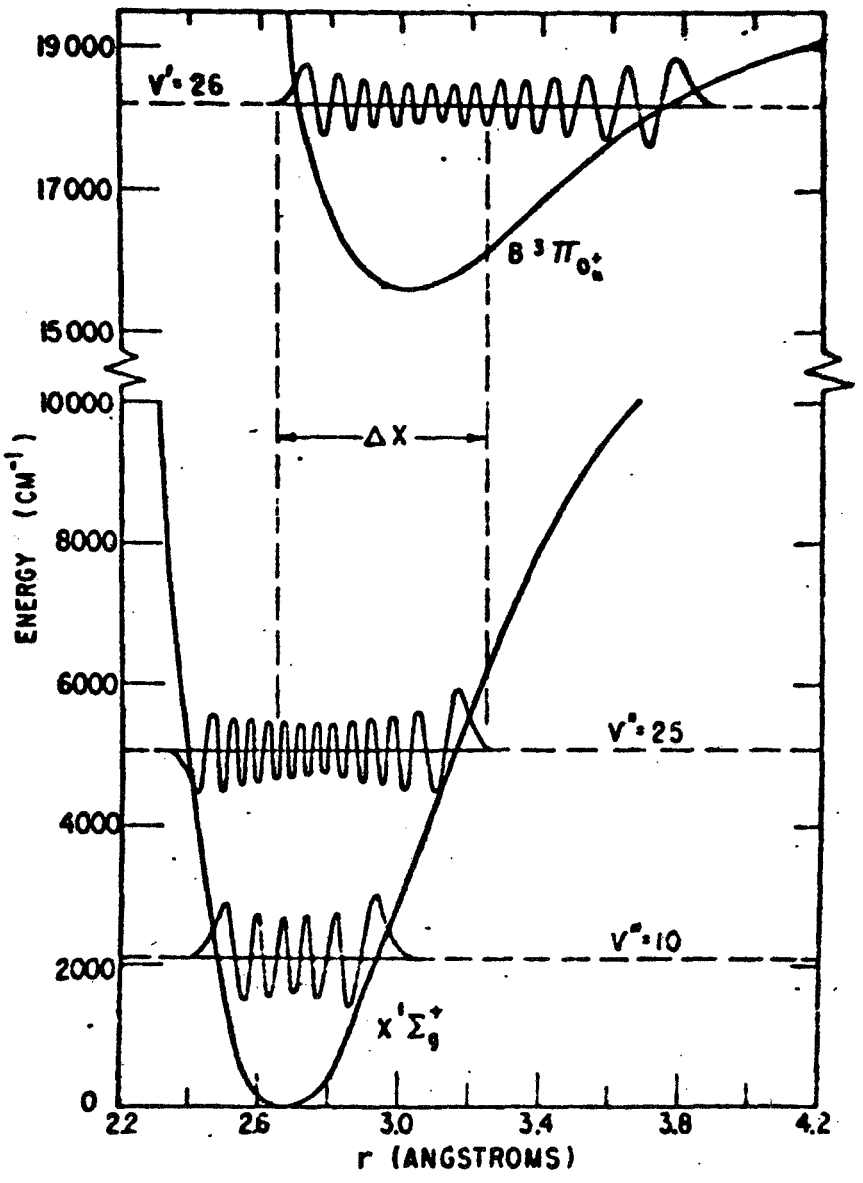

Figure 4.2-2 Potential Energy Curves and Examples of Wavefunctions

(Taken from: R. N. Zare, J. of Chemical Physics, Vol. 40, No. 7, Page 1938, 1 April 1964)

angular momentum and the angular momentum associated with nuclear rotation. How these angular momenta couple together depends on the type of molecule.

In diatomic molecules, there is axial symmetry about the internuclear axis. The component of the orbital angular momentum of the electrons along the internuclear axis is designated by Λ, for which $\Lambda = 0, 1, 2, 3...$These values of Λ correspond to the different electronic states in the molecule designated by Σ, Π, Δ, Φ,...The total electron angular momentum along the internuclear axis is designated by Ω.

The iodine molecule obeys Hund's coupling case (c) which is illustrated in Figure 4.2-3. In this coupling scheme, the interaction between the electron orbital angular momentum, $\vec{L}$, and the electron spin $\vec{S}$ is stronger than the interaction between either $\vec{L}$ or $\vec{S}$ with the molecular field along the internuclear axis. $\vec{L}$ and $\vec{S}$ couple together to form $\vec{J}_a$ which in turn couples to the internuclear axis and has a component Ω along this axis. Ω couples with $\vec{N}$, the end-over-end molecular rotation to form $\vec{J}$, the total angular momentum of the molecule, neglecting nuclear spin.

The ground state in I_2 is a $^1\Sigma^+_{0g}$ state. The superscript 1 implies that the multiplicity of the state is 1, in other words the electron spin is zero. The subscript 0 implies that Ω, the total angular momentum along the internuclear axis is zero. Furthermore, since I_2 is a molecule that obeys Hund's case (c), the total electronic angular momentum is zero when

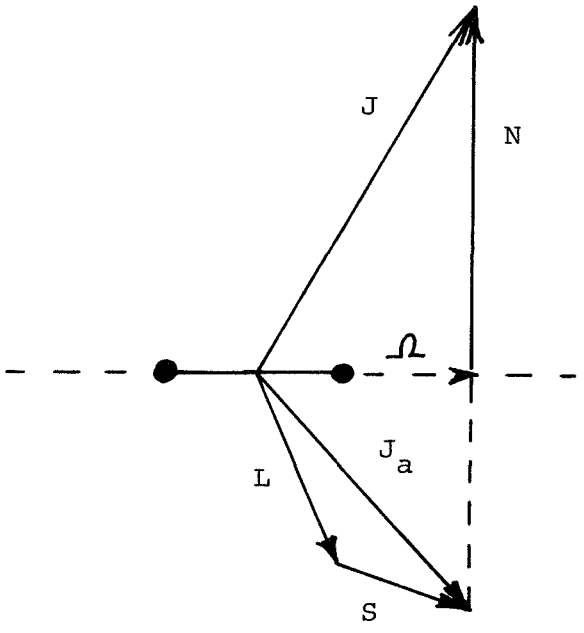

(a)

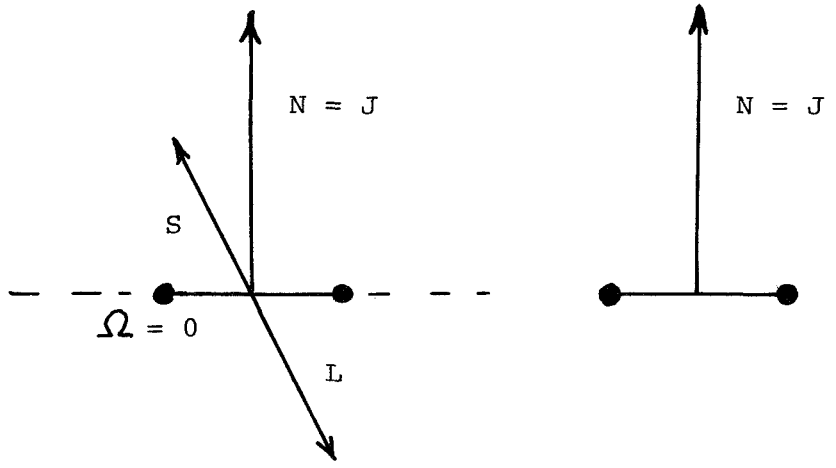

$B\,^3\Pi_{o^+u}$ STATE

$X\,^1\Sigma_{o^+g}$ STATE

(b)

FIGURE 4.2-3 VECTOR DIAGRAMS FOR (a) HUND'S CASE (c) - GENERAL
(b) HUND'S CASE (c) - APPLICABLE TO $X\,^1\Sigma_{o^+g}$ AND $B\,^3\Pi_{o^+u}$ STATES IN I_2

$\Omega = 0$. The subscript g, for "gerade" means that the electronic eigenfunction of the state is even or symmetric with respect to the center of the molecule.

The relevant excited state is a $^3\Pi_{+}$ state. In this electronic state the multiplicity is 3 which implies that the total electron spin is 1. The subscript 0 means that $\Omega = 0$ and, again, since I_2 obeys Hund's case (c), this means that $\vec{L}$ and $\vec{S}$ are opposite to each other to give a zero total electron angular momentum. In both the $^1\Sigma_{+}$ and $^3\Pi_{+}$ states, J is equivalent to N. The subscript u for "ungerade" implies that the electronic eigenfunction for $^3\Pi_{+}$ state is odd or anti-symmetric with respect to the center of the molecule.

For electric dipole transitions, the matrix element $\int \psi'^* |M| \psi'' d\tau$ must be non-zero which is only possible if ψ' and ψ'' have opposite symmetry since the electric dipole operator M is an odd function. The $^1\Sigma_{+}$ and the $^3\Pi_{+}$ states satisfy this condition. However, this is not the only restriction on transitions between the two states. Since $\Omega = 0$ in both states, there is a selection rule for J which is $\Delta J = \pm 1$ ($\Delta J = 0$ is forbidden) for electric dipole transitions. There are no selection rules for Δv for transitions between the two electronic states. As a consequence, the molecular level excited in the $^3\Pi_{+}$ state can decay in doublets, corresponding to $\Delta J = \pm 1$ to any of the vibrational levels in the $^1\Sigma_{+}$ state, providing that the overlap integral $\int \psi'_v \psi''_v dr$ is not zero.

This multi-wavelength decay of the excited level is called "fluorescence". The bandwidth of the fluorescence corresponds to the decay of the excited level to a range of vibrational energy levels in the lower electronic state that extend from the dissociation level to the lowest vibrational level, v" = 0. In I_2, the range of the fluorescence, after excitation by 5145 Å light, is 5000 Å - 1.3μ. It is possible to have fluorescence at a shorter wavelength than the exciting line. For example, if the laser induces a transition out of the v" = 2 level in the $X^1\Sigma^+_{og}$ state, it may be possible to observe fluorescence at a shorter wavelength than the exciting line if the decay of the excited level is to v" = 0 and v" = 1. The fluorescence lines at a wavelength shorter than that of the exciting line are called "anti-Stokes" lines.

There is one other electronic state below the $B^3\Pi^+_{ou}$ state in the I_2 molecule. However, this state, $A^3\Pi_{1u}$, has odd symmetry so that there is no electric dipole transition between the $B^3\Pi^+_{ou}$ and $A^3\Pi_{1u}$ states.

CHAPTER 5

THE APPARATUS

5.1 General

The apparatus used in the experiments consists of a vacuum system in which a molecular beam of iodine interacts with the 5145 Å light from an argon ion laser. The region where the laser beam meets the molecular beam will be referred to as the interaction region. The resonance fluorescence that is induced by the laser in the I_2 molecules is collected by an optical system and is detected on a photomultiplier.

The molecular beam is formed in the following manner. I_2 molecules, in a reservoir or oven, effuse through a narrow slit into the vacuum chamber. A collimating slit further down the apparatus determines the width of the beam that enters the interaction region.

In order to perform the experiments, a laser with a narrow spectral width, that can be scanned in frequency over several thousand MHz, is required. The narrow spectral width is obtained by using a laser oscillating in a single longitudinal mode and the scanning of the frequency of oscillation of the laser across the laser gain curve is achieved by varying the length of the laser cavity by means

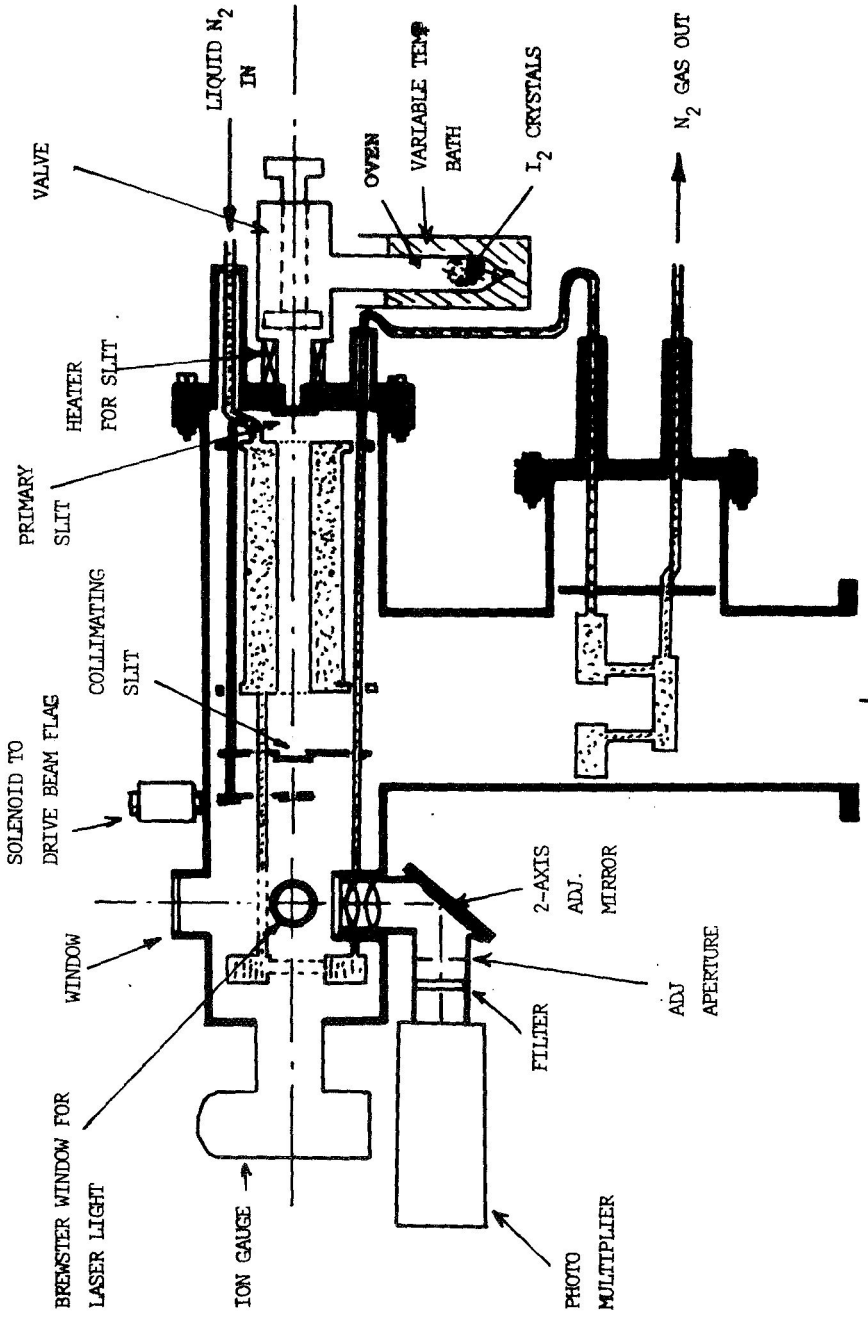

Figure 5.2-1 Iodine Molecular Beam Apparatus (Not to Scale)

of a piezo-electric crystal.

5.2 The Molecular Beam Apparatus

The molecular beam apparatus is shown in Figure 5.2-1. The oven contains about 10 grams of resublimed reagent grade Iodine crystals. The vapor pressure of the I_2 in the oven can be temperature controlled. At room temperature, the I_2 vapor pressure is 0.3 mmHg which is very convenient since this pressure is in the desired range. The oven or primary slit is 0.1 mm wide and 1 cm high. For molecular effusion through the slit, the width of the slit must be of the order of the mean free path of the gas at the oven pressure. With a 0.1 mm slit, oven pressures up to about 1 mmHg can be used. The slit itself is heated to avoid condensation of the I_2 on it.

The rate of molecular effusion out of the slit is given by

$$\frac{dN}{dt} = \frac{1}{4} N \bar{v}_0 A_s \text{ molec/sec} \quad \ldots\ldots\ldots\ldots 5.2\text{-}1$$

where N is the number of molecules per cm^3 in the oven, $\bar{v}_0$ is the average thermal velocity of the molecules in the oven which is $1.13\sqrt{\frac{2kT}{M}}$, k is Boltzman's constant, T is the temperature of the oven in degrees Kelvin, M is the mass of the molecule and A_s is the area of the oven slit. For an oven pressure of 0.3 mmHg, $N = 0.9 \times 10^{16}$ molec/cm^3, $\bar{v}_0 = 1.6 \times 10^4$ cm/sec for I_2 at room temperature, $A_s = 10^{-2}$ cm^2, so that the rate of

molecular effusion is

$$\frac{dN}{dt} = \frac{1}{4}\,(0.9 \times 10^{16})\cdot(1.6 \times 10^{4})\cdot 10^{-2} = 3.6 \times 10^{17} \text{ molec/sec}$$

The I_2 molecules that effuse out of the oven slit emerge into a region of good vacuum.

The width of the beam entering the interaction region is determined by a collimating slit, 0.75 mm wide by 1 cm high, placed 11 cm from the oven slit. The beam is mechanically chopped by a solenoid driven "beam flag" just before the interaction region. The beam finally enters an ion gauge at the end of the apparatus. The increase in pressure in the ion gauge gives a measure of the beam intensity.

The beam intensity, I, at a distance d from the oven slit is given by

$$I = \frac{1}{4} N\bar{v}_0 A_s \frac{1}{\pi d^2} \cos\theta \text{ molec/cm}^2\text{-sec} \quad \ldots\ldots \quad 5.2\text{-}3$$

where θ is the angle with respect to the normal to the slit and N, $\bar{v}_0$, A_s are the same as in equation 5.2-1. The beam intensity at the interaction region located 17 cm from the oven slit is 5×10^{14} molec/cm^2-sec for d = 17, θ = 0 and an oven pressure of 0.3 mmHg.

The laser light enters and leaves the apparatus through windows placed at Brewster's angle. The laser beam, which is collimated and has a 2 mm diameter, intersects the molecular beam at a point 1.5 cm from the beam flag. The interaction

volume is approximately a cylinder whose diameter is the laser beam diameter and whose height is the molecular beam width at the interaction region, i.e. 1.1 mm.

The resonance fluorescence is produced in the interaction volume and is collected by an f/0.5 optical system placed outside the vacuum chamber. The collected fluorescence light is brought to a focus at an adjustable iris in front of an EMI photomultiplier with an S-20 photocathode having a response that extends to about 8000 Å. The optical path is folded by means of a 45° mirror that has 2-axis adjustment. The design of the optical housing permits interference filters to be inserted in the optical path. The optics are aligned so that only light from the vicinity of the interaction volume can pass through to the photomultiplier; a grain of wheat light bulb is placed at the interaction region to simulate the source of fluorescence during the alignment.

The background pressure of I_2, as well as other gases, has to be sufficiently small so that the molecular beam is not scattered between the oven slit and the interaction region. The mean-free-path λ should be much larger than the distance d between the oven slit and the interaction region. For a given λ, the beam intensity I reaching the interaction region is

$$I = I_0 e^{-\frac{d}{\lambda}}$$

where I_0 is the initial beam intensity at the oven slit. For

a pressure of 10^{-6} mmHg, $\lambda = 5 \times 10^{-3}$ cm and for d = 17 cm, $\frac{I}{I_0}$ is greater than 0.99.

There is a further reason for maintaining a low background pressure of I_2. Since the laser beam passes across the apparatus, there will be resonance fluorescence induced in the background gas of I_2. The resonance fluorescence from the beam, however, may be distinguished from that of the background by mechanically chopping the beam and detecting only the fluorescence signal that is modulated at the chopping frequency. In this case, the fluorescence from the background gas of I_2 may contribute a large d.c. background in the measured fluorescence signal.

An estimate for the molecular beam density ρ at the interaction region is obtained from

$$\rho = \frac{I}{\bar{v}_b}$$

where I is the beam intensity and $\bar{v}_b$ is the average velocity of the molecules in the beam which is $1.33\sqrt{\frac{2kT}{M}} = 1.87 \times 10^4$ cm/sec. Typically, for $I = 5 \times 10^{14}$ molec/cm^2-sec as obtained above, the density in the beam at the interaction region is 3×10^{10} molec/cm^3. The equivalent pressure in the beam is $\frac{3 \times 10^{10}}{3 \times 10^{16}}$, i.e. 10^{-6} mmHg. The interaction volume in the background gas of I_2 is larger than that in the molecular beam. The acceptance angle of the optics, however, limits the amount of background fluorescence that is measured by the photomultiplier.

The noise associated with the fluctuations in the d.c. background fluorescence can exceed the Poisson noise in the fluorescence signal unless the I_2 background pressure is much lower than that in the beam.

The air in the system is pumped out with a 2" diffusion pump. The speed of the diffusion pump is 60 liters/sec which is not sufficient to maintain the I_2 pressure below 10^{-6} mmHg as required in the experiment.

An estimate for the pumping speed needed is obtained from the following relationship

$$\frac{F_{pump}}{F_{oven}} = \frac{P_{oven}}{P_{background}}$$

where F_{pump} is the pumping speed of the pump; F_{oven} is the pumping speed out of the oven and is given by 1/4 x (average velocity of I_2 in oven) x area of oven slit, i.e. $1/4\ \bar{v}_0\ A_s$ = 43 cm^3/sec; P_{oven} is the pressure of I_2. For $P_{background}$ less than 10^{-6} mm, F_{pump} must be greater than 1.3×10^4 liter/sec. For this purpose, a cryogenic pump i.e. a liquid N_2 trap is used which completely surrounds the beam in the region in front of the oven slit, as shown in the figure. The pumping speed of the trap is proportional to its surface area. With a trap area of 800 cm^2, a background pressure of 1×10^{-7} mmHg is obtained with the oven valve opened.

Figure 5.2-2 is a photograph of the beam apparatus and Figure 5.2-3 is a photograph showing some construction details of the beam forming part of the apparatus.

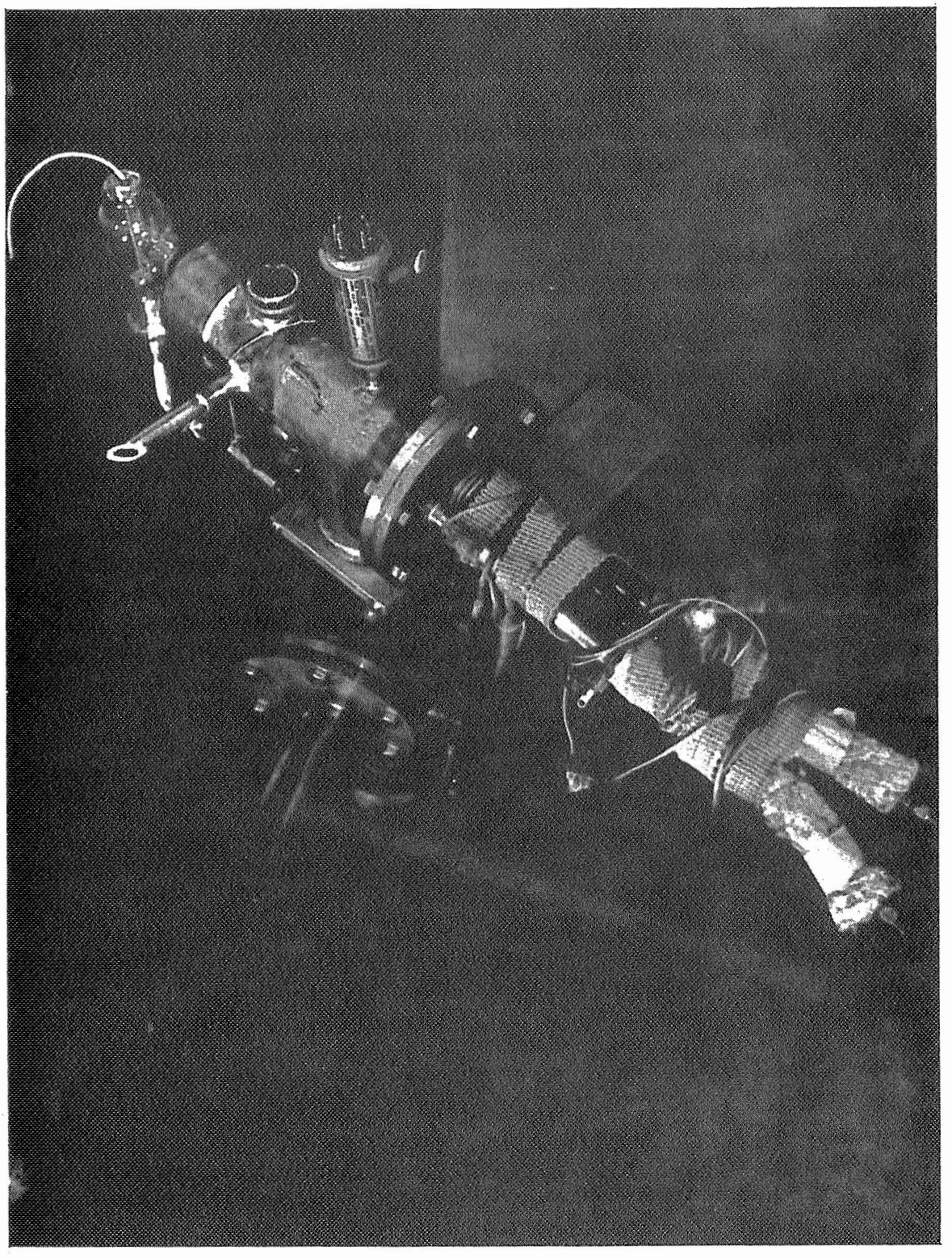

Figure 5.2-2 Photograph of Beam Apparatus

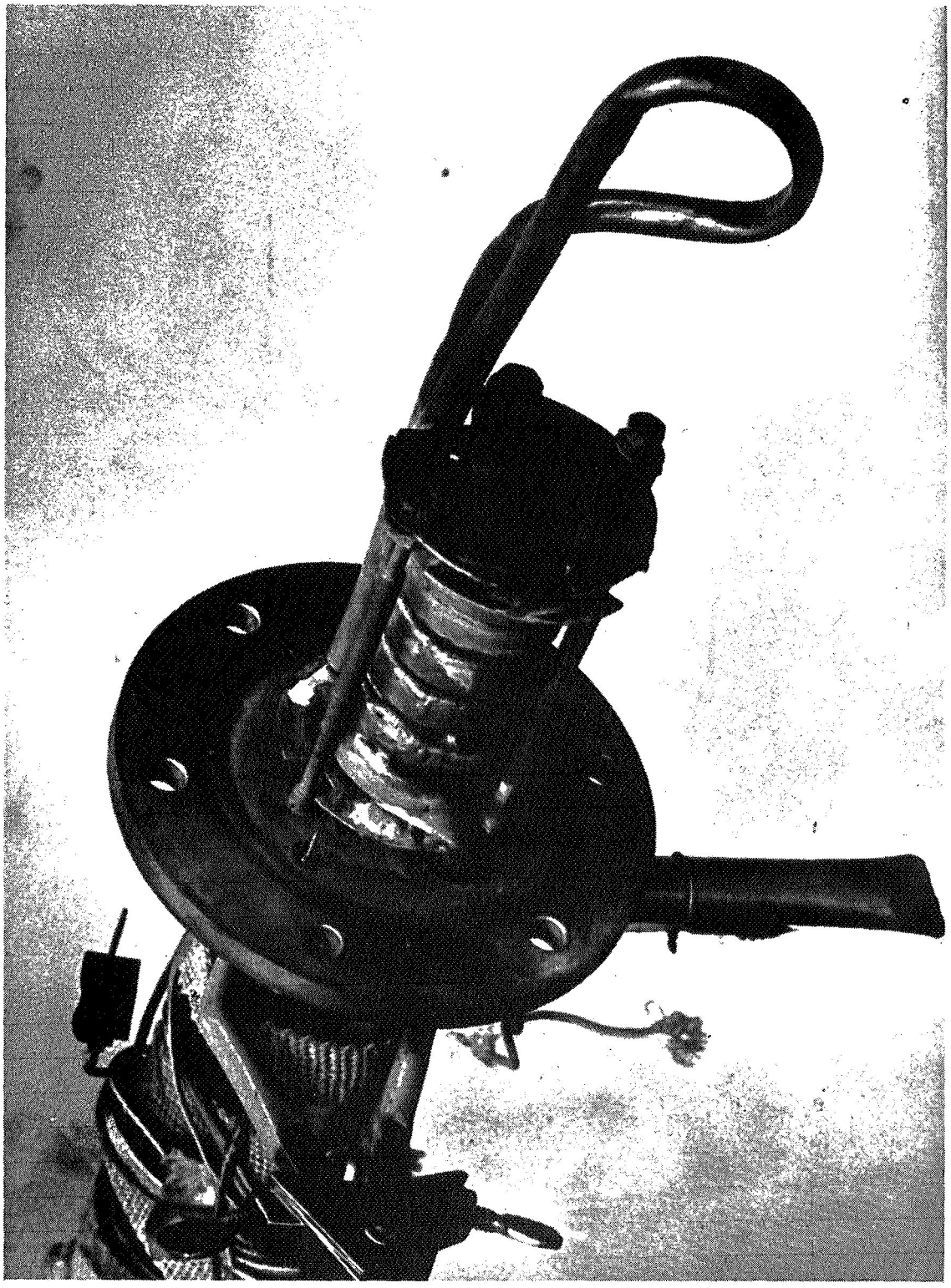

Figure 5.2-3 Photograph of Some Construction Details of Beam Apparatus

5.3 Argon Ion Laser

The argon ion laser is presently the most powerful cw laser (100 Watts) in the visible spectrum. First cw laser oscillation was reported by Gordon, et al.[31] At least six strong lasing transitions take place between excited states of the argon ion.

The excitation of the upper laser level is by electron impact but the exact excitation mechanism is not known. However, two hypotheses have been proposed. In the first, the ionic excited states are generated by multiple collisions of the argon atom with electrons.[31] In the second, the ionic excited states are generated in a single collision with the electrons.[32]

The population difference between the upper and lower laser levels which is responsible for the gain is further enhanced by a favorable lifetime ratio. The lower level couples directly to the ground state of the argon ion and therefore decays at a faster rate than the upper level.

The power output of the argon ion laser exhibits an I^6 dependence for low discharge currents (I), falling off to I^4 at medium currents and then to I^2 at still higher currents.[31] Observation of saturation in cw operation has not been reported. The steep current dependence certainly points to multiple step excitation.

An axial magnetic field of approximately 1000 gauss has been found to enhance the power output of the laser. This is

attributed to the increase in electron density with magnetic field. At optimum magnetic field, a power output of 100 mW/cm of discharge length has been achieved for a bore diameter of 2.5 mm and discharge current of 30 amps.[33]

The width of the gain curve is in the range of 7,000 - 10,000 MHz, which is several times larger than that for the He-Ne laser. The larger width of the argon laser is due to the increased doppler broadening caused by the fast moving ions. The natural width of the ionic transition which, in free ions is 100 MHz, is collision broadened by small angle ion-ion scattering to several hundred MHz.[34] Since this width is generally broader than the axial mode spacing of the cavity, strong mode competition effects take place.

A survey article by Paananen on the progress of argon ion lasers is found in reference (35).

5.3.1 Argon Ion Discharge Tube

The argon ion discharge tube is shown in Figure 5.3.1-1. It consists of a 30 cm long, 3 mm i.d., 4 mm o.d. quartz capillary which is surrounded by a 16 mm i.d. water jacket. Quartz was chosen to handle the high power dissipation in the discharge tube. The design of long life discharge tubes made up of graphite sections is discussed in reference (36). Materials such as ceramics and berylium are also being considered by argon laser manufacturers.

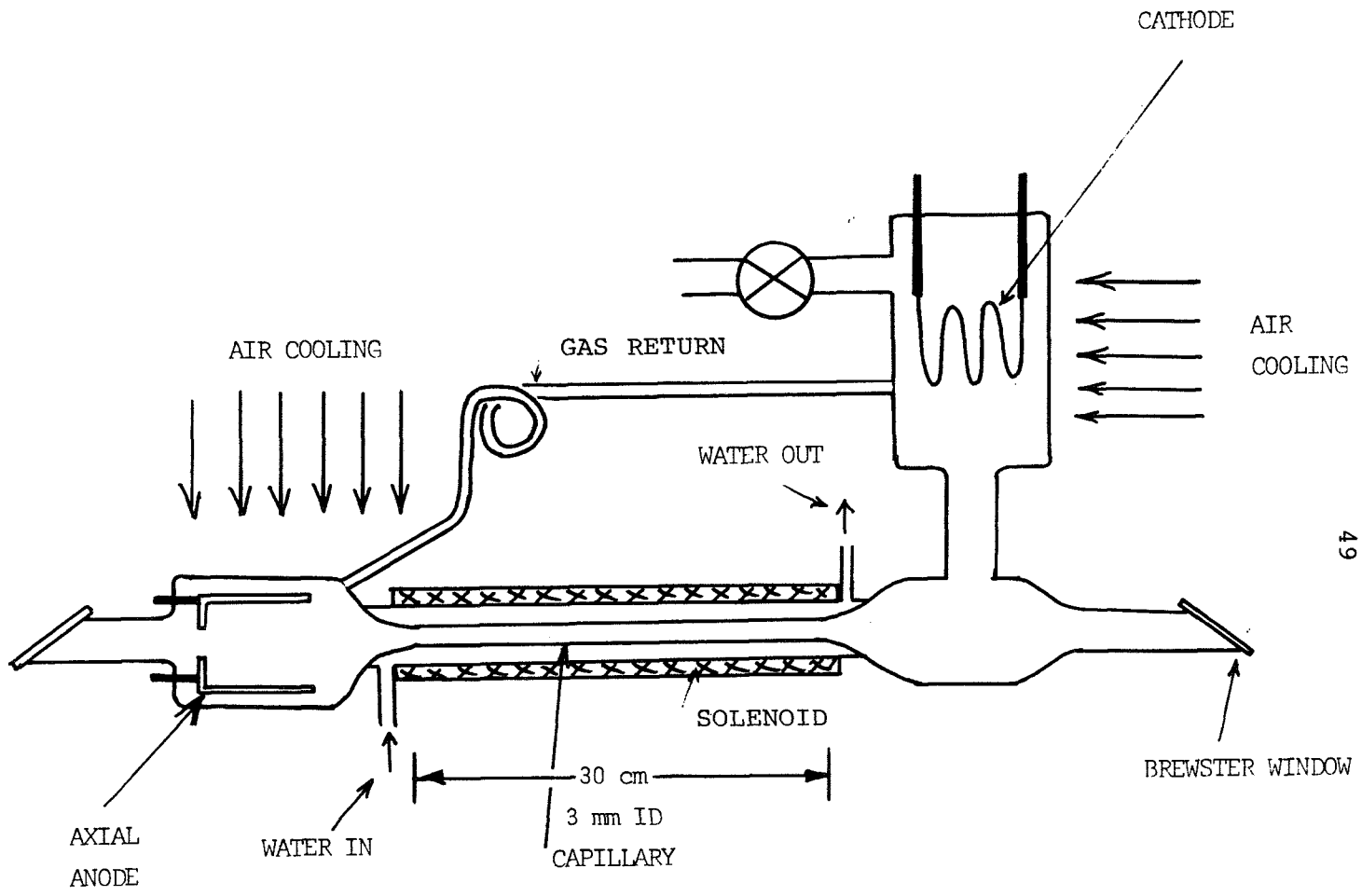

FIGURE 5.3.1-1 ARGON ION LASER DISCHARGE TUBE

The cathode, placed off axis, is a tungsten mesh coated with Barium-Strontium-Calcium oxide with an active surface area of 80 cm^2. A molybdenum anode is placed coaxial with the capillary and has a 3/16" hole at its center to allow the laser light to pass through. The gas return is an 8 mm i.d. tube having two 2 1/2" diameter loops. The Brewster windows were cemented on by means of Torr-Seal. With the exception of the pyrex cathode envelope and the pyrex gas return tubing, the discharge tube was made entirely out of quartz.

The axial magnetic field is provided by a solenoid made up of two layers of #16 coated copper wire wound around the water jacket.

The discharge tube was pumped down to about 2×10^{-7} mm Hg before the cathode was activated. The speed of cathode activation was increased greatly by the use of a "cold finger" directly below the cathode. The cold finger was maintained at liquid N_2 temperature throughout the activation. After cathode activation, research grade argon was introduced into the tube and the first few discharges were used to remove any moisture from the walls of the tube. The cathode and anode envelopes are cooled by forced air.

The 50 Amp cathode d.c. current is drawn from batteries which are continuously charged by a rectified a.c. supply. The magnet current is obtained from a 25 Amp filtered supply of standard design having a ripple of 0.25%. The anode

supply used the 240 volt, 0.4% ripple, d.c. line available in the Research Laboratory of Electronics in series with a water cooled rheostat to adjust the discharge current. The discharge was started by a pulse from a charged capacitor.

A general purpose pulsed anode supply, capable of providing 80 Amp, 500 μsec pulses by use of pulse forming networks at a repetition rate of 100 pulses/sec was designed and used for pulsed (or quasi-cw) laser operation.

5.3.2 Single Longitudinal Mode Cavity

For a typical cavity length of, say, 100 cm, the frequency separation between axial modes, $\frac{c}{2L}$, is 150 MHz. Many axial modes can therefore oscillate within the bandwidth of the laser gain medium.

In the experiment, the laser must have a narrow bandwidth to investigate the structure of the I_2 resonances. A laser is therefore needed that can oscillate in a single longitudinal mode which can be scanned in frequency over the bandwidth of the laser gain medium.

Several methods of achieving single mode operation have been proposed and demonstrated.[37-41] The reduction in laser power due to single mode operation is not as dramatic as first appears because of the broad collision width of the excited argon ion in the case of the argon laser. In fact, single mode power comparable to multi-mode power has been achieved.[42] A discussion of this large single frequency

power in the argon laser is given in a recent paper by Zory.[43]

The scheme adopted to achieve single mode operation is that described by Smith.[38] Smith's method is chosen because it is simple and provides the smallest cavity loss.

The scheme is shown in Figure 5.3.2-1. It consists of a long cavity with a close intermode spacing in which the gain medium is placed and a short empty cavity with intermode spacing greater than the width of the gain medium. The two cavities are coupled by means of a beam splitter. The length of the short cavity can be adjusted so that only one of the resonances of the short cavity coincides with a resonance in the long cavity within the laser gain curve. The combined cavity has effectively a high Q at the common resonance frequency and a low Q everywhere else. In other words, the three element combination on the left in Figure 5.4.2-1 behaves as a highly selective mirror which exhibits high reflectivity at only one of the many axial modes of the long cavity within the laser gain curve. The axial mode that is selected, is determined by the length of the short cavity. An analysis of these coupled cavities is given by Smith in reference (38). In principle, the on-resonance loss of the cavity is zero if the beam splitter transmits 50% and reflects 50% of the incident light, and the other mirrors are assumed perfectly reflecting. The corresponding on-resonance condition is $L_1 + L_2 = n \frac{\lambda}{2}$ and $L_2 + L_3 = m \frac{\lambda}{2}$

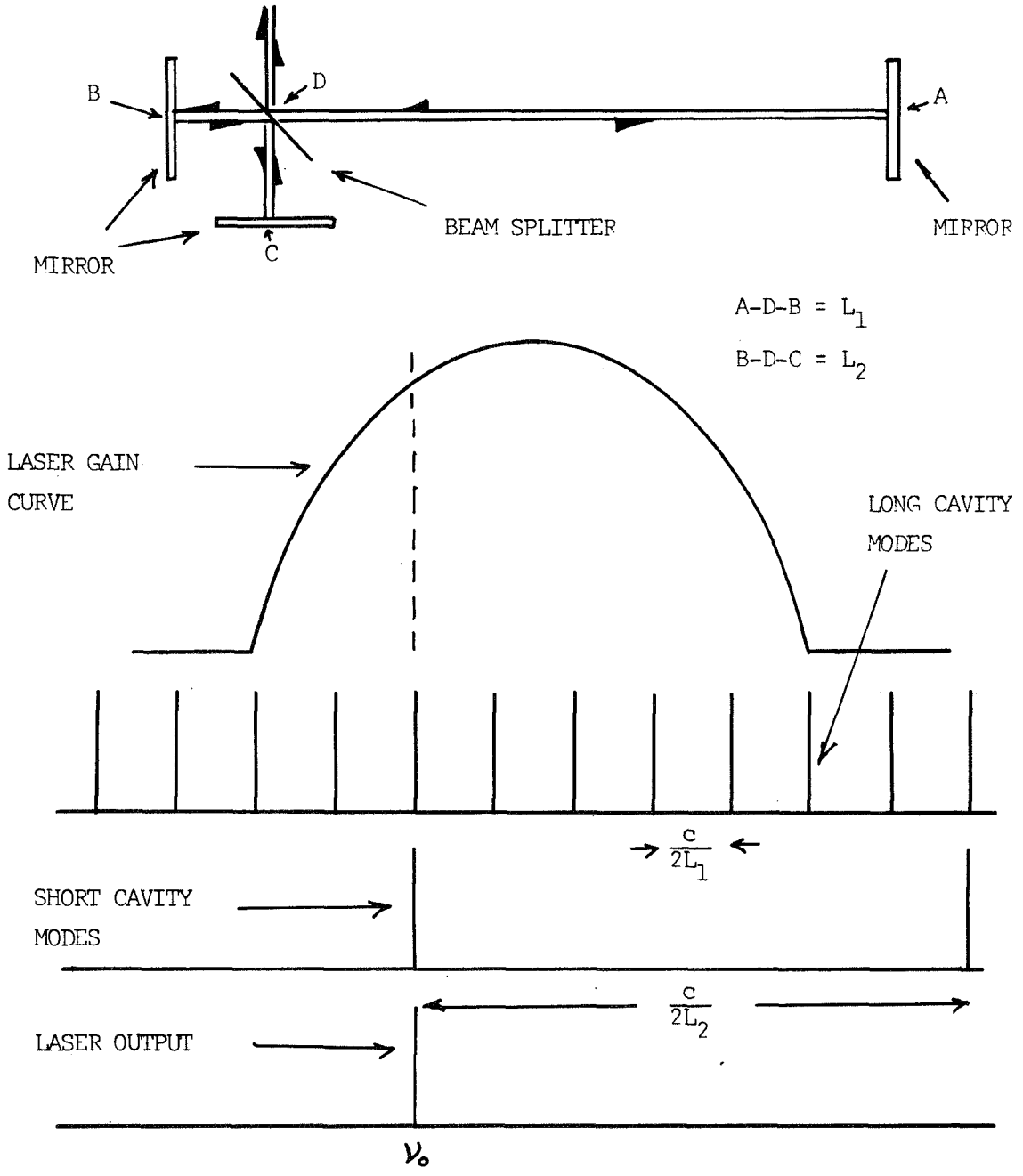

FIGURE 5.3-2-1 MICHELSON-TYPE SINGLE LONGITUDINAL MODE CAVITY

where m and n are integers. The loss at the neighboring long cavity resonance can be as large as 40% for m = n/10 which is adequate for good mode selection at low power levels.

The on-resonance condition implies that the light reflected out of the cavity by the beam splitter destructively interferes with the light passing out of the cavity through the beam splitter. This is responsible for the zero on-resonance cavity loss. The short cavity is often referred to as the Michelson cavity.

In addition to longitudinal modes, a cavity can support a set of transverse or radial modes.[44] Each transverse mode has a mode size, which is a measure of the decrease of the electric field amplitude with distance from the cavity axis, and a radius of wavefront curvature. The mode size and wavefront curvature are a function of position within the cavity. In order to have efficient coupling between the cavities in Figure 5.3.2-1 as well as complete destructive interference, the mode size and wavefront curvature in each cavity must match at the beam splitter.

The general properties of the TEM_{noo} mode in a low loss cavity consisting of two spherical mirrors with radii of curvature R_1 and R_2 and separated by a distance D are shown in Figure 5.3.2-2. The TEM_{noo} mode is the lowest order transverse mode, indicated by the subscript (00), and has a Gaussian field distribution. The mode has a minimum size or a "waist", where the wavefront is plane, at a distance Z_2 from mirror R_2 where[44]

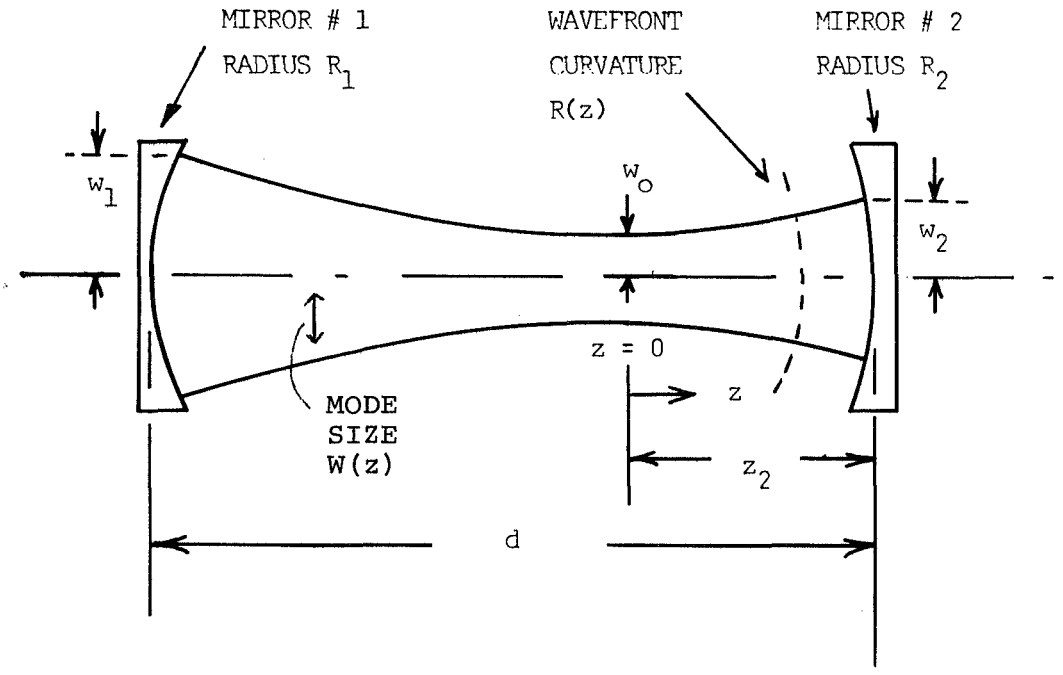

FIGURE 5.3.2-2 GENERAL PROPERTIES OF A TWO MIRROR RESONATOR

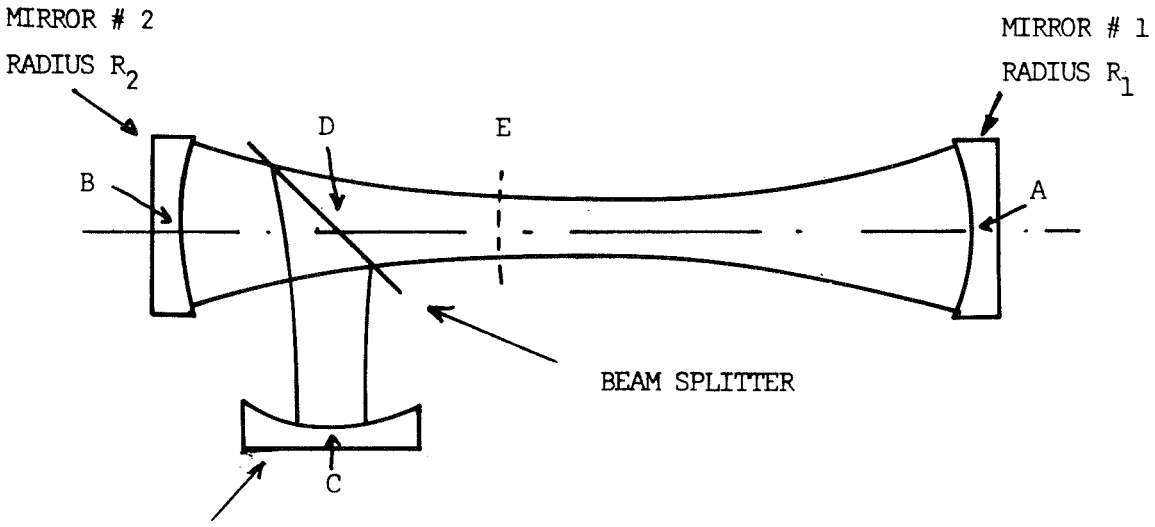

FIGURE 5.3.2-3 MODE MATCHING IN A GENERAL THREE MIRROR SINGLE LONGITUDINAL MODE CAVITY

$$Z_2 = \frac{d\ (R_1-d)}{(R_1 + R_2-d)}$$

The waist at Z = 0 has a diameter $2w_0$ where

$$w_0 = (\frac{\lambda d}{\pi})^{1/2}\ [\frac{(R_1-d)(R_2-d)(R_1 + R_2-d)^{1/4}}{d\ (R_1 + R_2-2d)^2}]$$

The mode size w_z at any distance z from the waist is given by

$$w_z = w_0\sqrt{1 + (\frac{\lambda z}{\pi w_0^2})^2}$$

and the radius of wavefront curvature R(z) at a distance z is given by

$$R(z) = z(1 + \frac{w_0^2\ \pi}{\lambda z})$$

Now in the case of the coupled cavities, R(z) and w(z) of the long cavity must match R(z) and w(z) of the short cavity at the beam splitter as shown in Figure 5.3.2-3. This condition is satisfied if the curvature of mirror R_3, which is at a distance D from mirror R_2, is identical with the wavefront curvature at the point E in the long cavity located at the same distance D from mirror R_2. With this value of R_3, the mode size and wavefront curvature are identical in the region between the beam splitter and mirror R_2.

For general cavity in Figure 5.3.2-3, R_3 is given by

$$R_3 = \frac{d(R_1-d)(R_2-D)^2 + D^2(R_2-d)(R_1 + R_2-d)}{D(R_2-d)(R_1 + R_2-d) - d(R_2-D)(R_1-d)}$$

as shown elsewhere in reference (45). For the case where mirror R_2 is plane, $R_1 > d$ and $D << R_3$, R_1, d as in argon ion lasers, R_3 is given by

$$R_3 \simeq (R_1-d)\ \frac{d}{D}$$

For the case where $R_1 = R_2 = R$ and $D << R$, d

$$R_3 \simeq -R$$

i.e., mirror R_3 is convex. This latter arrangement with 3 curved mirrors may be used to make the resonator less sensitive to tilts of the mirrors.

5.3.3 Design of the Single Longitudinal Mode Cavity

Figure 5.3.3-1 shows the main features of the single longitudinal mode cavity. The main cavity is plano-spherical and is 105 cm long. The radius of curvature of the spherical mirror is 147 cm. Both mirrors have a high reflectivity, > 99.5%, wideband multi-dielectric coating centered at 5145 Å. The spherical mirror is attached to a .2" long by 1/2" diameter piezo-electric cylinder which is used for adjusting the length of the long cavity.

The short cavity is also plano-spherical and is 3.5 cm long. The spherical mirror has a radius of 10 m and is attached to a 1" long by 1/2" diameter piezo-electric cylinder.

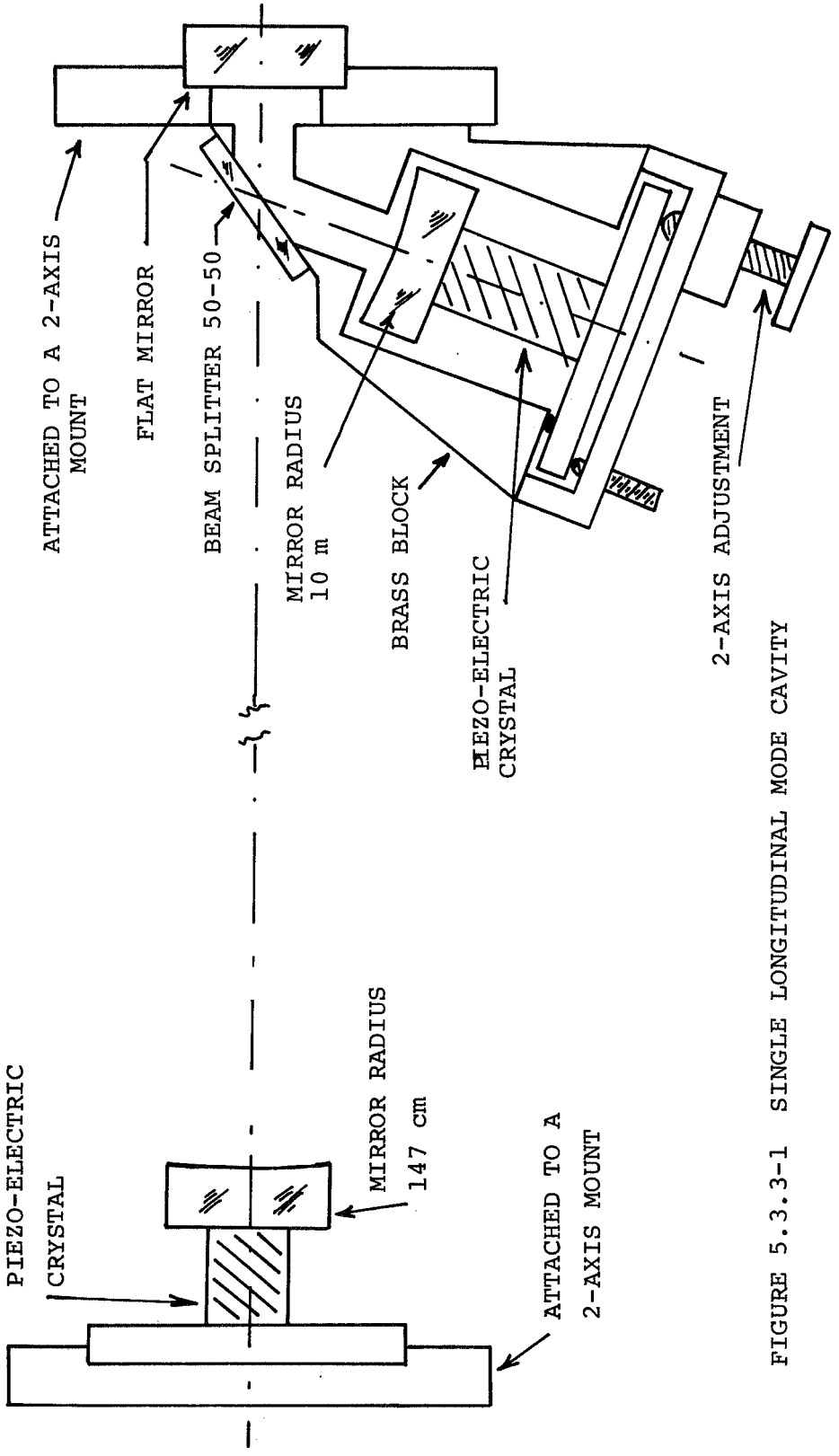

FIGURE 5.3.3-1 SINGLE LONGITUDINAL MODE CAVITY

The short cavity is machined out of a block of brass and is bolted to the adjustable part of the mount that carries the flat mirror. The relative angles between the faces of the block are cut to a tolerance of 0.1 of a degree. The piezo-electric cylinder, to which the spherical mirror is attached, is held in a stiff 2-axis ball suspension. The beam splitter is glued to the brass block with the 50% transmission-50% reflection coating on the surface facing the short cavity. The short cavity is designed so that the beam splitter is at Brewster's angle to minimize reflection losses at the uncoated surface. The spherical mirror has a high reflectivity > 99.5% at 5145 $\mathring{A}$ and a low reflectivity < 15% at 4880 $\mathring{A}$.

The long cavity mirror mounts are attached to an aluminum frame with 4" x 6" rectangular section.

The air spaces between the laser Brewster windows and the mirrors, as well as the entire short cavity, are enclosed by a plastic covering to isolate the air spaces from pressure fluctuations due to the forced air cooling.

Since the laser power needed for the experiment is small of the order of one hundred microwatts, there is no need for a specially coated dumping mirror to achieve optimum laser output power. The output power through the high reflectivity plane mirror is adequate.

The pressure of the argon in the discharge tube is about 150 microns which is found to give minimum lasing threshold

at 5145 Å. A plot of the lasing threshold as a function of argon pressure in a 105 cm long, plano-spherical cavity with high reflectivity mirrors is shown in Figure 5.3.3-2.

Figure 5.3.3-3 is a photograph of the single longitudinal mode argon ion laser.

5.3.4 Alignment of Coupled Cavities

The coupled cavities are aligned as follows:

(a) With the short cavity absent, the discharge tube capillary and the long cavity mirrors are aligned by an external He-Ne laser. The mirrors are then adjusted for minimum lasing threshold in pulsed operation.

(b) The short cavity is introduced with its spherical mirror deliberately misaligned. In spite of the 50% loss of the beam splitter, the laser can be made to oscillate at 4880 Å. The lowest current threshold in pulsed operation is as high as 20 Amps for the 4880 Å line. The 5145 Å line has a higher threshold and does not oscillate when the beam splitter is introduced. The initial laser alignment is not affected by the introduction of the beam splitter since this only introduces a lateral shift of the laser beam in the region between the beam splitter and the plane mirror. The position of the short cavity is then adjusted for minimum reflection from the uncoated surface which ideally should be zero.

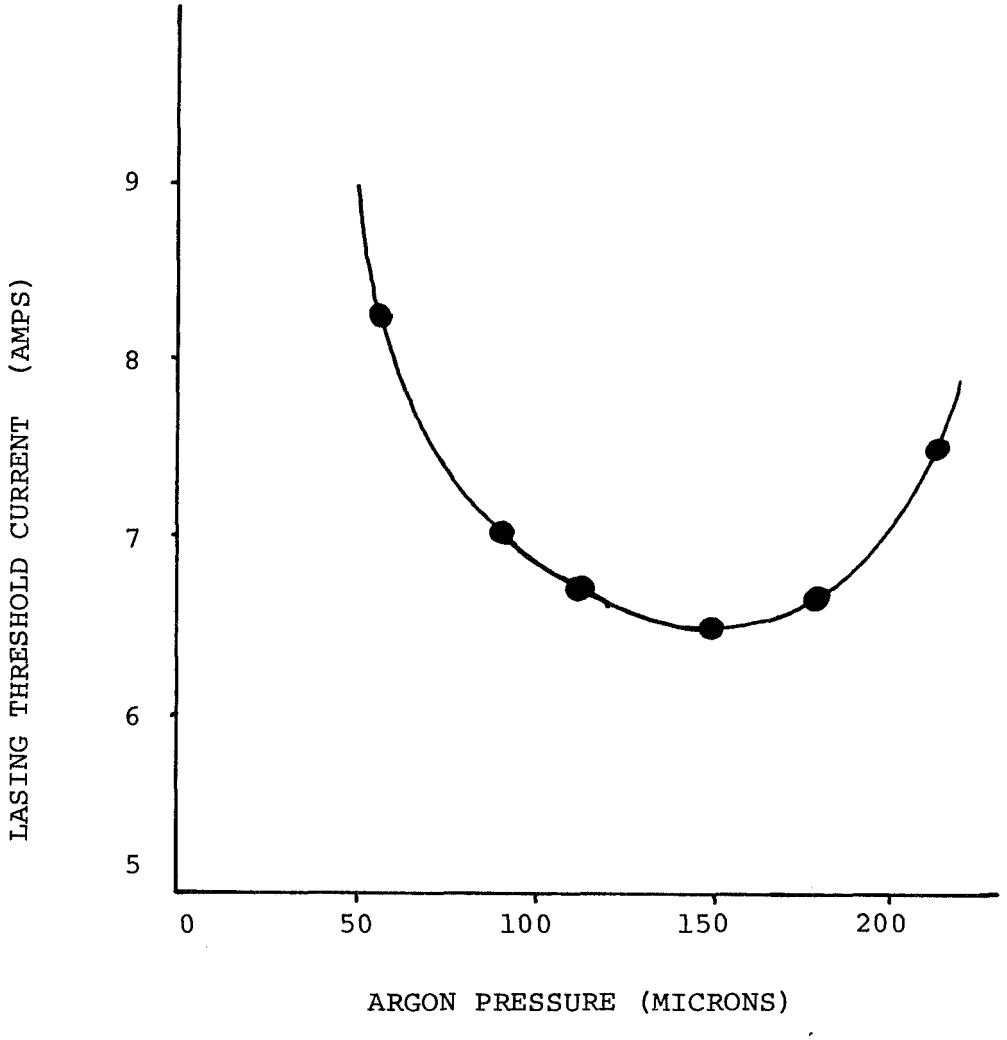

FIGURE 5.3.3--2 LASING THRESHOLD CURRENT VS. ARGON PRESSURE

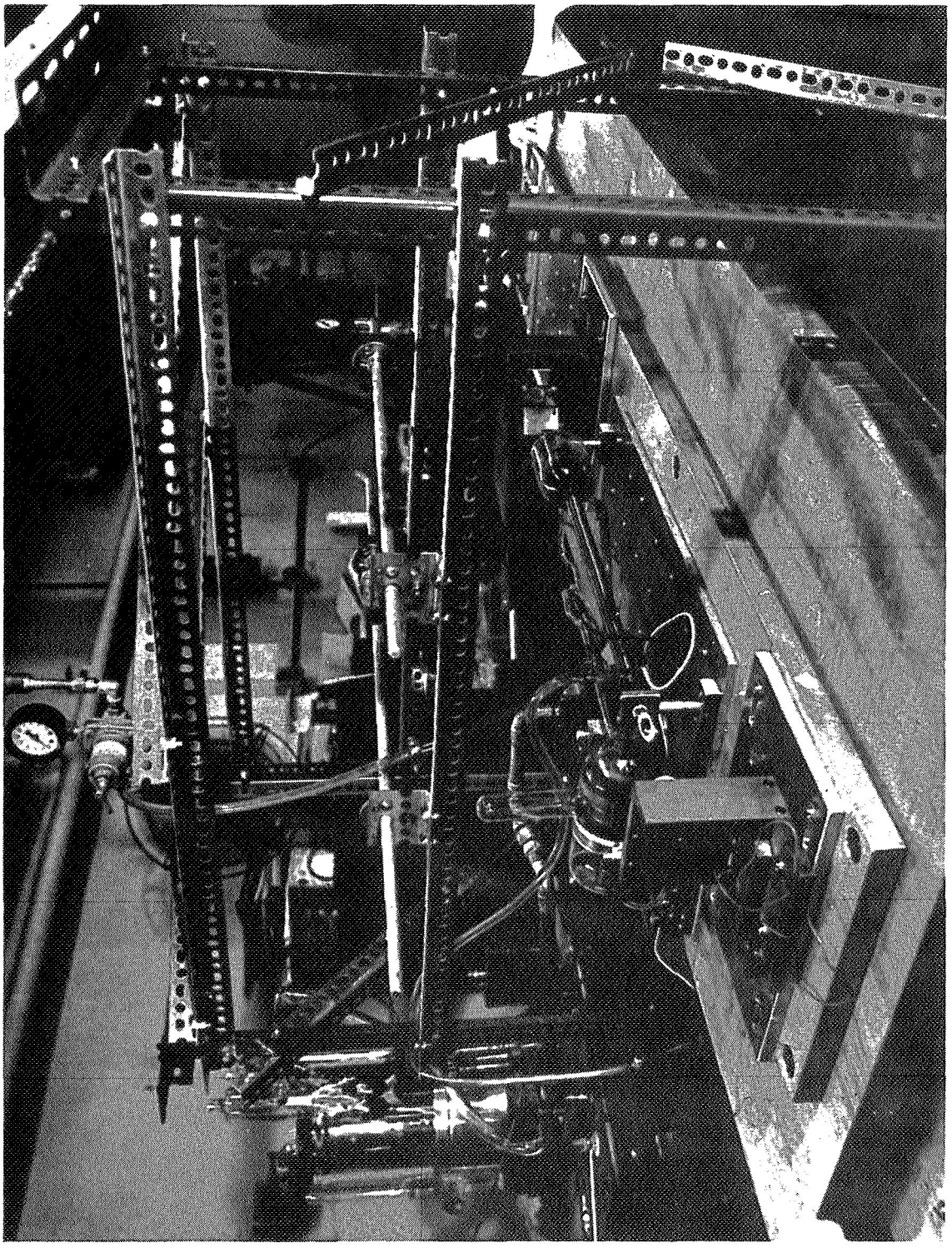

Figure 5.3.3-3 Photograph of Single Longitudinal Mode Argon Ion Laser

(c) With the laser oscillating at 4880 Å, a fraction of the laser beam is reflected into the short cavity by the beam splitter. The alignment of the short cavity consists of reflecting this beam back on itself by adjusting the spherical mirror in the short cavity. When this is carried out the two cavities are coupled and the laser output becomes much brighter. The single mode oscillation is predominantly at 5145 Å since the short cavity spherical mirror has only a 15% reflectivity at 4880 Å.

(d) Adjustment of all three cavity mirrors, including axial translation of the short cavity spherical mirror are then carried out to obtain minimum lasing threshold with the cw supply.

5.3.5 Continous Scanning of the Frequency of a Single Longitudinal Mode Laser

Normally, if the length of the short cavity is varied, the coupling between the two cavities changes and the laser output sweeps out the discrete structure of the longitudinal modes in the long cavity. To achieve continuous, rather than discrete, scanning of the laser frequency, the length of the long cavity must be continuously adjusted to maintain the coupling between the two cavities as the resonance frequency of the short cavity is swept across the laser gain curve.

The experimental arrangement to achieve continuous frequency scanning is shown in Figure 5.3.5-1. The single

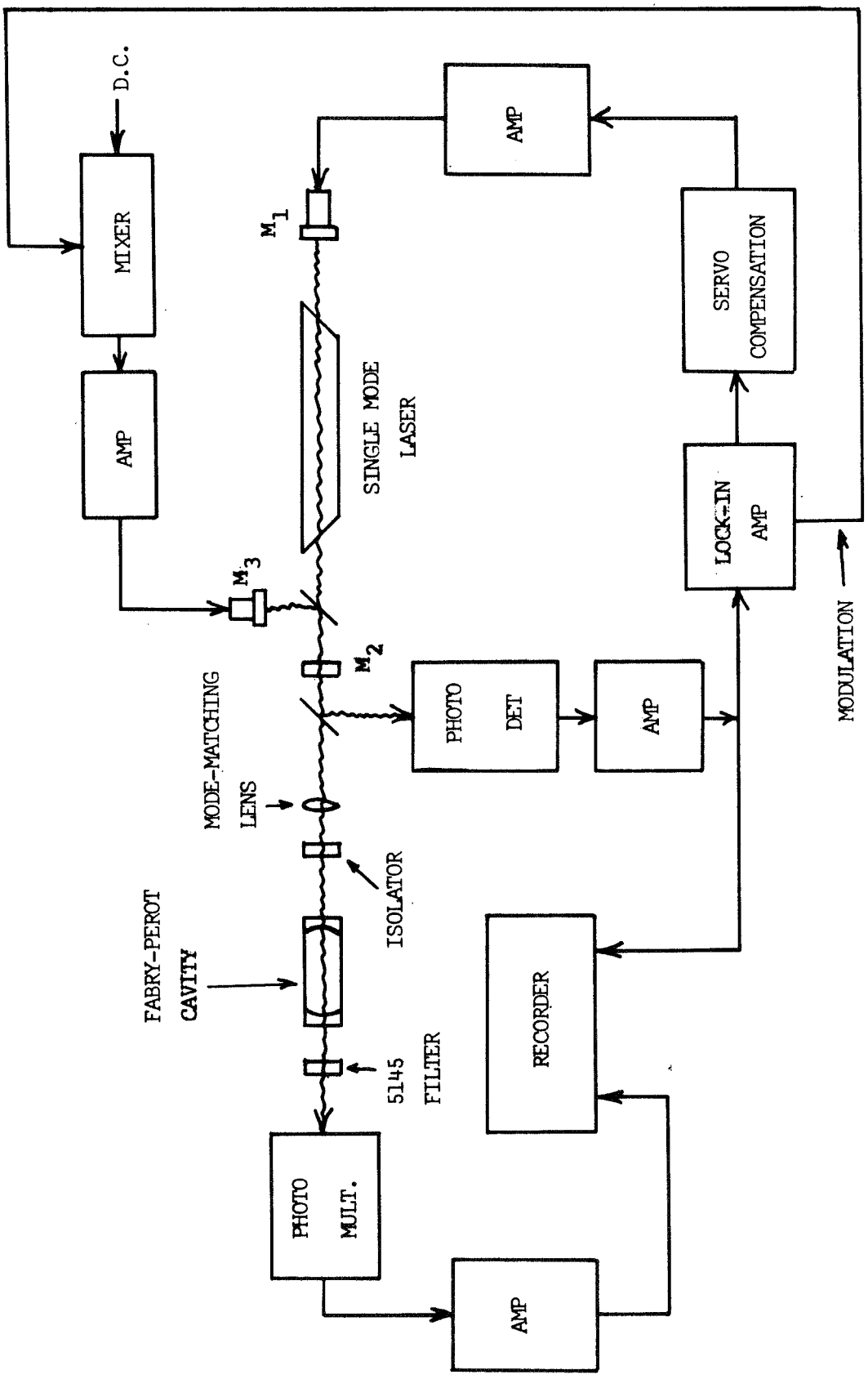

FIGURE 5.3.5-1 SINGLE LONGITUDINAL MODE SCANNABLE LASER (SPECTRAL WIDTH 2-17 MHz)

mode cavity is first tuned for peak laser output by adjusting the length of the short cavity. This implies that the long cavity resonance is coincident with that of the short cavity. The length of the short cavity is then sinusoidally modulated by applying an a.c. signal to the piezo-electric crystal holding the short cavity spherical mirror. The amplitude of the modulation is small so that the resonance frequency of the short cavity is kept within the frequency separation of adjacent cavity modes of the long cavity. As a result, the laser output is amplitude modulated and this is detected on a photodetector. After amplification, the photodetector output is subjected to phase sensitive demodulation in a lock-in amplifier. The d.c. output of the lock-in amplifier is proportional in magnitude and phase to the relative frequency separation between the long and short cavity resonances; at coincidence, the output signal is zero. The output of the lock-in amplifier is fed into a servo-amplifier to drive the piezo-electric crystal holding the long cavity spherical mirror M_1. This feed-back procedure adjusts the length of the long cavity so as to maintain the long cavity resonance in coincidence with that of the short cavity.

In order to scan the frequency of the laser, a slow ramp voltage is applied to the mixer to sweep the resonance frequency of the short cavity over the laser gain curve. Because of the feedback loop, the long cavity resonance tracks the short cavity resonance over the frequency range of the gain curve.

The modulation frequency used is 4 kHz and is limited by the frequency response of the crystal assembly at M_3. The bandwidth of the tuned amplifier in the signal channel of the lock-in amplifier is 10 kHz. Some lead-lag compensation in the wideband servo-amplifier is used to stabilize the feedback loop.

The spectral width of the laser output varied from 2-17 MHz when scanned at the rate of 10 MHz per second, as discussed in the next section. The principle causes of this spectral width may be attributed to (a) the instability of the short cavity; the laser frequency faithfully follows the fluctuations in the center frequency of the short cavity and (b) the fast fluctuations in the optical length of the long cavity that are outside the servo bandwidth.

If the feedback loop is opened and the laser cavity is subjected deliberately to a noisy environment, the resonance frequencies of the long cavity are no longer discrete but tend to be smeared over the entire gain curve. The result of varying the length of the short cavity, in this case, is a single mode output with a broad spectral width of 100 MHz that is continuously scanned in frequency across the laser gain curve. This simple scheme was used in the early experiments.

5.3.6 Measurement of Laser Spectral Width

The transmission of light through a Fabry-Perot inter-

ferometer as a function of the light frequency is a set of periodic narrow resonances and may be used for the measurement of the laser spectral width. The center frequencies of these transmission resonances may be varied by changing the optical path length of the cavity, e.g. by varying the gas pressure inside the cavity.

The ratio of transmitted intensity I_t to the incident intensity I_o through a Fabry-Perot interferometer of length L with perfectly flat mirrors that have identical reflectivity ρ and transmission t, is given by Airy's[46] formula as

$$\frac{I_t}{I_o} = \left(\frac{t}{1-\rho}\right)^2 \frac{1}{1 + \frac{4\rho}{(1-\rho)^2} \sin^2 \frac{2\pi\nu L}{c}} \quad \ldots\ldots 5.3.6\text{-}1$$

When $\nu = \frac{Nc}{2L}$ where N is an integer, the transmission is a maximum. The spectral range is the frequency spacing between maxima, i.e. c/2L. The width, $\Delta\nu_w$, of the resonance of the interferometer, defined by the frequency separation between points where the intensity drops by a half, is given by

$$\Delta\nu_w = \frac{(1-\rho)}{\pi\rho} \frac{c}{2L} \quad \ldots\ldots\ldots\ldots 5.3.6\text{-}2$$

and the ratio of the width to the frequency is

$$\frac{\Delta\nu_w}{\nu} = \frac{(1-\rho)}{\pi\rho} \frac{c}{2L} \cdot \frac{1}{\nu} = \frac{1}{Q}$$

For ρ = 99%, L = 7.5 cm, t = 0.8% assuming a 0.2% loss in each mirror, then

$$\Delta\nu_w = 6\text{MHz}$$

$$\left.\frac{I_t}{I_o}\right|_{max} = 0.6$$

The peak value of the ratio $\frac{I_t}{I_o}$ can be re-written in terms of the loss ℓ_m in the mirror where $t + \rho + \ell_m = 1$ so that

$$\left.\frac{I_t}{I_o}\right|_{max} = \left(\frac{t}{1-\rho}\right)^2 = \left(\frac{t}{t+\ell_m}\right)^2$$

Clearly, if t is increased then the transmission through the cavity increases but the width of the resonance, which depends on $\frac{(1-\rho)}{\rho}$ or $\frac{(t+\ell_m)}{1-(t+\ell_m)}$ gets wider. A compromise has to be found, for a given mirror loss ℓ_m, between the width desired and the peak transmission ratio that can be tolerated.

In a Fabry-Perot interferometer with spherical mirrors, the resonance frequency of the transverse modes as a function of mirror radii R_1 and R_2 and cavity length L is given by the following expression[44]

$$\nu_{n\ell p} = \frac{c}{2L}\left[n + \frac{1}{\pi}\left(+ 2p + 1\right) \cos^{-1}\sqrt{\left(1-\frac{L}{R_1}\right)\left(1-\frac{L}{R_2}\right)}\right]$$

and for $R_1 = R_2 = R$

$$\nu_{n\ell p} = \frac{c}{2L}\left[n + \frac{1}{\pi}\left(\ell + 2p + 1\right) \cos^{-1}\left(1-\frac{L}{R}\right)\right]$$

where n is the longitudinal mode number, i.e. the number of half wavelengths between the cavity mirrors; ℓ, p are the transverse mode numbers. Several low order transverse mode patterns are shown in Figure 5.3.6-1.

In order to couple the spherical Fabry-Perot interferometer

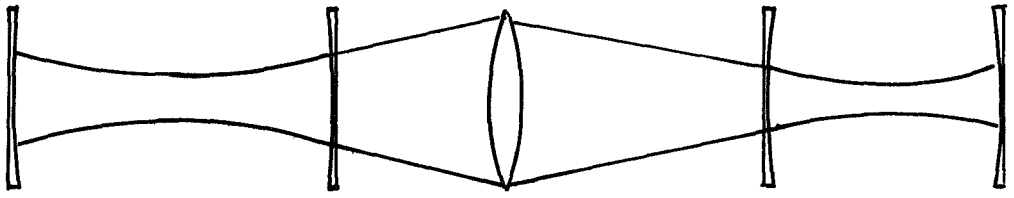

LASER CAVITY

MODE MATCHING LENS

FABRY-PEROT CAVITY

(a)

0,0 1,0 2,0 0,1

(b)

FIGURE 5.3.6-1 (a) MEASUREMENT OF LASER SPECTRAL WIDTH USING A FABRY-PEROT INTERFEROMETER

(b) MODE PATTERNS OF FABRY-PEROT CAVITY (CYLINDRICAL SYMMETRY)

efficiently to the laser light, the azimuthal symmetry of the laser mode and the interferometer mode must be identical. For example, a laser that is oscillating in the lowest order transverse mode, i.e. TEM_{00} mode, has to excite the TEM_{00} of the interferometer. A lens is used to match the laser TEM_{00} mode to the interferometer TEM_{00} mode as shown in Figure 5.3.6-1. The details of the matching of the modes are given in reference (47).

Some of the advantages of a spherical Fabry-Perot interferometer over a plane parallel one are the markedly lower diffraction loss and the higher stability of this cavity. The mode dimension at the mirrors is typically 1 mm for the TEM_{00} mode so that $\lambda/10$ spherical mirror are usually adequate.

The design of the spherical Fabry-Perot interferometer is shown in Figure 5.3.6-2. Each mirror has a 46.9 cm radius of curvature and is coated with 99% broadband reflection coating centered at 5145 Å and also at 6328 Å. The spacer between the mirrors is an invar cylinder 7.5 cm long, 2.5 cm o.d. and 1.25 cm i.d. The ends of the cylinder are cut parallel to within 10 seconds of arc and are turned down to 1.9 cm circle, true to within one part on 10^4. The invar cylinder is inserted inside a brass tube and the mirrors are pressed against either end of the invar cylinder by means of 3-point clamps. The interferometer is supported on two Vee blocks inside a vacuum chamber. Two windows, set at a slight angle with respect to the interferometer axis, allow the laser light

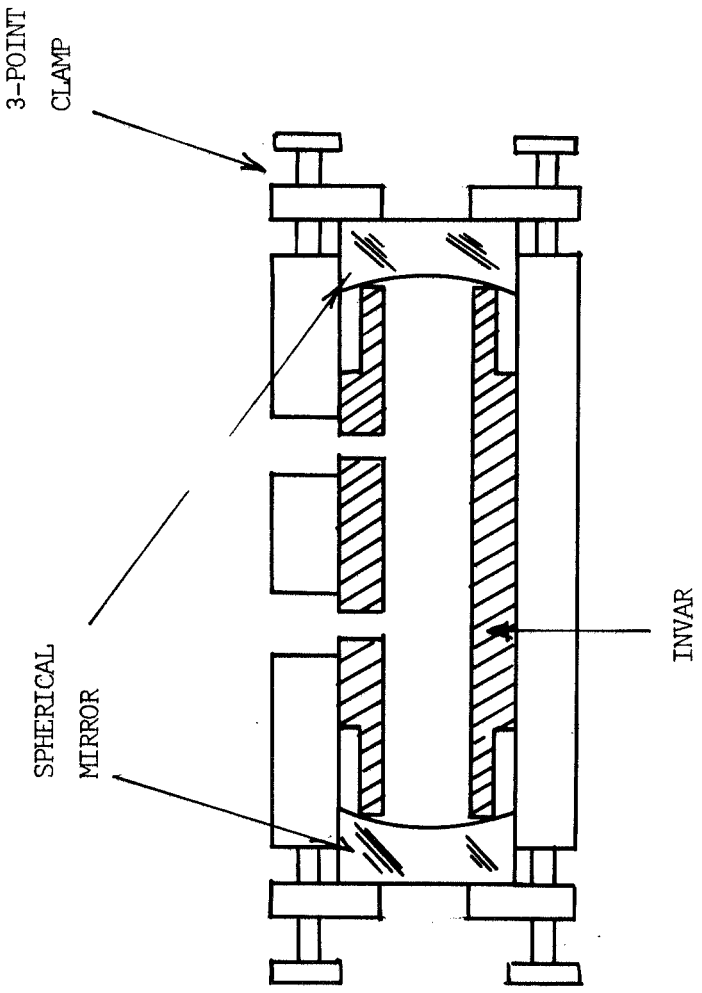

FIGURE 5.3.6-2 SPHERICAL FABRY-PEROT CAVITY

to pass through the vacuum chamber. The leak rate of air into the vacuum chamber is controlled by a micrometer needle valve.

The inherent width of the Fabry-Perot interferometer was determined by using a frequency stabilized 6328 Å He-Ne laser (Spectra-Physics model 108) which has a spectral width of less than 1 MHz. A convex lens was used to match the laser mode to the interferometer mode. However, complete suppression of the other transverse modes was not attempted. An isolator, consisting of a linear polarizer and a quarter wave plate, was placed between the laser and the Fabry-Perot so as to suppress reflections from the Fabry-Perot back into the laser cavity.

The transmission through the Fabry-Perot as a function of pressure is shown in Figure 5.3.6-3. Several of the transverse modes between the two consecutive (00) longitudinal modes have been identified visually and the relative frequency separation between the modes have been consistent with equation 5.3.6-3. The width of the resonances, i.e. the inherent cavity width is measured as 10 MHz at 6328 Å. The frequency separation between consecutive (00) transverse modes, $\frac{c}{2L}$, is 2000 MHz and is used to calibrate the frequency axis in Figure 5.3.6-3.

The inherent resonance width at 5145 Å should also be 10 MHz since the mirrors of the interferometer have equal reflectivity at both 6328 Å and 5145 Å. The interferometer width given in equation 5.3.6-2 is independent of the wavelength of the light.

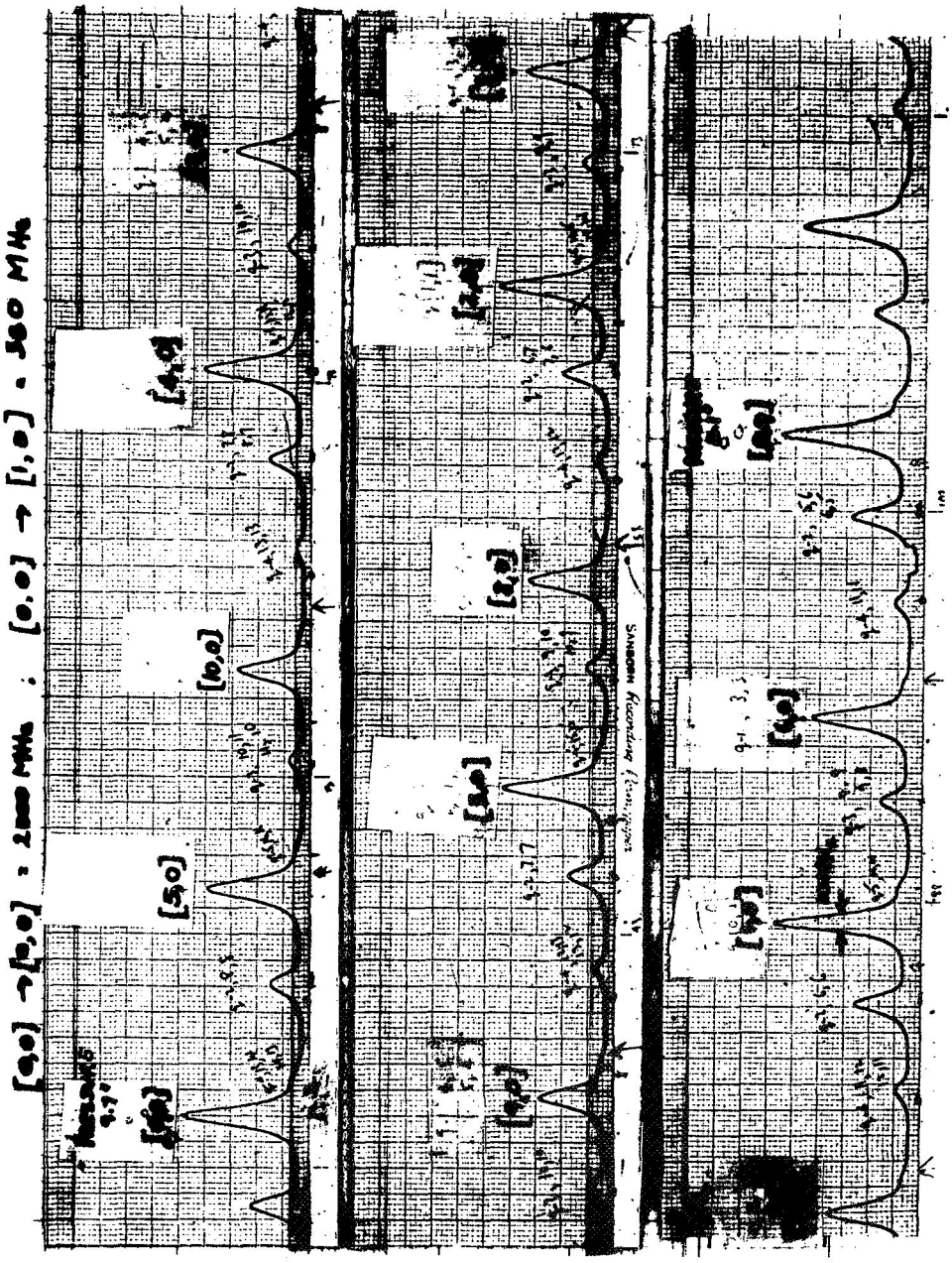

Figure 5.3.6-3 Transmission Through Fabry-Perot as a Function of Pressure Using Stabilized 6328 A He-Ne Laser

The calculated width is 6.7 MHz and is close to the measured value of 10 MHz.

The spectral width of the single mode argon ion laser was measured in a similar way. Figure 5.3.6-4 shows the transmission through the Fabry-Perot interferometer at constant pressure, as the laser, with the servo loop open, is scanned in frequency. The spectral width of the laser is found to be about 100 MHz. This value is inferred from the known separation between the (0,0) and (1,0) transverse modes of the interferometer.

Figure 5.3.6-5 shows the transmission of the Fabry-Perot at constant pressure as the single mode laser, with the servo loop closed, is scanned in frequency. The laser spectral width in this case is found to vary between 2 - 17 MHz, after allowing for the 10 MHz inherent width of the Fabry-Perot.

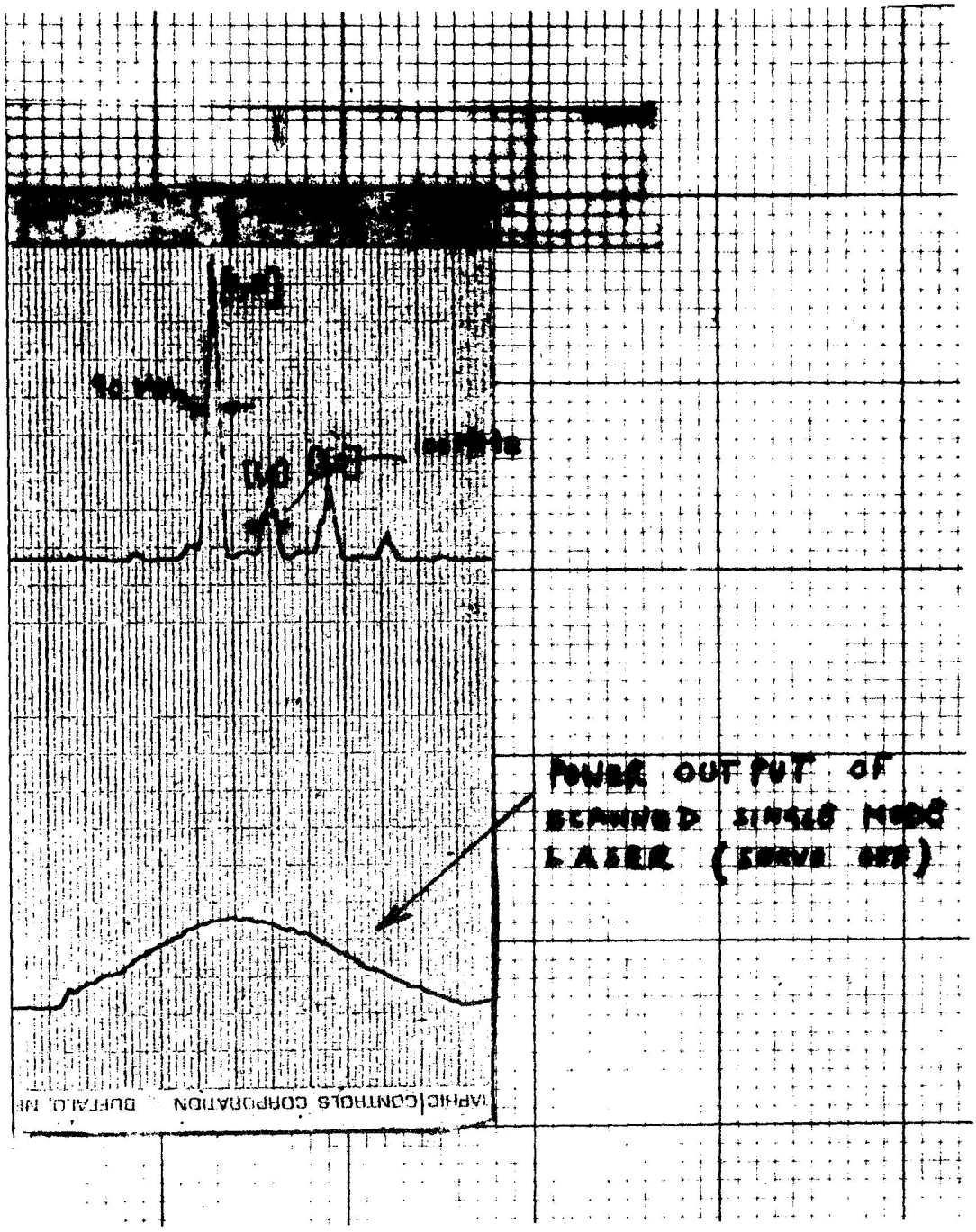

Figure 5.3.6-4 Transmission Through Fabry-Perot as Single Mode Laser is Scanned in Frequency

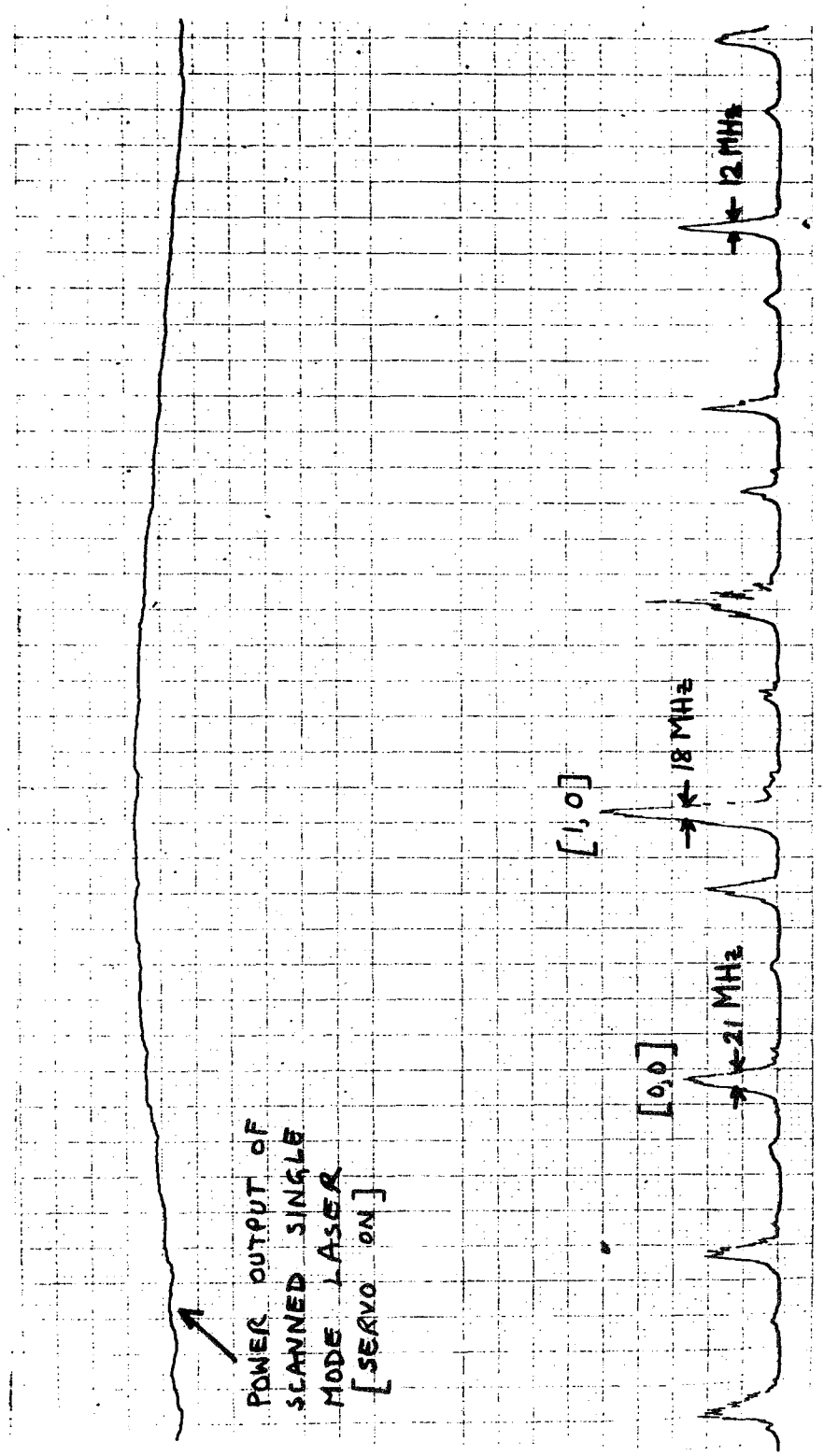

Figure 5.3.6-5 Transmission Through Fabry-Perot as Single Mode Laser is Scanned in Frequency (Servo on). Integration Time 0.1 Second

CHAPTER 6

EXPERIMENTS PERFORMED AND RESULTS

6.1 Measurement of Absorption of 5145 Å Laser Light in an I_2 Gas Cell

The experimental arrangement for the measurement of absorption of 5145 Å laser light in a gas of I_2 is shown in Figure 6.1-1.

In the experiment the light from the single mode laser is split into two beams. One beam is passed through an absorption cell of I_2 and is then detected on a photodetector. The other beam goes directly to another photodetector. The intensity in the second beam provides a reference for measuring the absorption out of the first beam as the laser is scanned in frequency.

A qualitative demonstration of the absorption of the laser light is the appearance of a yellowish fluorescence along the path of the beam in the gas cell (I_2 pressure is 0.3 mmHg) in contrast with the green color of the 5145 Å laser beam on either side of the cell.

The absorption cell is 120 cm long, 3.2 cm diameter and contains ten grams of resublimed analytical reagent grade Iodine crystals. The vapor pressure of the I_2 in the cell is controlled by varying the temperature of the I_2 reservoir

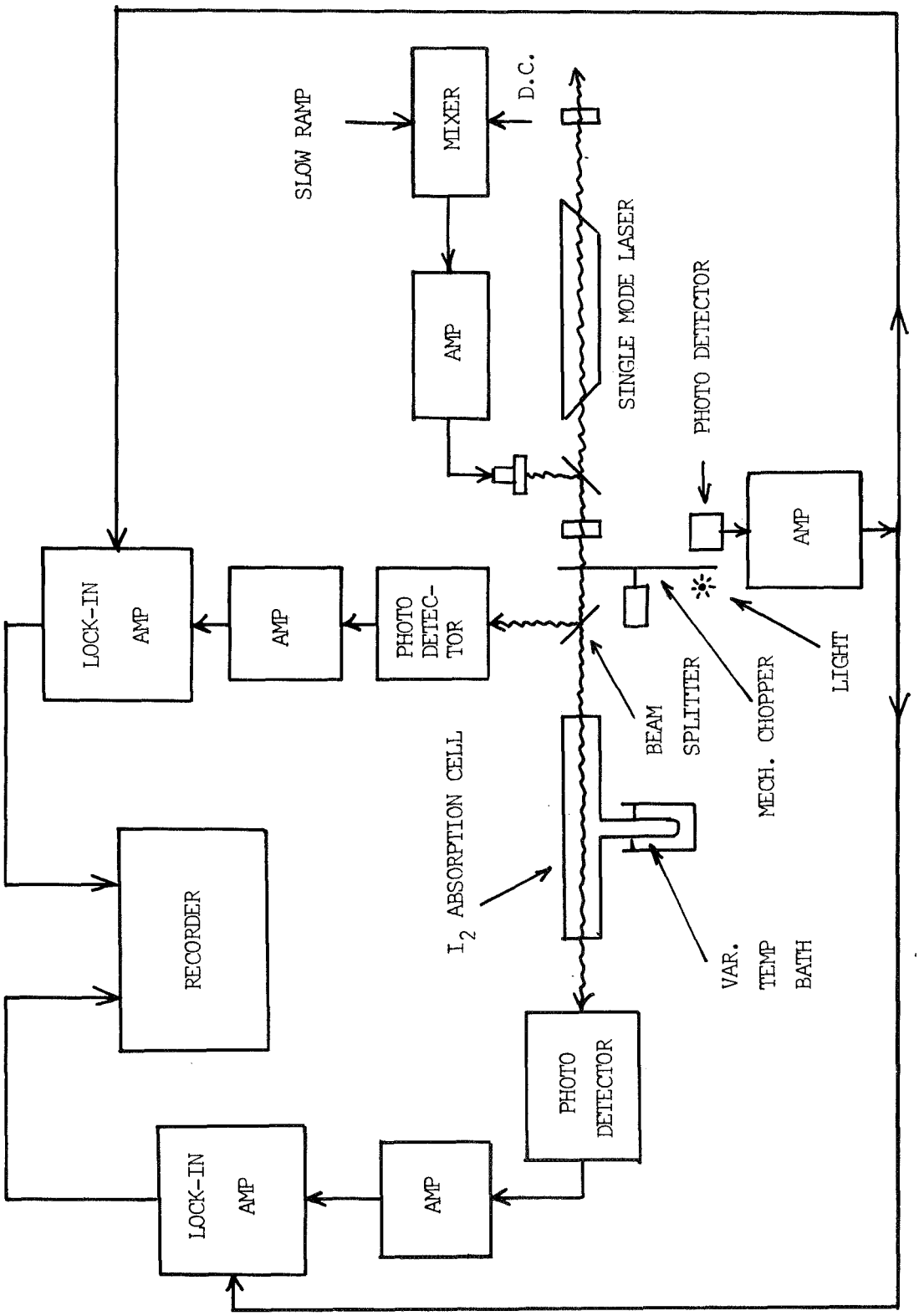

FIGURE 6.1-1 SET-UP FOR ABSORPTION CELL EXPERIMENTS

attached to the cell.

The light from the laser is mechanically chopped at 93 Hz. The output of each photodetector is passed through an amplifier followed by phase sensitive demodulation in a lock-in amplifier. The reference to the lock-in amplifiers is obtained from the chopper by means of an optical pick-off.

Figure 6.1-2 shows simultaneous recordings of direct laser power and laser power after passing through the absorption cell as a function of laser frequency for several values of I_2 pressure. The total bandwidth of the laser scan is 3800 MHz. In Figure 6.1-2(a) the absorption is not noticeable because the I_2 pressure is too low; in Figure 6.1(b) and (c) absorption of the laser light takes place at a frequency above the center of the laser gain curve; Figure 6.1-2(d) shows that at a pressure of 0.3×10^{-1} mmHg, absorption also takes place at a frequency below the center of the gain curve.

The light intensity after passing through the cell is given by

$$I(\nu) = I_0(\nu)\ e^{-k_\nu \varkappa} \quad \ldots\ldots\ldots \quad 6.1\text{-}1$$

where $I_0(\nu)$ is the incident light intensity at a frequency ν; $I(\nu)$ is the intensity of the light at a frequency ν after passing through the cell; k_ν is the absorption coefficient at a frequency ν and $\varkappa$ is the length of the path in the absorption cell.

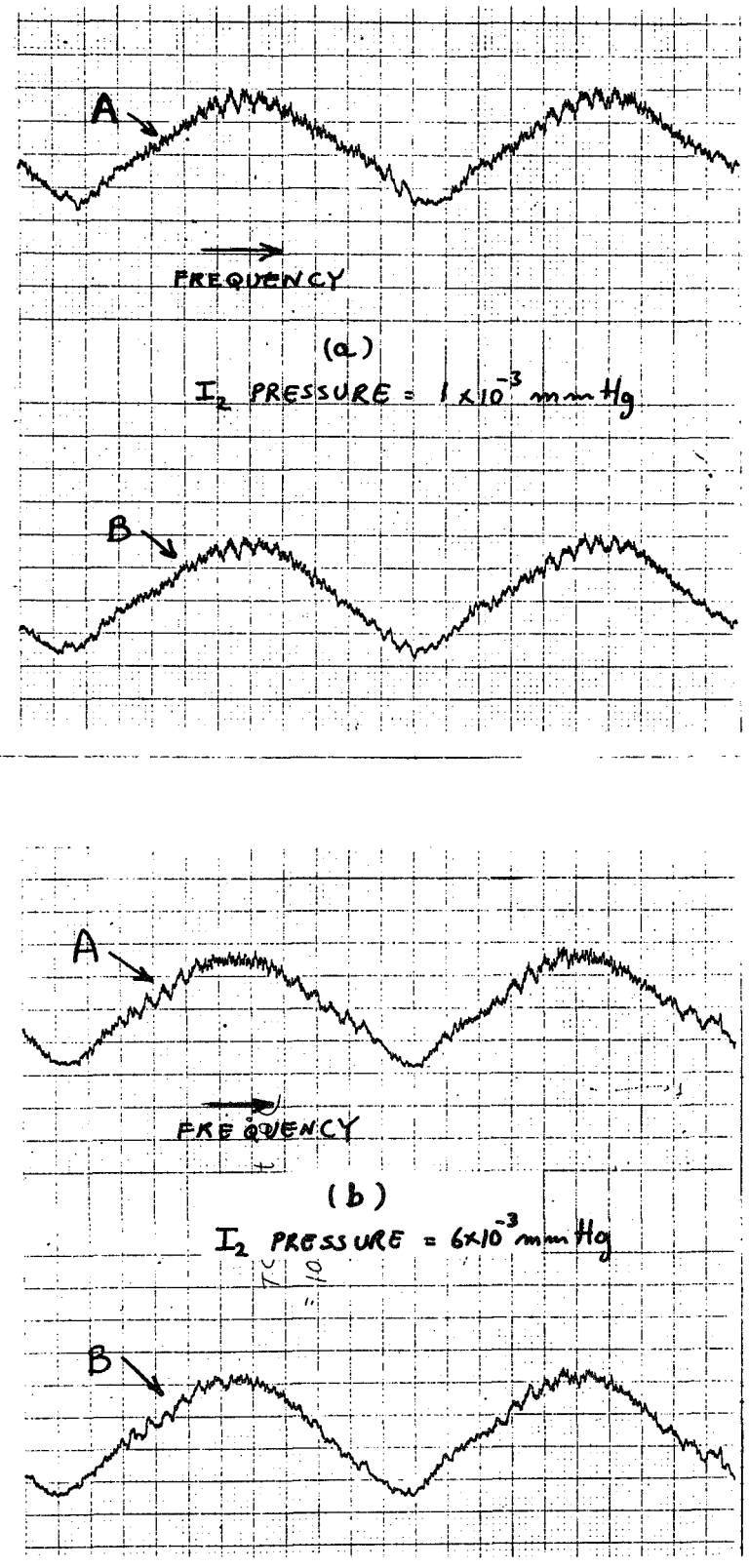

Figure 6.1-2 Simultaneous Recording of (A) Direct Laser Power, and (B) Laser Power After Passing Through Absorption Cell, as the Laser Frequency is Scanned Over 3800 MHz.

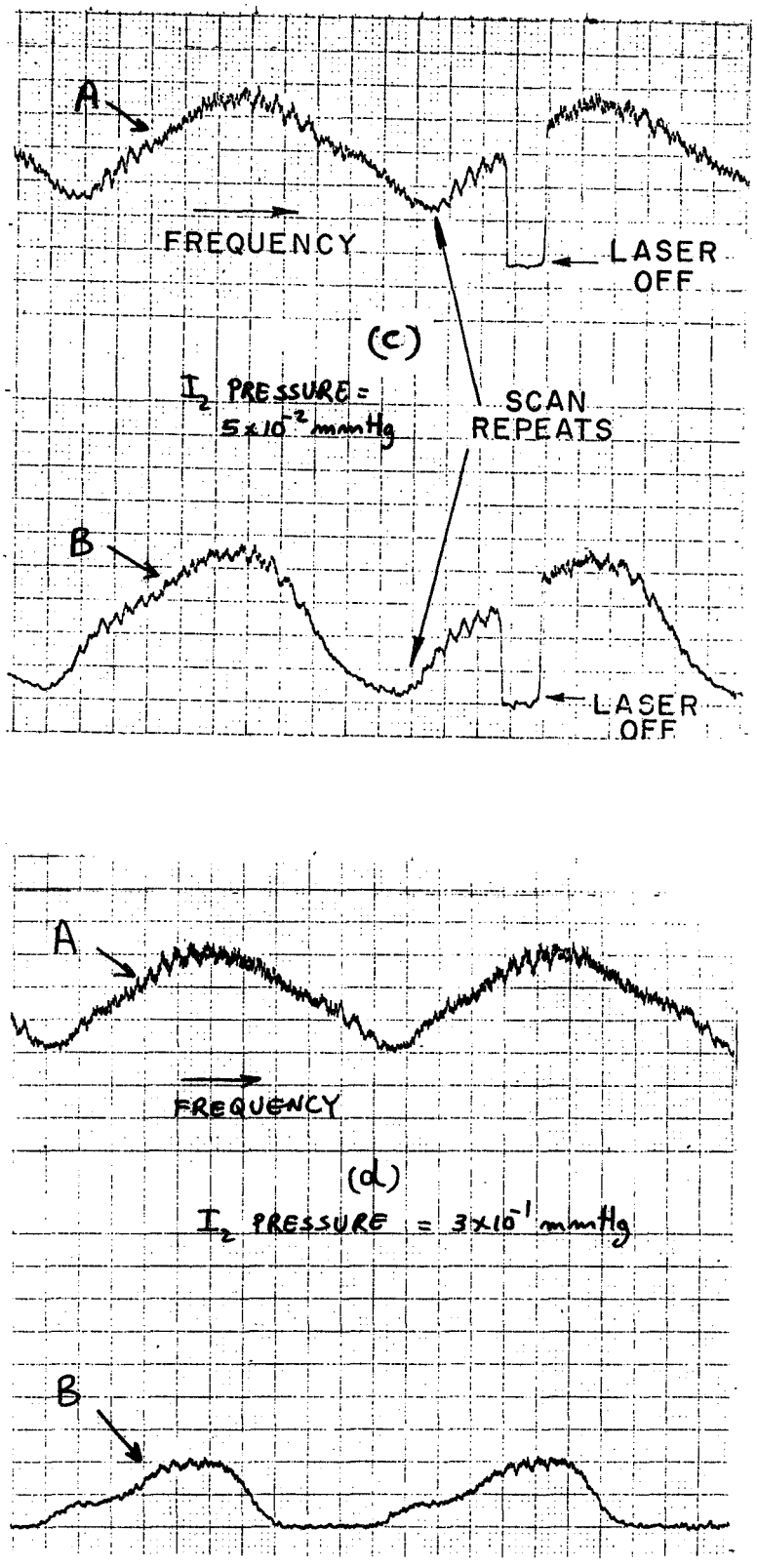

Figure 6.1-2 (continued) Simultaneous Recording of (A) Direct Laser Power, and (B) Laser Power After Passing Through Absorption Cell, as the Laser Frequency is Scanned Over 3800 MH_z.

$I_0(\nu)$ is obtained from the intensity in the reference beam after a scale adjustment. The scale adjustment is the ratio of the measured intensity of the beam through an empty absorption cell, i.e. when the I_2 is trapped out, to the intensity in the reference beam.

The absorption coefficient k_ν is given by

$$k_\nu = \frac{1}{x} \ln \left(\frac{I(\nu)}{I_0(\nu)}\right)$$

and is plotted as a function of laser frequency in Figure 6.1-3, for an I_2 pressure of 5×10^{-2} mmHg. It is evident from this plot that absorption of the laser light is taking place on either side of the center of the gain curve. The peak of the absorption coefficient at the center of the strong line is 23 times larger than that of the weak one.

A slight ambiguity arises in the region where the scan repeats, as indicated in Figure 6.1-2(c), because the bandwidth of the gain curve is a little wider than the mode spacing of the short cavity. The laser power measured in the region where the scan repeats has contributions from both ends of the gain curve and therefore tends to decrease the value of the absorption coefficient in that region.

6.2 Observation of Laser Induced Resonance Fluorescence in a Molecular Beam of Iodine

The experimental set-up for the observation of the laser

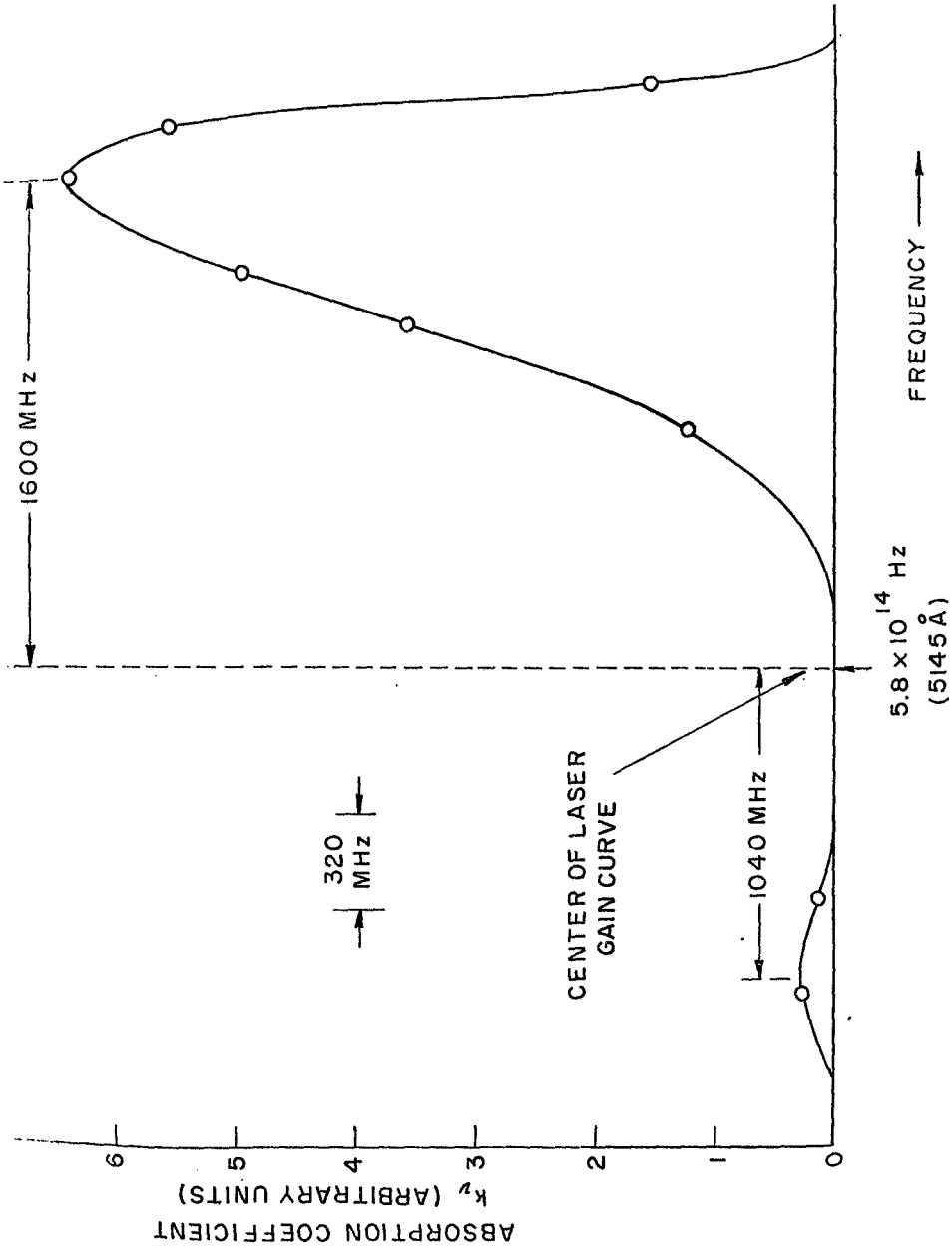

Figure 6.1-3 Absorption Coefficient vs. Frequency

induced resonance fluorescence in a molecular beam of I_2 is shown in Figure 6.2-1.

Light from the single mode cw laser is passed through the molecular beam of I_2 at right angles. The intensity of the laser beam is measured by a photo-detector on the other side of the beam apparatus. The molecular beam is modulated by a 29 Hz sinusoidal signal applied to the solenoid driving the beam flag. The laser induced resonance fluorescence in the iodine molecules is detected on the photomultiplier below the interaction region as the laser is scanned in frequency.

The photomultiplier output is amplified and then subjected to phase sensitive demodulation in a lock-in amplifier. The d.c. output of the lock-in amplifier corresponds to the 29 Hz component in the resonance fluorescence signal.

Figure 6.2-2 shows a simultaneous recording of the cw laser power and the resonance fluorescence signal as the laser frequency is scanned over 3400 MHz. The single mode laser in this case is operated with the feedback loop opened, i.e. the laser spectral width is about 100 MHz, as measured by the spherical Fabry-Perot interferometer.

The resonance fluorescence signal first appears when the laser frequency is about 600 MHz above that of the center of the laser gain curve and the fluorescence extends over approximately 1300 MHz.

Figure 6.2-3 shows another simultaneous recording of cw laser power and resonance fluorescence signal under a higher

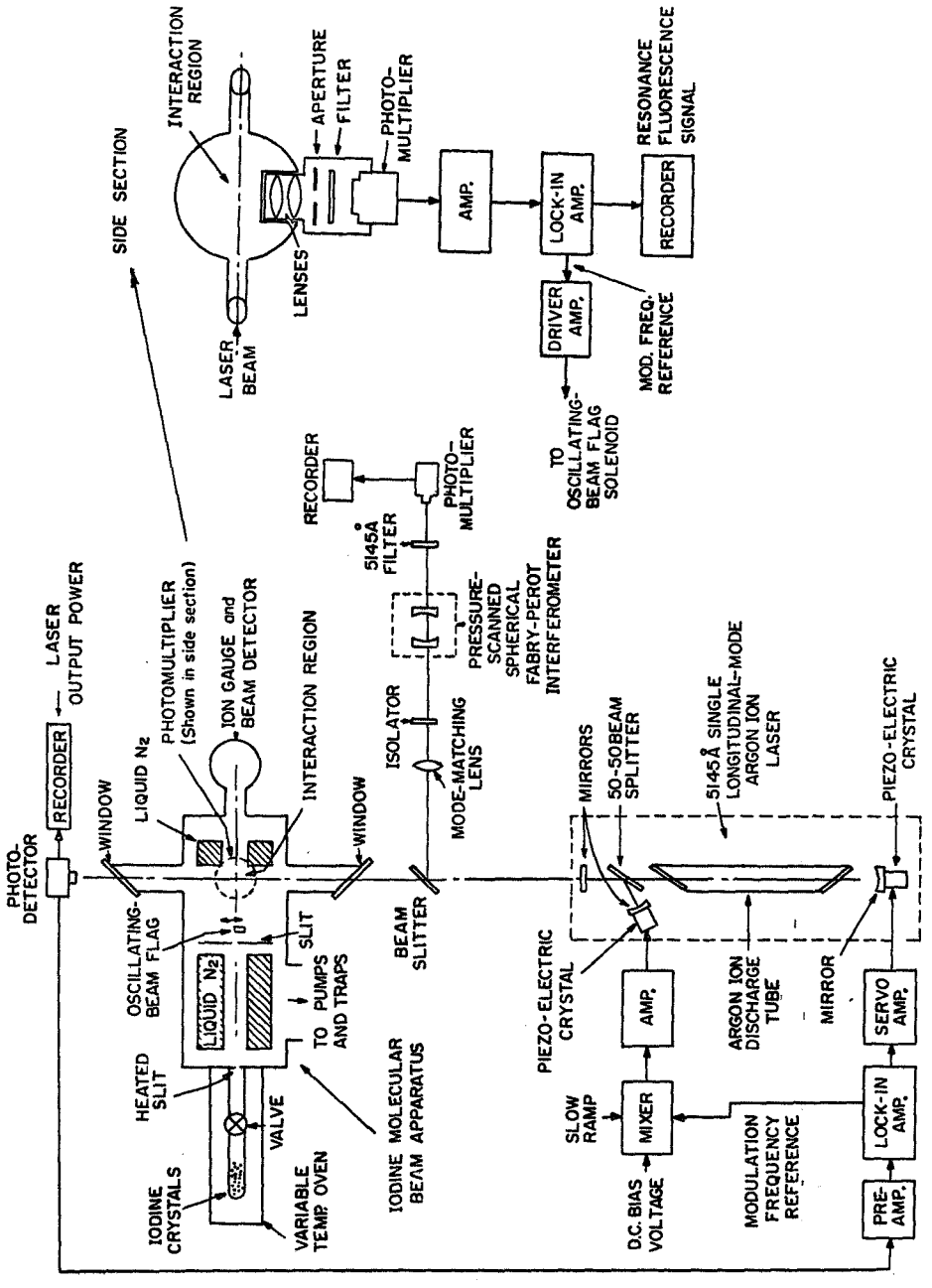

Figure 6.2-1 Experimental Set-up for Observation of Laser Induced Resonance Fluorescence in a Molecular Beam of Iodine

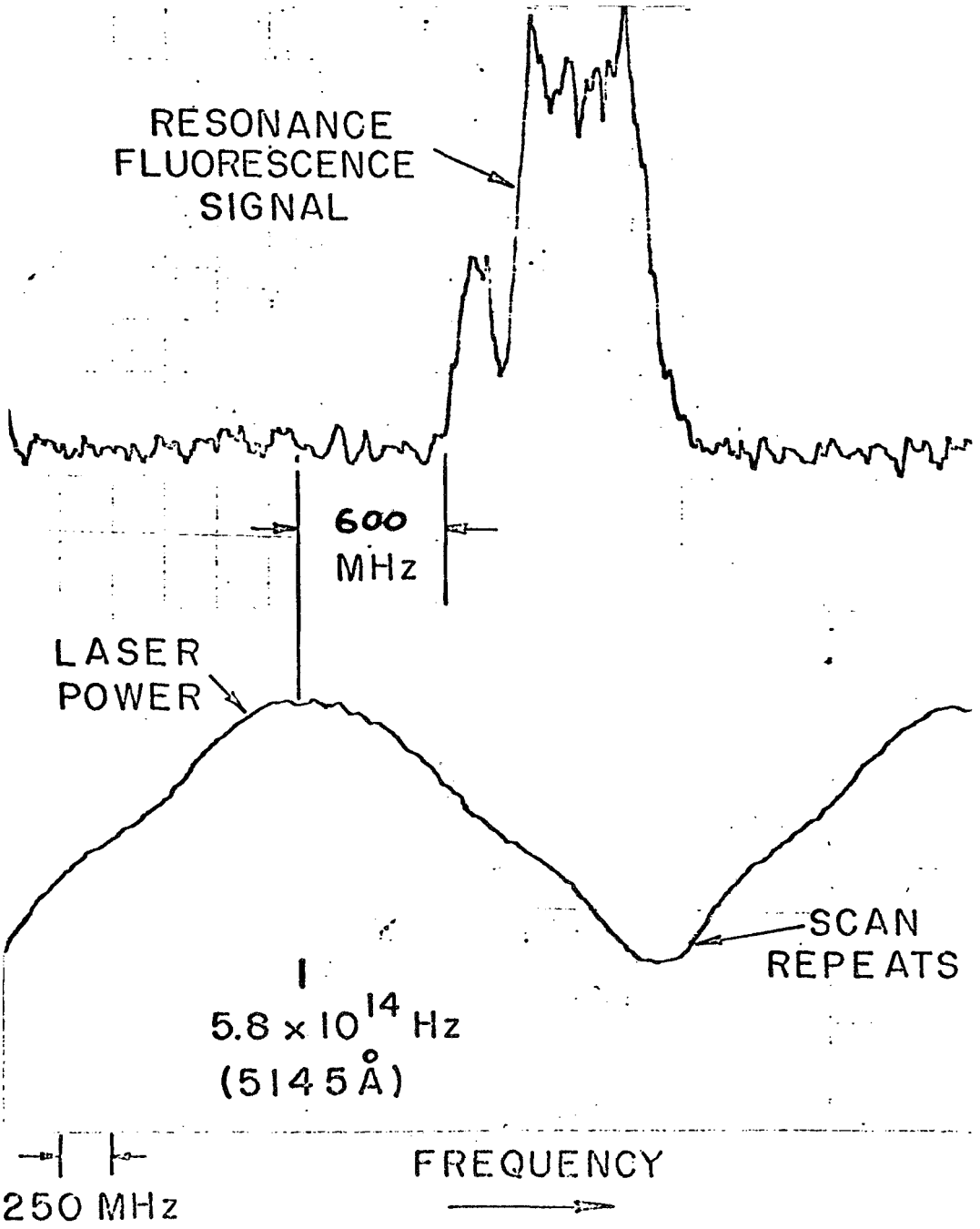

Figure 6.2-2 Simultaneous Recording of CW Laser Power and Resonance Fluorescence Signal as the Laser Frequency is scanned over 3400 MH_z. (Laser Spectral width 100 MH_z; Integration time 0.03 seconds)

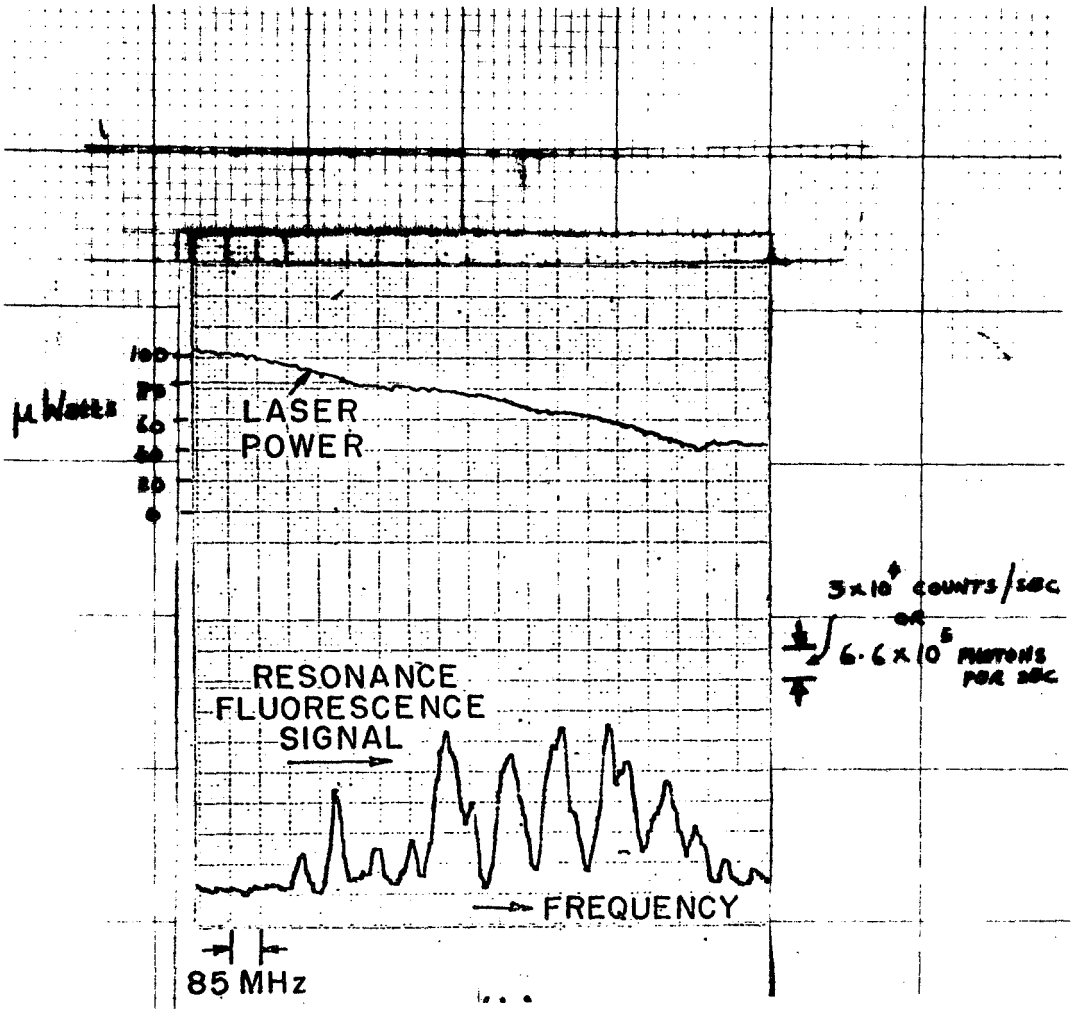

Figure 6.2-3 Simultaneous Recording of CW Laser Power and Resonance Fluorescence Signal as the Laser Frequency is Scanned over 3400 MH_z. (Laser Spectral Width 2-17 MH_z; Integration time 0.03 seconds)

resolution. The single-mode laser in this case is operated with the servo loop closed so that the laser spectral width is in the range 2-17 MHz.

Figure 6.2-3 shows that I_2 has many resonances in the frequency range scanned by the laser. The width of several of the resonances is about 22 MHz.

The doppler width of the molecules in the beam is determined primarily by the geometry of the slits and is 2.25 MHz in this case. This implies that the laser spectral width of 2-17 MHz is the dominant or limiting width in the experiment. Other sources of linewidth broadening are small and are discussed in Chapter 9.

The width of the narrow resonances observed is therefore comparable with the limiting width in the apparatus. This suggests that the natural width of the I_2 resonances may be narrower than 22 MHz. In the next section, the natural width of these resonances is inferred from a measurement of the lifetime of the excited state of I_2 in the beam. The structure of the resonances is discussed in Chapter 8.

Table 6.2-1 summarizes some of the pertinent data relevant to the conditions of the experiment.

The total fluorescence yield as a function of laser power is shown in Figure 6.2-4. Curve #1 represents the total fluorescence; curve #2 represents the fluorescence yield in the first 700 MHz of the fluorescence bandwidth; curve #3 represents the fluorescence yield in the first 500 MHz of the

Oven pressure.....0.3 mmHg

Background pressure of I_2 in apparatus.....1.2×10^{-7} mmHg

Increase in ion gauge reading

when I_2 beam is on.....1.0×10^{-7} mmHg

Beam modulation frequency.....29 Hz

Doppler width of molecular beam

as determined by geometry of slits.....2.25 MHz

Laser cw power (Fig. 6.2-3).....4 μW/mm

Laser spectral width.....2-17 MHz

Laser beam diameter.....2.2 mm

Laser frequency scan speed.....10 MHz/sec

Background noise (Fig. 6.2-3)....less than 1×10^4 counts/sec

Fluorescence signal (Fig. 6.2-3)...6×10^3 counts/sec per mm

(equivalent to 1.3×10^5 photons/sec per mm)

Integration time (Fig. 6.2-3).....0.03 sec

Frequency scale (Fig. 6.2-3).....17 MHz per mm

Paper speed (Fig. 6.2-3).....1 mm per sec

Table 6.2-1

RELEVANT EXPERIMENTAL DATA

ASSOCIATED WITH FIG. 6.2-3

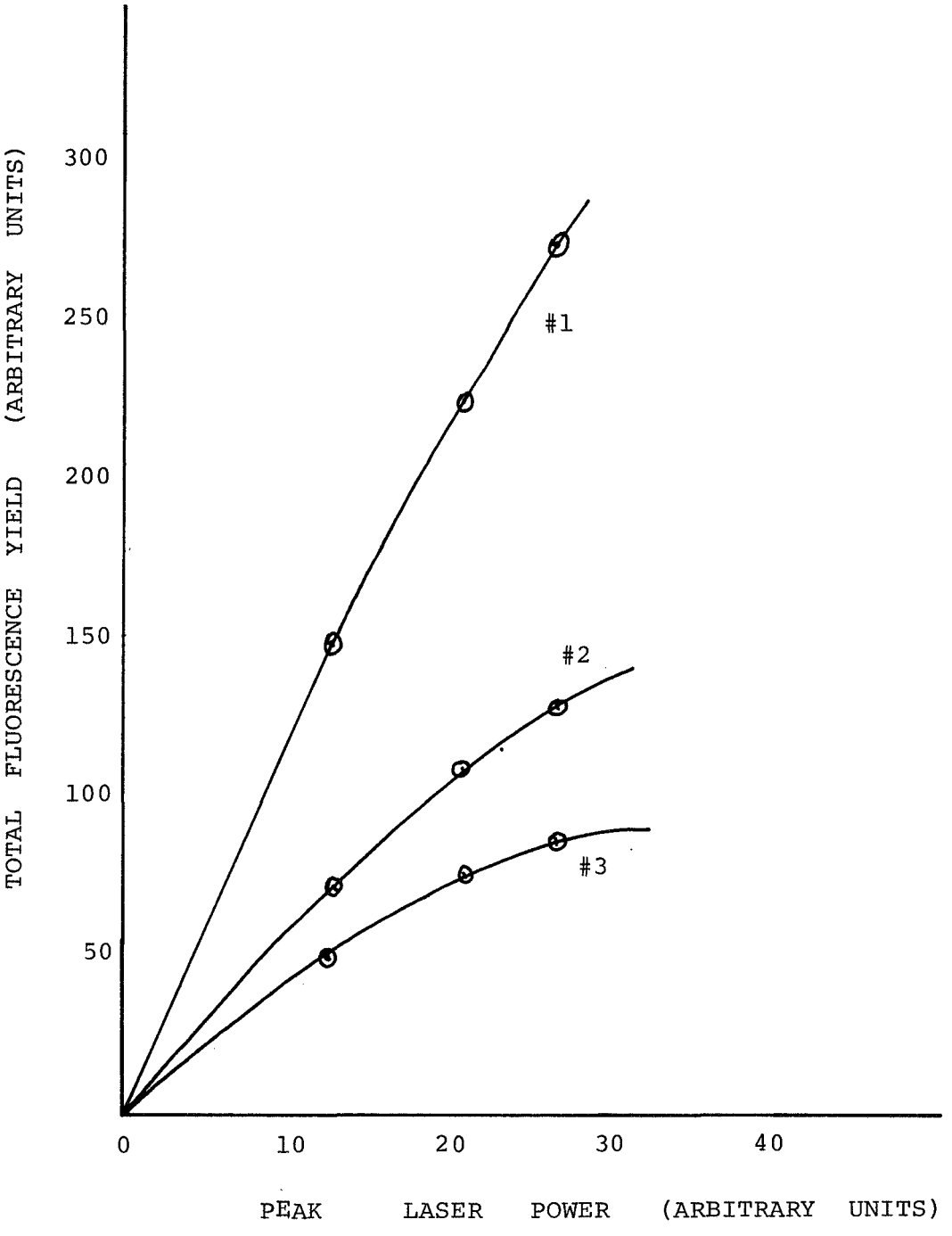

FIGURE 6.2-4 TOTAL FLUORESCENCE YIELD VS. PEAK LASER POWER

fluorescence bandwidth. Curve #3 clearly shows that saturation of the I_2 transitions is taking place in the region where there is sufficient laser power. An estimate for the average cw laser power to saturate the I_2 transitions is 160 μ watts or a laser power spectral density of 4.0×10^{-10} watts/cm^2-Hz for an average laser spectral width of 10.0 MHz and a laser beam diameter of 2.2 mm.

Figure 6.2-2 shows that the fluorescence signal drops to zero when the laser power goes to zero which raises the question of how far up in frequency does the induced fluorescence really extend? This was settled by increasing the laser excitation to extend the bandwidth of the laser. To avoid the risk of damaging the laser by passing a much higher d.c. current, a quasi-cw, high current excitation was employed. The d.c. discharge current was maintained at a quiescent value of 5 Amps and was increased to 40 Amps for 500 μ-seconds at a repetition rate of 50 pulses per second. Figure 6.2-5 shows the fluorescence signal with a quasi-cw laser operation. The bandwidth of the fluorescence is within 10% of that shown in Figure 6.2-2. The signal to noise ratio is very much reduced because of the low duty cycle (2.5×10^{-2}) and because of the saturation of the I_2 resonances at low laser power levels.

6.3 Lifetime Measurement of the Excited State of I_2 in the Beam

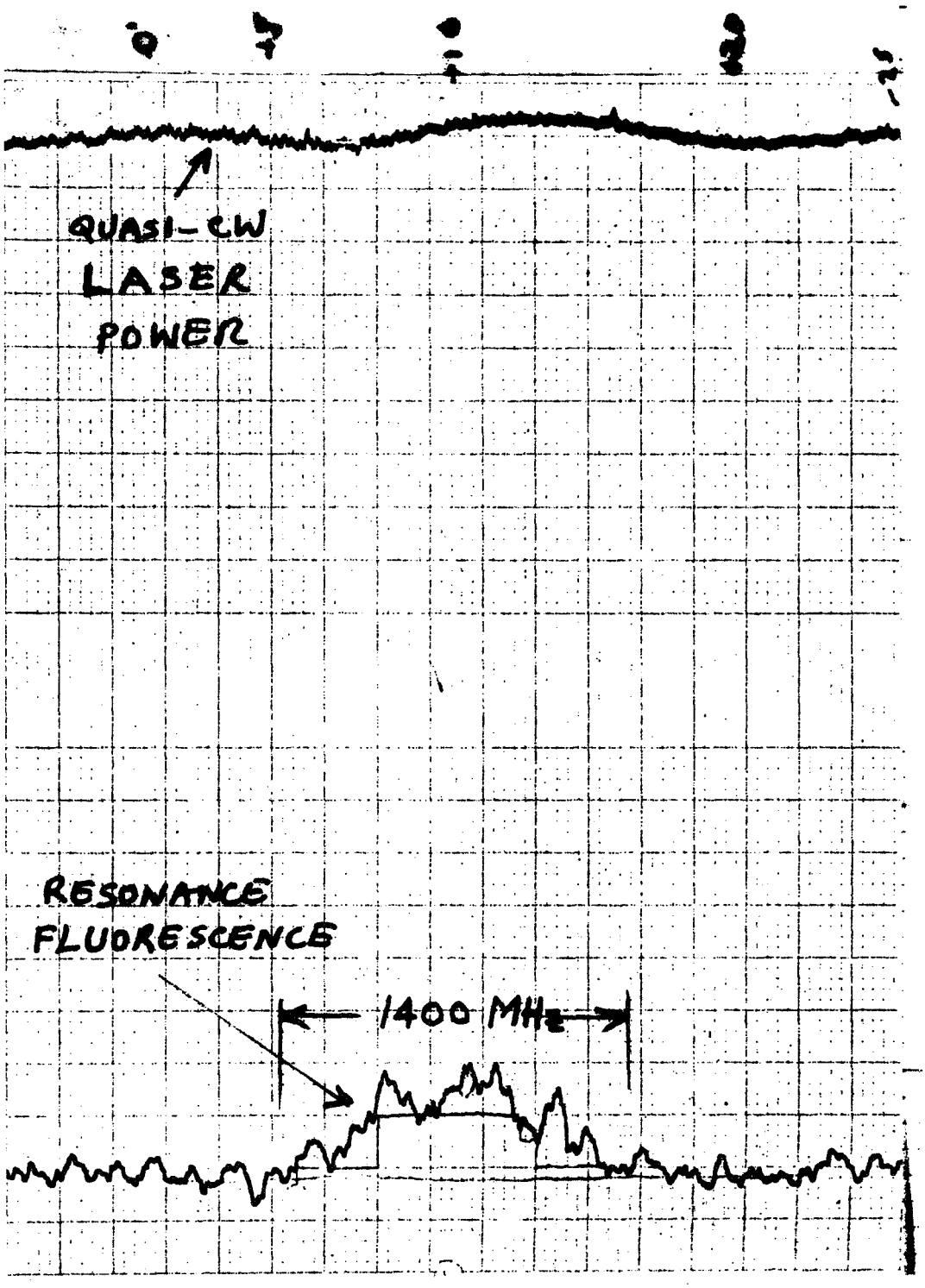

Figure 6.2-5 Fluorescence Signal with High Current Quasi-CW Laser Operation (Duty Cycle 2.5×10^{-2})

The measurement of the lifetime of the relevant excited state of I_2 in the beam was motivated by the fact that the width of several I_2 resonances shown in Figure 6.2-3 is comparable with the laser spectral width. This implied that the natural width of these resonances may be narrower than 22 MHz.

The experiment consists of exciting the I_2 molecules in the beam with very short laser pulses and then measuring the time dependence of the resonance fluorescence. The time constant of the decay gives the lifetime of the excited level.

Figure 6.3-1 shows the experimental arrangement for the lifetime measurement. Short laser pulses are obtained by the use of a rapidly rotating mirror which sweeps the light beam across a small aperture in front of the molecular beam apparatus. The rotating mirror is doublesided and is attached to the shaft of an 18,000 RPM motor. The axis of rotation of the mirror shown in the figure is perpendicular to the plane of the paper. The laser beam diameter is 2 mm and is equal to the diameter of the aperture. The separation between the aperture and the rotating mirror is 150 cm. The calculated width of the light pulse through the aperture is 1.4 μ-seconds.

The pulsed fluorescence signal, detected by the photomultiplier, is first amplified and then sampled in a sampling gate. The width of the sampling gate is 1/2 μ-second and the position of the gate is varied slowly over a sampling sweep

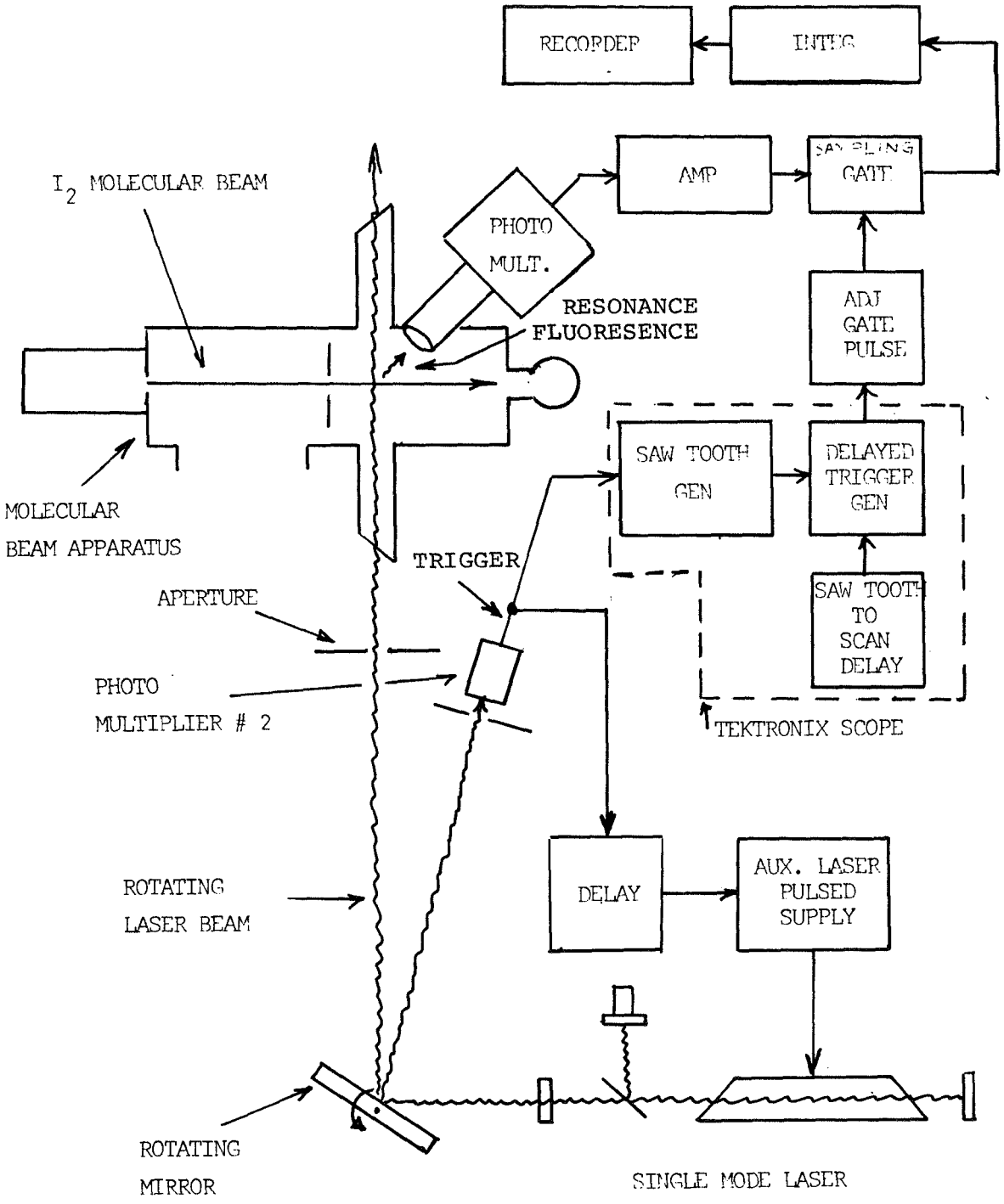

FIGURE 6.3-1 SET-UP FOR LIFETIME MEASUREMENT

of 16 μ-seconds.

The timing is achieved as follows. The rotating laser beam is detected by photomultiplier #2 several microseconds before the laser beam enters the molecular beam apparatus. The output pulse from photomultiplier #2 is used as a trigger to start the sweep in the Tektronix scope. The delayed trigger generator in the scope produces a trigger pulse at a pre-set delay with respect to the start of the sweep in the scope. This delayed trigger generates the 1/2 μ-second gate pulse to control the sampling gate. The delay of the gate pulse with respect to the start of the sweep is varied slowly from zero up to a delay of 16 μ-seconds in 50 seconds. This is achieved by sweeping the delay in the delayed trigger generator using a slow sawtooth waveform generator in the scope.

In the pulsed excitation of the I_2 molecules, the transition probability is smaller than in cw operation for the same cw laser power. This is due to the duration of the pulse, 1.8 μ-seconds, being shorter than the average time of 10^{-5} seconds that the molecules spend in the laser field in cw operation. An expedient that works quite successfully is to increase the laser power momentarily by pulsing the laser discharge just as the laser beam is to pass through the beam apparatus. The timing trigger for the discharge pulse is obtained from photomultiplier #2 after a suitable fixed delay. The average laser power in the pulse is 1 watt/cm^2 or a power

spectral density of 10^{-8} watts/cm^2-Hz. In this way, the cw laser beam is used for the timing and the momentary increase in the laser power is used to saturate the I_2 transitions.

An attempt was made to obtain short laser pulses by pulsing the discharge instead of using a rotating mirror. Laser output pulses shorter than 5 μ-seconds could not be obtained by pulsing the discharge.

The lifetime measurements were performed in the following way. First, the laser pulse was measured with the molecular beam off. This established the origin of the time coordinate. A scatterer was introduced on one of the Brewster windows in the beam apparatus to make the light pulse visible to the photomultiplier. The molecular beam was then turned on to record the fluorescence signal.

Figure 6.3-2(a) shows the photomultiplier signal with the molecular beam off and (b) shows the photomultiplier signal with the molecular beam on.

The decay of the fluorescence is analyzed after the laser pulse is over. The decay is found to be exponential with an average time constant of 3 μ-seconds.

Radiation entrapment of the resonance fluorescence is negligible since the background I_2 pressure is 1×10^{-7} mmHg.

The natural width of the resonance transition between two states, say 1 and 2 is given by

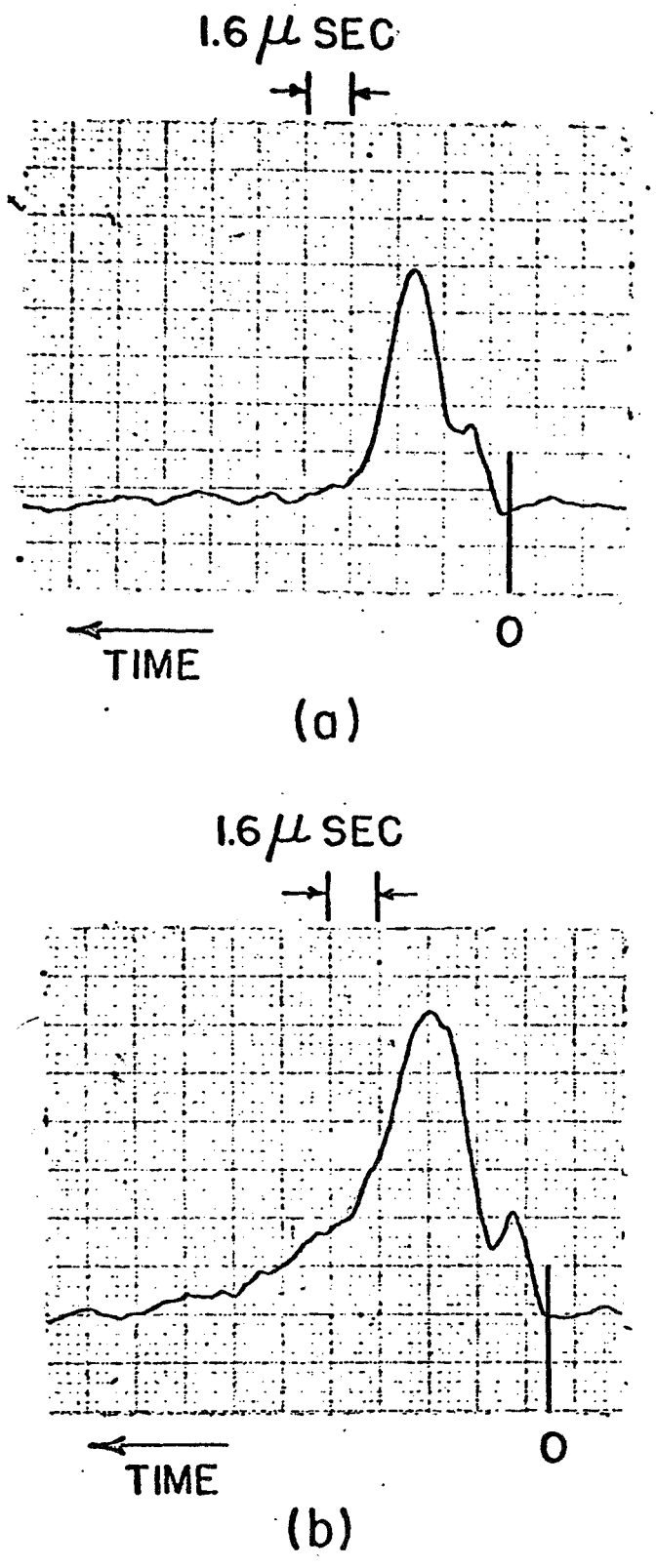

Figure 6.3-2 Sampling Data Obtained with Pulsed Laser Light. (A) Photo-multiplier Output Attributable to Laser Light Scattered in the Apparatus Vs. Time with Molecular Beam Off (B) Photo-multiplier Output with Molecular Beam On, Showing the Decay of the Resonance Fluorescence Signal

$$\Delta B = \frac{1}{2\pi} \left(\frac{1}{\tau_1} + \frac{1}{\tau_2}\right)$$

$$= \frac{1}{2\pi} \left(\sum_j A_{1j} + \sum_k A_{2k}\right)$$

where ΔB is the natural width of the transition; $\sum_j A_{1j}$ is the sum of all the spontaneous transition rates from state 1; $\sum_k A_{2k}$ is the sum of all the spontaneous transition rates from state 2; τ_1 and τ_2 are the lifetimes of state 1 and state 2, respectively. For a ground state transition, the lifetime of the upper state determines the natural width of the resonance line and is given by

$$\Delta B = \frac{1}{2\pi\tau}$$

where τ is the lifetime of the excited state. In this case, τ = 3 μ-seconds which implies that the natural width of the I_2 transitions is

$$\Delta B = \frac{1}{2\pi} \frac{1}{3 \times 10^{-6}} = 50 \text{ kHz}$$

CHAPTER 7

DATA ANALYSIS

7.1 General

The dipole moment matrix element associated with the I_2 transition is calculated by two independent methods. One uses the saturation data and the other uses the lifetime data.

In addition, the fraction of the I_2 molecules that take part in the observed fluorescence is also calculated by two methods. One uses the fluorescence yield at saturation and the other uses the gas cell absorption data.

7.2 Dipole Moment Matrix Element from Saturation Data

The probability of a transition, $P_{1\to2}$, from state 1 to state 2, see Appendix A, is given by

$$P_{(1\to2)} = \frac{8\pi^3}{3h^2c} \mu_{12}^2 I(\nu) t \quad \ldots\ldots\ldots \quad 7.2\text{-}1$$

where μ_{12} is the dipole moment matrix element; $I(\nu)$ is the spectral intensity of the laser and t is the time the molecule spends in the laser radiation field.

At saturation, $P_{(1\to2)} \to 1/2$ and not 1 due to the velocity distribution of the molecules in the beam,[15] so that at saturation equation 7.2-1 becomes

$$\frac{1}{2} = \frac{8\pi^3}{3h^2c} \mu_{12}^2 I(\nu)_{sat} t \quad \ldots\ldots\ldots 7.2\text{-}2$$

An estimate for the laser spectral density $I(\nu)$ is obtained from

$$P_a = \int_0^\infty I(\nu)\, d\nu \simeq I_o(\nu)\, \Delta\nu_\ell$$

where P_a is the laser power per cm^2; $I_o(\nu)$ is the peak laser intensity and $\Delta\nu_\ell$ is the laser spectral width. This gives, approximately,

$$I_o(\nu) \simeq \frac{P_a}{\Delta\nu_\ell}$$

The cross sectional area of the laser beam is $\frac{\pi\ell^2}{4}$ where ℓ is the beam diameter, so that

$$I_o(\nu) = \frac{4P}{\pi\ell^2\, \Delta\nu_\ell} \quad \ldots\ldots 7.2\text{-}3$$

where P is the measured laser power.

The time, t, the I_2 molecule spends in the laser field is

$$t \simeq \frac{\ell}{\bar{v}_b} \qquad 7.2\text{-}4$$

where $\bar{v}_b$ is the average velocity of the molecules in the beam.

Substituting equations 7.2-3 and 7.2-4 into equation 7.2-2, we get

$$\frac{1}{2} = \frac{32\pi^2}{3h^2c} \frac{\mu_{12}^2}{\ell\bar{v}_b} \frac{P_{sat}}{\Delta\nu}$$

where P_{sat} is the cw laser power needed to saturate the I_2

transition. The square of the dipole moment matrix element is then given by

$$\mu_{12}^2 = \frac{3h^2 c \ell \bar{v}_b \, \Delta\nu_\ell}{64\pi^2 P_{sat}} \quad \ldots\ldots 7.2\text{-}5$$

From section 6.2, P_{sat} = 160 μwatts; ℓ = 2.2 mm, $\Delta\nu_\ell\,|_{average}$ = 10.0 MHz; $\bar{v}_b = 1.87 \times 10^4$ cm/sec so that

$$\mu_{12} = 2.7 \times 10^{-19} \text{ e.s.u.}$$

7.3 Dipole Moment Matrix Element from Lifetime Data

The lifetime of the excited state or state 2 is given in equation 4.2-4 as

$$\tau_2 = \frac{1}{\sum_i A_{2i}} = \frac{3hc^3}{64\pi^4 \sum_j \nu_{2j}^3 \mu_{2j}^2} \quad \ldots\ldots 7.3\text{-}1$$

If the ratio of the transition probability from state 2 to state 1 to the total transition probability out of state 2 is α_{21}, then from equation 4.2-2, we have

$$\alpha_{21} = \frac{A_{21}}{\sum_i A_{2i}} = \frac{\nu_{21}^3 \mu_{21}^2}{\sum_i \nu_{2i}^3 \mu_{2i}^2} \quad \ldots\ldots 7.3\text{-}2$$

α_{21} is called the branching ratio. From equations 7.3-1 and 7.3-2, we get

$$A_{21} = \alpha_{21} \sum_i A_{2i} = \frac{\alpha_{21}}{\tau_2}$$

so that the square of the dipole moment matrix element becomes

$$\mu_{21}^2 = \frac{3hc^3}{64\pi^4 \nu_{21}^3} \frac{\alpha_{21}}{\tau_2} \quad \ldots\ldots\ldots\ldots 7.3\text{-}3$$

The lifetime of the excited state, τ_2, has been measured in section 6.3 as 3×10^{-6} seconds.

The branching ratio is defined as

$$\alpha_{21} = \frac{\text{fluorescence at the laser frequency (5145 Å)}}{\text{total fluorescence}}$$

and has to be determined. In order to measure the fluorescence at the laser frequency (5145 Å), a narrow band, 80 Å wide, multi-dielectric transmission filter centered at 5145 Å was placed in front of the S-20 photomultiplier. Since the fluorescence of the excited state is in doublets that correspond to $\Delta J = \pm 1$ transitions, two closely spaced lines fall within the bandwidth of the filter. The measured fluorescence through the filter is therefore twice that at the laser frequency. The photocathode efficiency at 5145 Å is 10%. The total fluorescence which, in this case can extend from 5000 Å - 1.3μ, may be estimated by making two assumptions. One, the fluorescence is uniformly distributed over its entire frequency range and two, that 6/10 of the total fluorescence falls within the bandwidth of the S-20 photomultiplier where the average photocathode efficiency is assumed to be 5%. With the above assumptions, the branching ratio, α_{21}, is found to be 1/14.

Substituting the above value for α_{21} and τ_2 in Equation 7.3-3

we get $\mu_{21} = 1.0 \times 10^{-19}$ e.s.u.

The μ_{21} from the branching ratio and lifetime data is about 4 times smaller than the μ_{21} obtained from the saturation data. The main source of error in Equation 7.2-5 is the instantaneous laser spectral density $P_{sat}/\Delta\nu_{\ell}$ and in Equation 7.3-3 is the branching ratio α_{21}. The magnitude of the instantaneous laser spectral density assumed is a minimum value since the laser is known to display discontinuous jumps in frequency rather than continuous broadening behavior where the instantaneous spectral width can be very narrow. A narrow width would decrease μ_{21} in the direction of the values obtained from the branching ratio. The branching ratio data is also approximate. However, without the knowledge of the spectral distribution of the fluorescence, this is a fair approximation.

The value for μ_{21} obtained from the lifetime data is considered more reliable than that from the beam saturation data so that $\mu_{21} = 1.0 \times 10^{-19}$ e.s.u. will be used in the calculations to follow.

7.4 Fraction of Molecules Taking Part in Transition from Absorption Cell Data

The absorption of light at a frequency ν and intensity $I(\nu)$ through a column of gas of length dx is given by

$$dI(\nu) = -(N_1 W_{12} - N_2 W_{21})\, h\, \nu\, dx \quad . \quad . \quad . \quad . \quad . \quad . \quad 7.4\text{-}1$$

where W_{12} and W_{21} are the transition rates from state 1 to state 2 and from state 2 to state 1, respectively; N_1 and N_2 are the populations in state 1 and state 2.

The transition rate W_{12} is obtained by differentiating the transition probability $P_{(1\to2)}$ given in equation 7.2-1, so that

$$W_{12} = \frac{d}{dt}\left[P_{(1\to2)}\right] = \frac{8\pi^3}{3h^2c}\,\mu_{12}^2\, I(\nu) \quad \ldots\ldots 7.4\text{-}2$$

For a gas that obeys a Boltzman distribution, $N_2 \simeq 0$ at room temperature because of the large energy separation between the ground and excited states, so that equation 7.4-1 becomes

$$\frac{dI(\nu)}{dx} = -N_1 W_{12} h\nu$$

and substituting for W_{12} from equation 7.4-2, we get

$$\frac{dI(\nu)}{dx} = \frac{8\pi^3}{3hc}\, N_1\, \mu_{12}^2\, I(\nu)\nu \quad \ldots\ldots\ldots 7.4\text{-}3$$

Now from equation 6.2-1

$$\frac{dI(\nu)}{dx} = -k_\nu\, I(\nu)$$

therefore,

$$k_\nu = -\frac{dI(\nu)}{dx} \,/\, I(\nu) \quad \ldots\ldots\ldots 7.4\text{-}4$$

Substituting Equation 7.4-2 into 7.4-3, we get the following expression for the absorption coefficient

$$k_\nu = -\frac{8\pi^3}{3hc}\, N_1 \nu\, \mu_{12}^2 \quad \ldots\ldots\ldots 7.4\text{-}5$$

This relationship is not complete since the absorption line of the molecules has a certain lineshape. If $g(\nu - \nu_0)$ is the normalized lineshape function centered at ν_0, then

$$\int_0^\infty g(\nu - \nu_0)d\nu = 1$$

and $W_{12} \rightarrow W_{12}\, g(\nu - \nu_0)$. The lineshape function can then be included in equation 7.4-4 as follows

$$k_\nu = - \frac{8\pi^3\nu}{3hc} N_1 \mu_{12}^2 g(\nu - \nu_0)$$

The integral of the absorption coefficient then becomes

$$\int_0^\infty k_\nu \, d\nu = - \frac{8\pi^3\nu}{3hc} N_1 \mu_{12}^2 \int_0^\infty g(\nu - \nu_o) \, d\nu$$

$$= \frac{8\pi^3\nu}{3hc} N_1 \mu_{12}^2 \quad \ldots\ldots\ldots \quad 7.4\text{-}6$$

Using equation 7.4-5, the population fraction N_1/N_0, where N_0 is the number density of the molecules in the gas cell, can be expressed as

$$\frac{N_1}{N_0} = \frac{3hc}{8\pi^3\nu\mu_{12}^2 N_0} \int_0^\infty k_\nu \, d\nu \quad \ldots\ldots\ldots \quad 7.4\text{-}7$$

The value of the integral of k_ν is obtained from the area under the absorption coefficient vs. frequency curve in Figure 6.1-3. N_0 is determined from the pressure of the I_2

in the absorption cell which is the equilibrium vapor pressure at the temperature of the I_2 reservoir.

Using $\mu_{12} = 1 \times 10^{-19}$ e.s.u. determined from the lifetime data, the population fraction is $\frac{N_1}{N_0} = 2.6 \times 10^{-3}$.

7.5 Fraction of Molecules Taking Part in Transition from Molecular Beam Data

In order to determine the fraction of molecules taking part in the transition from the molecular beam data we have to know (a) the total fluorescence at saturation which corresponds to the number of excited molecules and (b) the density of I_2 molecules in the beam.

At saturation, half the number of the molecules that can partake in the transition are excited. The total number of photons, η_{ph}, emitted in the fluorescence corresponds directly to the number of excited molecules so that the population fraction is given by

$$\frac{N_1}{N_0} = \frac{2\eta_{ph}}{N_0} = \frac{2\,\frac{d\eta_{ph}}{dt}}{\frac{dN_0}{dt}} = \frac{2V_{out}}{G_0\,\frac{dN_0}{dt}} \qquad \ldots\ldots 7.5\text{-}1$$

where N_1 is the number density of the molecules that can partake in the transition; N_0 is the total number density of the molecules in the beam; V_{out} is the amplitude of the output signal of the measuring system; and G_0 is the effective gain of the measuring system.

Since many resonances are observed, V_{out} is the effective output signal if all the I_2 resonances involved are superimposed on each other. Since these resonances are spread out, V_{out} can be determined by dividing the area under the total fluorescence signal at saturation by the dominant width which is that of the laser. The saturated fluorescence data in Figure 6.2-5 for quasi-cw operation is used for this purpose. The laser spectral width in quasi-cw operation is 100 MHz. V_{out} is then given by

$$V_{out} = \frac{\text{area under total fluorescence signal at saturation x duty cycle of quasi-cw supply}}{\text{spectral width of laser}}$$

$$= 1.3 \times 10^{3} \text{ volts}$$

The effective gain of the measuring system G_0 is the product of many terms. The absolute magnitude of these terms are difficult to determine, e.g. collection solid angle, photocathode efficiency, photomultiplier gain, etc. In addition, G_0 includes an assumption that the bandwidth of the fluorescence is uniformly distributed from 5000 Å - 1.3 μ and that the photomultiplier collects 6/10 of the fluorescence with a 5% efficiency. G_0 is estimated to be 1.1×10^{-6} volt/fluorescence photon.

The total number of photons radiated in the fluorescence per second is therefore

$$\frac{d\eta_{ph}}{dt} = \frac{V_{out}}{G_0} = 1.1 \times 10^{9} \text{ photons/sec}$$

The beam strength $\frac{dN_0}{dt}$ can be obtained from the flow rate of molecules into the ion gauge, see Figure 7.5-1. In the steady state, the flow rate of molecules into the ion gauge is equal to the flow rate out of the ion gauge so that

$$\left.\frac{dN}{dt}\right|_{in} = \left.\frac{dN}{dt}\right|_{out} = F_g \cdot \rho_g$$

where F_g is the pumping speed out of the ion gauge and ρ_g is the density of the I_2 in the gauge. $F_g = 1/4\ \bar{v}\ \pi r^2\ 1/k = 1.05 \times 10^4\ cm^3/sec$ where $\bar{v}_g$ is the average velocity of I_2 in the gauge $= 1.6 \times 10^4$ cm/sec; r is the radius of gauge opening = 1.2 cm; 1/k is the pumping speed factor of a long circular cylindrical tube = $8/3\ \frac{r}{\ell} = 0.58$ where ℓ is the length of tube between the bulk of the volume of the gauge and the beam chamber = 5.5 cm. ρ_g = pressure of I_2 in gauge $\times 3 \times 10^{16} = 2.1 \times 10^9$ molec/cm^3.

The flow rate of molecules through the interaction volume is

$$F_g\ \rho_g\ \frac{A_{int}}{A_{beam}} = 3.9 \times 10^{12}\ \text{molec/sec}$$

where A_{beam} is the total cross sectional area of the beam at the interaction region and A_{int} is the cross sectional area of the interaction volume in the direction of the molecular beam.

The calculated value for the beam strength at the interaction region by use of Equation 5.2-3 is 9.4×10^{12} molec/sec.

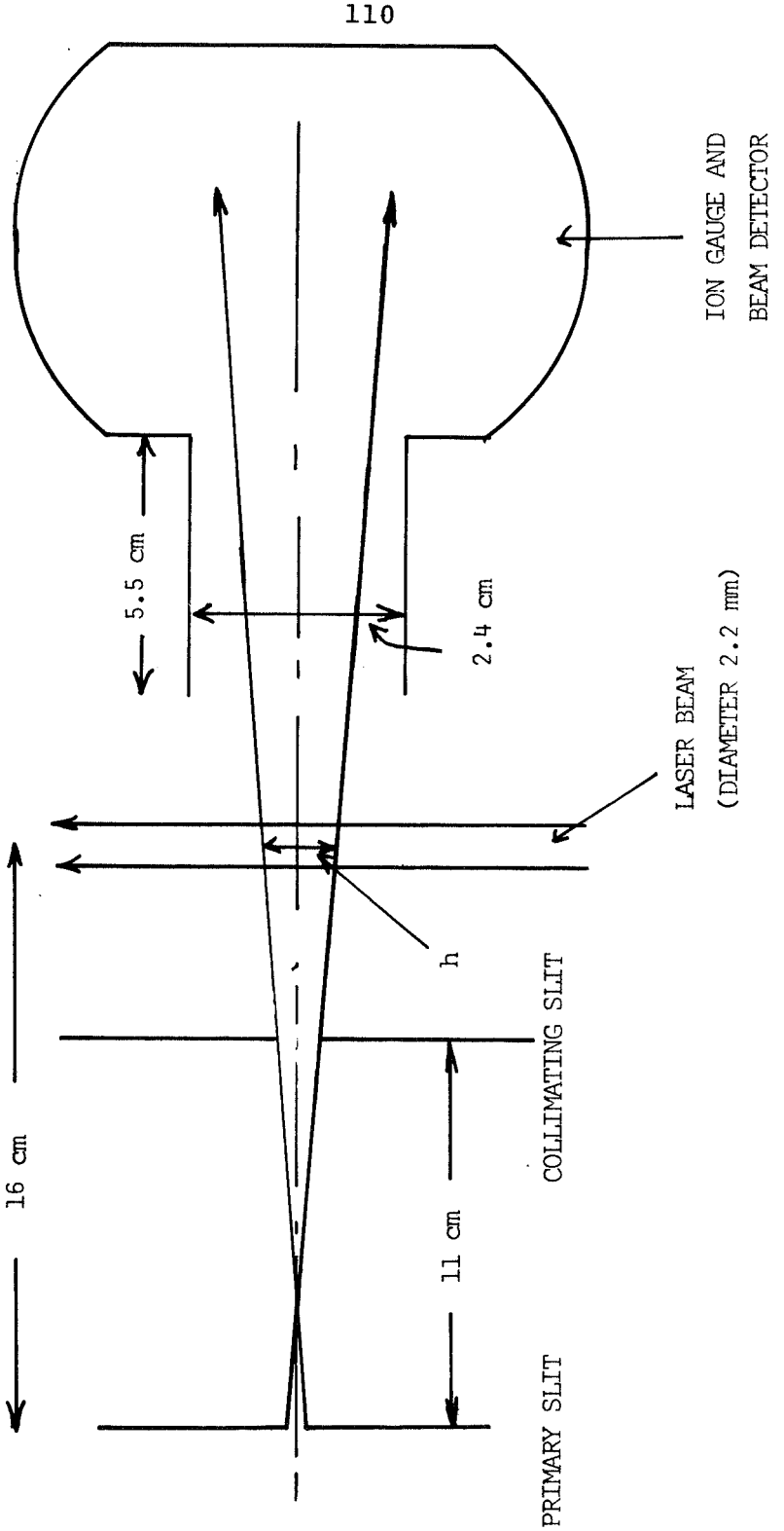

FIGURE 7.5-1 GEOMETRY OF THE INTERACTION AREA AND BEAM DETECTOR

This value is too high because the effusion rate of molecules out of the oven is faster than the evaporation rate of I_2.[48] Consequently, the vapor pressure in the oven is less than the equilibrium vapor pressure associated with the oven temperature. This is supported by the following observations:

(a) When the oven valve is first opened, the ion gauge reading increased to about 4×10^{-7} mmHg and then dropped to its steady value of 1×10^{-7} mmHg and (b) the fluorescence signal was also larger when the oven valve is first opened.

Now substituting in Equation 7.5-1 for $\frac{V_{out}}{G_0} = 1.1 \times 10^9$ photons/sec, $\frac{dN_0}{dt} = 3.9 \times 10^{12}$ molec/sec and allowing a duty factor of 1/2 for the mechanical chopper, we get

$$\frac{N_1}{N_0} = \frac{2\ V_{out}}{G_0\ (1/2\ \frac{dN_0}{dt})} = 1.3 \times 10^{-3}$$

This value of the population fraction is in fair agreement with 2.6×10^{-3} obtained in Section 7.4 using the absorption cell data and μ_{12} from the measured lifetime data.

CHAPTER 8

INTERPRETATION OF OBSERVED I_2 SPECTRUM

8.1 General

An attempt is made, in this chapter, to explain the structure of the resonances observed in the I_2 molecular beam on the basis of

(a) the calculated gross structure of the I_2 spectrum in the region of 19320 cm^{-1} laser line using the available molecular constants,

(b) the estimated hyperfine structure in the I_2 molecule,

(c) the estimated splittings due to the interaction of the I_2 molecule with external fields.

8.2 Calculation of I_2 Spectrum Using Available Molecular Constants

The I_2 spectrum in the region around 19320 cm^{-1} (5145 Å) is calculated by the following expression[29]

$$\begin{aligned}\Delta W = &\Big\{T_e' + w_e'.(v' + 1/2) + (x_e w_e)'.(v' + 1/2)^2 + (y_e w_e)'.\\ &(v + 1/2)^3 + \ + (z_e w_e)'.(v' + 1/2)^4 + (t_e w_e)'.(v' + 1/2)^5 +\\ &\ldots + \left[B_e' - \alpha_e' (v' + 1/2) \ + \ \gamma_e' (v' + 1/2)^2 + \right.\\ &\left.\delta_e' (v' + 1/2)^3 + \ldots\right] \left[J'(J' + 1) + D_e' J'^2 (J' + 1)^2\right]\Big\} +\\ &- \Big\{T_e'' + w_e''.(v'' + 1/2) + (x_e w_e)''.(v'' + 1/2)^2 + (y_e w_e)''.\\ &(v + 1/2)^3 \ + \ (z_e w_e)''.(v'' + 1/2)^4 + (t_e w_e)''.(v'' + 1/2)^5 + \ldots\end{aligned}$$

$$+ \left[B_e'' - \alpha_e''.(v'' + 1/2) + + \gamma_e''.(v'' + 1/2)^2 + \delta_e''.(v'' + 1/2)^3 + \ldots\right] \left[J''(J'' + 1) + D_e'' J''^2 (J'' + 1)^2\right]\Big\} \quad 7.5\text{-}1$$

where Δw is the frequency of the transition in wavenumbers between two electronic states with vibrational quantum numbers v' and v" and rotational quantum numbers J' and J". The molecular constants T_e, w_e, $x_e w_e$, $y_e w_e$, $z_e w_e$, $t_e w_e$, B_e, α_e, γ_e, δ_e and D_e are obtained from references (26) and (27) and are given below

	$X^1\Sigma_{og}^+$ state	$B^3\Pi_{ou}^+$ state
T_e	= 0	15770.59
w_e	= 214.51886	125.273
$x_e w_e$	= - 0.60738	- 0.7016
$y_e w_e$	= -1.307×10^{-3}	- 5.67×10^{-3}
$z_e w_e$	= -5.04×10^{-6}	3.2×10^{-5}
$t_e w_e$	= -1.6×10^{-7}	-
B_e	= 0.037389	0.028969
α_e	= 1.21×10^{-4}	1.5×10^{-4}
γ_e	= 1.9×10^{-8}	- 4.0×10^{-7}
δ_e	= 8.57×10^{-11}	- 3.5×10^{-8}
D_e	= -4.54×10^{-9}	3.5×10^{-9}

The transitions from the three lowest vibrational levels

in the ground state, i.e. v" = 0, 1, 2 with $\Delta J = \pm 1$ that fall within ± 10 cm^{-1} of the 19320 cm^{-1} laser line have been calculated on a computer and are shown in numerical order in Appendix B.

The population of the levels in the ground state depends on the values of v" and J", subject to a Boltzman distribution. The population fraction or partition function F(v",J") is given by [49]

$$F(v'', J'') = (2J''+ 1)\, \frac{hcB''_e}{kT} e^{-\frac{J''(J''+1)\, hcB''_e}{kT}} \left(1 - e^{-\frac{hcW''_e}{kT}}\right) e^{-\frac{v''hcW''_e}{kT}} \qquad 7.5\text{-}2$$

where B''_e is the rotational constant in the ground state; w''_e is the vibrational constant in the ground state; T is the temperature of the enclosure and k is Boltzman's constant. The partition function associated with the ground state of the calculated transitions has been computed and is included in Appendix B.

It should be noted that the molecular constants for the upper electronic state, $B^3\Pi^+_{ou}$ were calculated[27] from the molecular spectrum that extended up to v' = 26. It is almost certain that the extrapolation to v' = 43, the lowest value of v' in the transitions listed in Appendix B, will necessitate the knowledge of the $(w_e t_e)$ anharmonic term which is at present not available. As evidence for this, the last known anharmonic correction term $(z_e w_e)' (v' + 1/2)^4$ contributes 114 cm^{-1} to

the energy separation of the levels at v' = 43. The existing constants are clearly inadequate to explain a spectrum within 0.03 cm^{-1}. However, the molecular constants are not entirely useless, since the relative spacing of the rotational lines within one vibration band given by the constants is probably correct.

8.3 Estimation of the Hyperfine Structure in the I_2 Molecule

The treatment of the spectrum in Section 8.2 neglected the effects due to the interactions of the nuclei with each other as well as with electric and magnetic fields inside the molecule.

8.3.1 Nuclear Spin-Spin Interaction

The nuclear spin-spin interaction between the magnetic dipole of the two nuclei is described by the following Hamiltonian[15]

$$H_{ss} = \frac{1}{R^3} \left| \vec{\mu}_1 \cdot \vec{\mu}_2 - \frac{3(\vec{\mu}_1 \cdot R)(\vec{\mu}_2 \cdot R)}{R^2} \right|$$

where $\vec{\mu}_1$, $\vec{\mu}_2$ are the magnetic moments of the nuclei and R is the distance between the nuclei. An estimate in terms of frequency of the order of magnitude of the splitting due to the nuclear spin-spin interaction $\Delta\nu_{ss}$ is given by

$$\Delta\nu_{ss} \sim \frac{\mu^2}{hR^3} = 1 \text{ kHz}$$

where μ ~ 1 nuclear magneton = 5×10^{-24} ergs/gauss and $R = 10^{-8}$ cm.

The contribution of the nuclear spin-spin interaction is a slight broadening of the order of 1 kHz to the 50 kHz natural linewidth.

8.3.2 Nuclear Spin-Molecular Rotation Interaction

The interaction of the nuclear magnetic moment with the internal molecular magnetic field generated by the molecular rotation is described by the following Hamiltonian[15]

$$H_{IJ} = ChI_R J$$

where C is a constant, characteristic of the molecule; I_R is the total nuclear spin; J is the rotational quantum number. The splitting in each level in terms of frequency as predicted by the Hamiltonian is given by

$$\Delta\nu_{IJ} \sim CI_R J$$

The constant C has not been measured in I_2. However, a conservative estimate for C may be obtained from the following simplified treatment in which one considers the effect of the rotation of one iodine nucleus around the other nucleus. The interaction energy W is given by

$$W = \mu_I \cdot B$$

where μ_I is the nuclear spin magnetic moment of one iodine

nucleus and B is the magnetic field at this nucleus due to the rotation of the other nucleus. The effective charge associated with the rotating nucleus can vary from 0 to one electron charge, depending on the amount of shielding provided by the valence electrons. For our purpose, we shall assume that this effective charge is + e, i.e. there is complete slip between the valence electrons and the nucleus.

The magnetic field B may be calculated from

$$B = \int \frac{i\, d\vec{\ell} \times \vec{r}}{cr^2} = \frac{i\, 2\pi r}{cr^2} = \frac{ew}{cr}$$

where i is the current associated with the rotating charge of + e; r is intermolecular separation and w is the angular velocity of the molecule. The magnitude of w is obtained from the following angular momentum relationship

$$Aw = \sqrt{J(J+1)}\,\hbar$$

where A is the moment of inertia of the molecule which may be expressed in terms of the molecular rotational constant $B_e = \frac{\hbar}{4\pi cA}$. The magnetic field B then becomes

$$B = \frac{4\pi\sqrt{J(J+1)}\,B_e}{r} \simeq \frac{4\pi}{r} J\, B_e$$

The magnetic moment of the iodine nucleus μ_I is $g_I\, I\, \mu_N$ where g_I is the nuclear g-factor, I is the nuclear spin and μ_N is the nuclear magneton. Finally, the interaction energy W may

be re-written as

$$W = \mu_I \cdot B = g_I \, I \, \mu_N \frac{4\pi J \, B_e}{r}$$

Since the roles of the nuclei can be interchanged, the total interaction energy is 2W which corresponds to a frequency splitting

$$\Delta\nu_{IJ} = \frac{2W}{h} = \frac{g_I \, I_R \, \mu_N \, 4\pi \, J \, B_e}{hr}$$

where I_R is the total nuclear spin and the constant C is then given by

$$C = \frac{4\pi \, g_I \, \mu_N \, B_e}{hr} \simeq 15 \text{ Hz}$$

The magnitude of the frequency splitting $\Delta\nu_{IJ}$ for $I_R = 5$ (since I for the iodine atom is 5/2) is $\Delta\nu_{IJ} = 75$ J Hz and for J = 15 this splitting is about 1 kHz. Again this contributes a small broadening to the 50 kHz natural width.

8.3.3 Nuclear Electric Quadrupole Interaction

The interaction of the quadrupole moment of the iodine nuclei with the gradient of the molecular electric field at each nucleus, in a homonuclear diatomic molecule is described by the following Hamiltonian[15]

$$H_Q = \frac{eqQ}{2(2J-1)(2J+3)I_1(2I_1-1)} \left[1-\frac{I_R(I_R+1)+4I_1(I_1+1)}{(2I_R-1)(2I_R+3)}\right]\left[3(\vec{I}_R\cdot\vec{J})^2+\frac{3}{2}(\vec{I}_R\cdot\vec{J}) - \vec{I}_R^{\,2}\,\vec{J}^{\,2}\right] \qquad 8.3.3\text{-}1$$

where q is the electric field gradient at the nucleus due to the electrons; Q is the nuclear electric quadruple moment of the iodine nucleus; I_1 is the spin of each nucleus; I_R is the vector sum of the spins of the nuclei and J is the rotational quantum number.

An evaluation of the matrix elements of the Hamiltonian in an F, m_F, representation[47] gives the energy of the hyperfine structure states as

$$W_{E_2} = \frac{5eqQ}{10I_1(2I_1-1)(2J-1)(2J+3)} \left[1 - \frac{I_R(I_R+1)+4I_1(I_1+1)}{(2I_R-1)(2I_R+3)} \right] \times$$

$$\left[\frac{3}{4} C(C+1) - I_R(I_R+1)J(J+1) \right] \quad \ldots\ldots\ldots \quad 8.3.3\text{-}2$$

where $C = 1/2\ F(F+1) - I_R(I_R+1) - J(J+1)$ and where $\vec{F} = \vec{I}_R + \vec{J}$.

In order to determine the frequency spread of the hyperfine structure associated with an electronic transition, we need to know (a) W_{E_2} for both the $X'\Sigma^+_{og}$ and the $B^3\Pi_{+}_{ou}$ electronic states and (b) the relevant selection rules. For the iodine molecule, $I_1 = 5/2$; $I_R = 5, 4, 3, 2, 1, 0$, $Q = -0.59 \times 10^{-24} cm^2$; but q or eqQ has not been measured in either the $X'\Sigma^+_{og}$ or the $B^3\Pi_{+}_{ou}$ states and they have to be estimated. eqQ in the iodine atom, however, has been measured as -1146.356 MHz.[68]

The eqQ for the $X'\Sigma^+_{og}$ state in I_2 is estimated by the following heuristic argument. The I_2 molecule in the $X'\Sigma^+_{og}$ state dissociates into two iodine atoms in the $P_{3/2}$ state,

i.e. the ground state of the iodine atom. The covalent bonding of the I atoms in I_2 results from the absence of any favored position for the $P_{3/2}$ electrons in the molecule. The $P_{3/2}$ electrons are those atomic electrons which are shared between the two iodine atoms in the molecule. The $P_{3/2}$ electrons are indistinguishable so that, in effect, the electric field at the nuclei is the same as in the atom. eqQ in the I_2 molecule should then be twice the eqQ in the iodine atom.

Some evidence in support of this estimate is obtained from a plot of $\frac{eqQ\ (molecule)}{eqQ\ (atom)}$ as measured in different Halogen Halide molecules versus the electro-negativity difference of the two Halogen atoms in the molecule. The electro-negativity difference is, loosely speaking, related to the difference in time the binding electrons spend near each atom in the molecule. The plot, shown in Figure 8.3.3-1, is approximately a straight line and indicates that at an electro-negativity difference of zero, i.e. for covalent bonds such as that in I_2, the ratio $\frac{eqQ\ (molecule)}{eqQ\ (atom)}$ is approximately one. In other words

$$eqQ(X'\Sigma^+_{0g}\ \text{in}\ I_2) = 2eqQ(I\ \text{atom}) = -2292.7\ \text{MHz}.$$

An estimate for the eqQ in the $B^3\Pi^+_{0u}$ state is made by another heuristic argument. The I_2 molecule in the $B^3\Pi^+_{0u}$ state dissociates into one iodine atom in the $P_{3/2}$ or ground state of the atom and the other iodine atom in the $P_{1/2}$ state

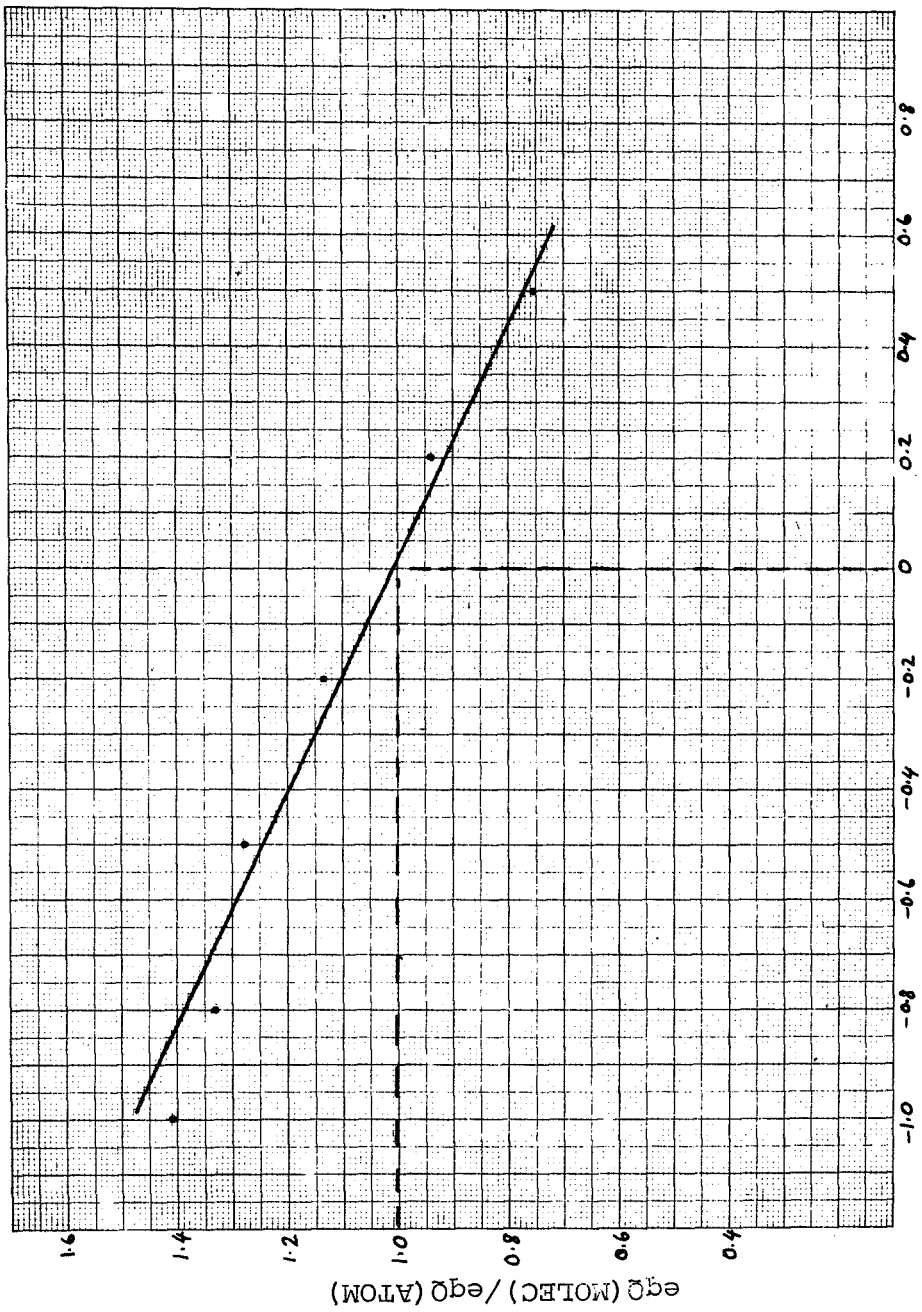

FIGURE 8.3.3-1 A PLOT OF $\frac{eqQ\,(MOLEC)}{eqQ\,(ATOM)}$ VS. ELECTRO-NEGATIVITY DIFFERENCE

ELECTRO-NEGATIVITY DIFFERENCE

which is the first excited state in the atom. Now if we view the bonding electrons in the I_2 molecule as a $P_{3/2}$ and a $P_{1/2}$ electron, the $P_{1/2}$ electron does not contribute any q as discussed in Ramsey.[47] Assuming that these electrons spend equal time in the region of each I atom then, effectively, $q(B^3\Pi_{+}_{ou}$ state) is 1/2 $q(X'\Sigma_{+}_{og}$ state). There may be further reduction in $q(B^3\Pi_{+}_{ou}$ state) due to the fact that the $P_{3/2}$ electron in the molecule may have a larger separation from the nuclei than the $P_{3/2}$ electron in the I atom. An estimate for eqQ ($B^3\Pi_{+}_{ou}$ state) is therefore $0<eqQ(B^3\Pi_{+}_{ou}$ state) < 1/2 eqQ ($X'\Sigma_{+}_{og}$ state).

The selection rules for transitions between the hyperfine structure states in two electronic levels are:

$$\Delta I_R = 0;\ \Delta J = \pm 1;\ \Delta F = 0, \pm 1$$

The $\Delta I_R = 0$ rule is due to the weak coupling of the nuclear spin to the electronic and molecular motion, so that the nuclear spin is unchanged in an electronic transition. The $\Delta J = \pm 1$ selection rule is that discussed in Chapter 4. In addition, not every I_R state can be in every J state. Since the iodine nuclei obey Fermi-Dirac statistics, the total molecular wavefunction must be antisymmetric. This implies that only certain values of I_R can be associated with specific values of J, thus, limiting the number of lines. In Table 8.3.3-1, those states for which the total molecular wavefunction is

antisymmetric are grouped together. The allowed transitions, $\Delta I = 0$, are indicated as well.

$X'\Sigma^+_g$	ψ_e	(symmetric)	$B^3\Pi^+_u$	ψ_e	(antisymmetric)
$J = 0,2,4,..$	ψ_J	(symmetric)	$J = 1,3,5,..$	ψ_J	(antisymmetric)
$I = 0,2,4.$	ψ_I	(antisymmetric)	$I = 0,2,4.$	ψ_I	(antisymmetric)
$X'\Sigma^+_g$	ψ_e	(symmetric)	$B^3\Pi^+_u$	ψ_e	(antisymmetric)
$J = 1,3,5,..$	ψ_e	(antisymmetric)	$J = 0,2,4,..$	ψ_J	(symmetric)
$I = 1,3,5.$	ψ_I	(symmetric)	$I = 1,3,5.$	ψ_I	(symmetric)

Table 8.3.3-1 - Allowed Transitions

A complete calculation of the molecular spectrum due to a quadrupole interaction has been carried out for:

$$eqQ(X'\Sigma^+_g) = -2292.7 \text{ MHz}$$

$$eqQ(B^3\Pi^+_u) = 0 \text{ and } -2292.7 \text{ MHz}$$

$$J = 0 \rightarrow 20$$

In addition, the relative strengths of the quadrupole transitions have been computed. The general expressions for the strengths of transitions between $J \rightarrow J-1$ are given

below[49]

$$F \to F-1: \quad \frac{B(J + F + I + 1)(J + F + I)(J + F - I)(J + F - I - 1)}{F}$$

$$F \to F: \quad \frac{B(J + F + I + 1)(J + F - I)(J - F + I)(J - F - I - 1)(2F + 1)}{F(F + 1)}$$

$$F \to F+1: \quad \frac{B(J - F + I)(J - F + I - 1)(J - F - I - 1)(J - F - I - 2)}{(F + 1)}$$

Typical splittings and their relative strengths are shown in Figure 8.3.3-2.

8.4 External Field Dependence of I_2 Transitions

The interaction of the I_2 molecule with an external magnetic field includes terms that have linear and also quadratic field dependence.

The linear field dependence arises from

(a) an interaction of the external magnetic field with the nuclear spin magnetic moment μ_I. This contributes a frequency splitting $\Delta\nu_I$ given by

$$\Delta\nu_I \sim \frac{\mu_I H}{h}$$

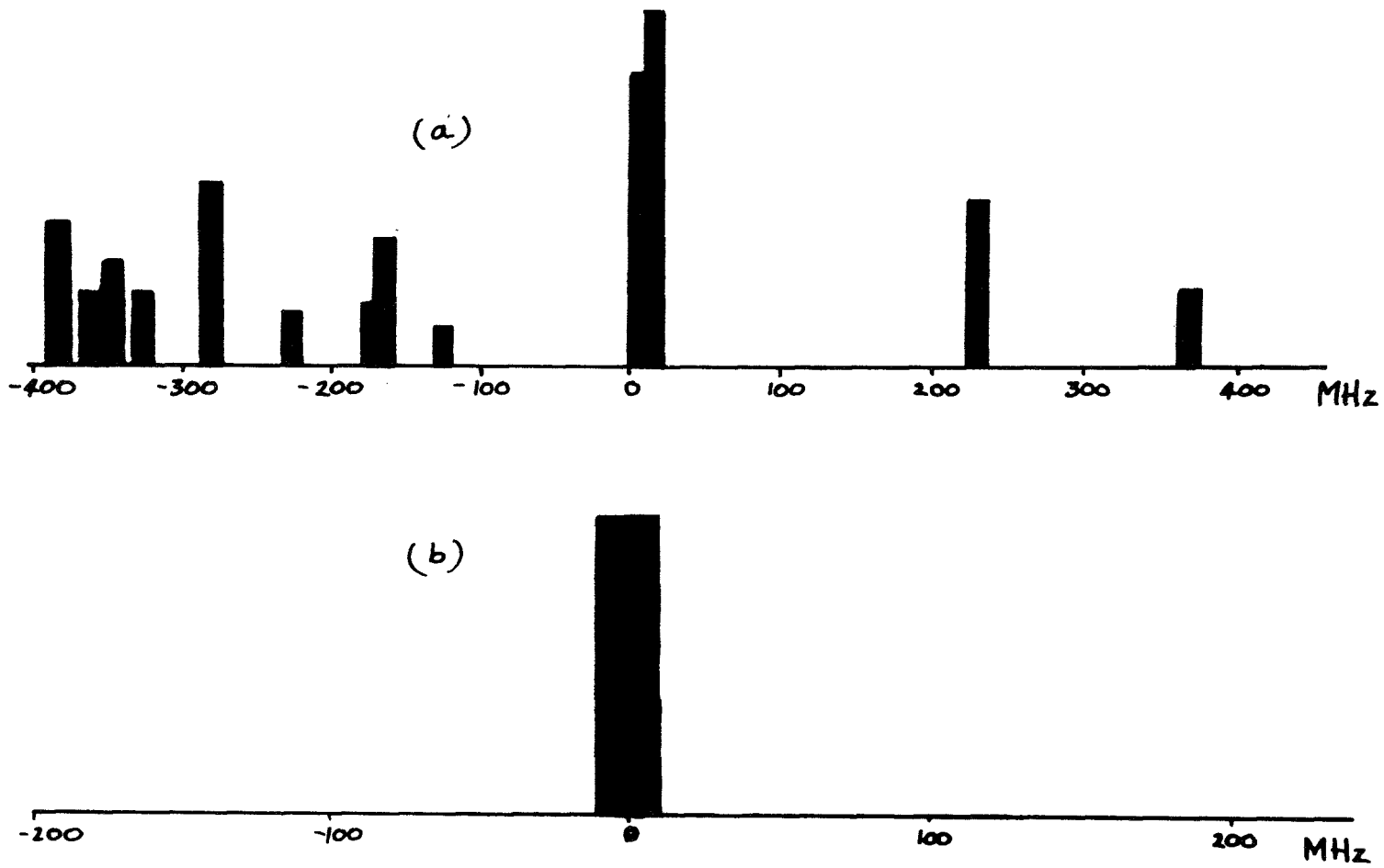

Figure 8.3.3-2 TYPICAL CALCULATED QUADRUPOLE SPLITTINGS

(a) For J" = 9 → J' = 8; eqQ(X' $\Sigma_{g^+_g}$) = -2290 MH_z; eqQ(B $^3\Pi_{0^+_u}$) = 0

(b) For J" = 9 → J' = 8; eqQ(X' $\Sigma_{\quad}$) = -2290 MH_z; eqQ(B $^3\Pi_{0^+_u}$) = -2290 MH_z

Spectral width of every quadrupole transition is assumed to be 10 MH_z, similar to that expected in the experiment

where H is the external magnetic field. For H ≃ 1 gauss, like the earth's field and μ_I assumed to be a full nuclear magneton $\mu_N = 5 \times 10^{-24}$ ergs/gauss, then $\Delta\nu_I \sim 1$ kHz.

(b) an interaction of the external magnetic field with the molecular rotation magnetic moment μ_J. A conservative estimate for μ_J may be made if we assume complete slip between the Iodine nuclei and the valence electrons as mentioned in Section 8.3.2. The magnetic moment due to the rotation of the nuclei with an effective charge +e is

$$\mu_J = \frac{2i\pi r_o^2}{c} = \frac{2er_o w\ \pi r_o^2}{c\ 2\pi r_o} = \frac{e}{c}\, r_o^2 w$$

where r_o is half the internuclear separation and w is the angular velocity of the molecule. The angular velocity w is obtained from the angular momentum relationship

$$Mr_o^2 w = \sqrt{J(J+1)}\ \hbar \simeq J\hbar$$

where M is the mass of the molecule. The molecular rotation magnetic moment then becomes

$$\mu_J = \frac{eJ\hbar}{Mc}$$

This expression may be written in terms of a nuclear magneton $\mu_N = \frac{e}{2m_p c}$ where m_p is the mass of a proton so that

$$\mu_J = 2\frac{m_p}{M}\ \mu_N\ J$$

The frequency splitting $\Delta\nu_J$ due to the molecular magnetic moment is

$$\Delta\nu_J = \frac{\mu_J H}{h} = 2\,\frac{m_p}{M}\,\mu_N\,JH$$

For H = 1 gauss, J = 15, $\Delta\nu_J \sim 120$ Hz.

There is no interaction with the electrons since the electron magnetic moment is zero.

The quadratic field dependence arises form the interaction of the induced magnetic moment with the external magnetic field. The induced magnetic moment depends on H, hence the quadratic field dependence. The molecular magnetic polarizability or diamagnetic susceptibility is of order $\frac{e^2a^2}{Mc^2}$ (15) where a is the molecular diameter and M is the mass of the molecule. The induced magnetic moment is then $\frac{e^2a^2}{Mc^2}$ H and the interaction with the external field contributes a frequency splitting $\Delta\nu_{im}$ given by

$$\Delta\nu_{im} = \frac{e^2a^2}{hMc^2}\,H^2 \simeq 10^{-7}\text{Hz}$$

for H = 1 gauss.

The interaction of the I_2 molecule with an external electric field involves only terms that have quadratic field dependence. There is no linear field dependence because there is no first order perturbation energy. Since there is no permanent molecular dipole moment, the only contribution to

the quadratic field dependence is from the induced electric dipole moment. The molecular electric polarizability goes like the volume of the molecule and is of order a^3. This contributes a frequency splitting $\Delta\nu_p$ given by

$$\Delta\nu_p \sim \frac{a^3}{h} E^2$$

where E is the external electric field. For E = 1 volt/cm, $\Delta\nu_p$ is 5×10^{-3} Hz.

8.5 Interpretation of Observed Spectrum

In this section an attempt is made to explain the observed spectrum. The relevant experimental data may be summarized as follows:

(a) The frequency distribution of the observed resonances is shown in Figure 6.2-3.

(b) Several resonances have a width of 22 MHz while others have a width of 100-150 MHz. Since the dominant width in the apparatus can be as much as 20 MHz, this implies that the narrow resonances observed are probably due to single transitions while the broader transitions are due to several closely spaced lines which are not resolved.

(c) The fraction of molecules in the interaction volume that partake in the observed spectrum is measured as 2×10^{-3}.

(d) In Section 4.2, it is pointed out that only the three lowest vibrational levels in the ground state, namely v" = 0,1,2

can be involved. The v" = 2 level has been eliminated because of the apparent absence of anti-Stokes fluorescence at 5050 Å which was established by placing a narrow band transmission filter centered at 5050 Å in front of the photomultiplier. Anti-Stokes fluorescence at 5050 Å is the fluorescence that terminates on the v" = 0 level as a result of a laser induced transition out of the v" = 2 level in the ground state. This conclusion, however, is not valid if the overlap integral, $\int \psi_{v}' \psi_{v}'' \, dr$ for the upper vibrational level v' and the lower vibrational level v" = 0, is zero.

In addition, the estimates made in this chapter for the splittings of the lines show that the molecular electric quadrupole interaction with the assumed values for eqQ contributes the largest splitting. The quadrupole splitting may be as large as 800 MHz while the splitting due to the other interactions considered is of the order of 1 kHz.

Let us now examine the I_2 transitions in Appendix B, which have been calculated with the presently available molecular constants, that fall near the laser frequency as shown in Figure 8.5-1. The closest transition to the laser frequency is that between v" = 0, J" = 13 and v' = 43, J' = 12 and is only 0.004 cm^{-1} or 140 MHz away. The partition function for the lower level of this transition is 3×10^{-3} which is in agreement with the measured fraction of molecules that partake

in the observed spectrum.

The estimated quadrupole splittings associated with this transition may be large enough to explain the total frequency spread of the observed resonances. However, the calculated splittings are not as numerous or as closely spaced to explain the observed spectrum.

Furthermore, the calculated spectrum shows several other transitions in the vicinity of the laser frequency as indicated in Figure 8.5-1. The frequency distribution of these transitions, with or without quadrupole splittings do not in any way resemble the observed spectrum.

As anticipated in Section 8.2, the presently available I_2 spectrum is not adequate to identify the I_2 transitions that fall within the laser gain curve. However, a general examination of the calculated spectrum within ± 10 cm^{-1} of the laser frequency does indicate that it is highly unlikely to have a cluster of many transitions in a bandwidth of 1300 MHz. This implies that the quadrupole splittings are partly responsible for the closely spaced structure observed.

In order to make a better attempt at identifying the transitions involved, it is clear that more reliable molecular constants are needed for the $B^3\Pi_{0_u^+}$ state. This would establish more precisely the relative spacing between the presently calculated vibration bands to determine which transitions fall within the laser gain curve. The relative spacing between the rotation levels in the same vibration band has already

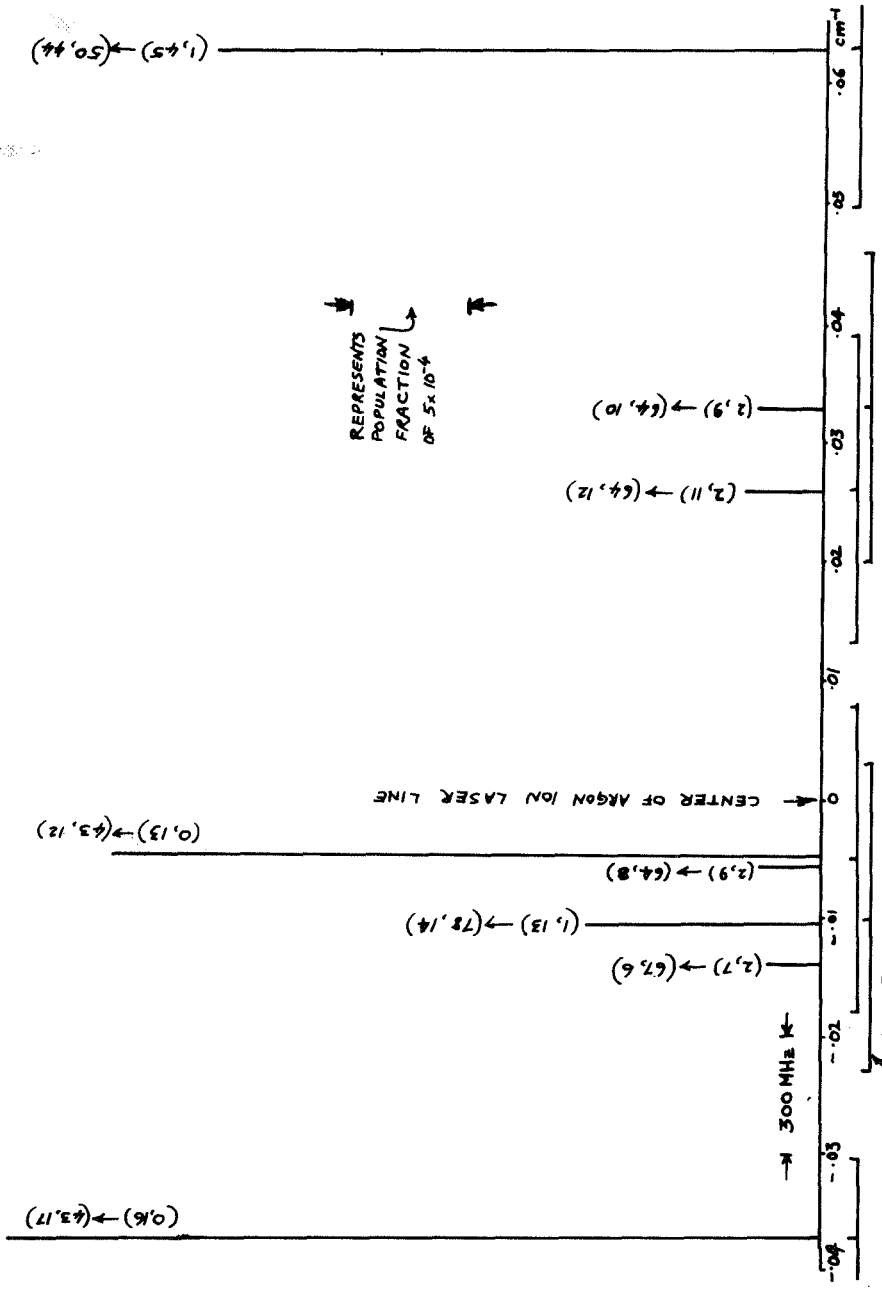

Figure 8.5-1 Calculated I_2 Spectrum Near 5145 Å Argon Laser

been shown to be sufficiently accurate with the present data.

Aside from better molecular constants, it may be possible to identify the I_2 transitions by superposing the 5145 Å laser line over the I_2 absorption spectrum in a high resolution spectrometer. This being pursued at present by Professor Steinfeld.[67]

A method for establishing the rotational levels of the observed transitions is to examine the external field dependence, i.e. the splittings of the transitions in an external magnetic field. However, this only becomes feasible when the laser width is narrowed down to less that 100 kHz and when the laser drift is small.

CHAPTER 9

PROPOSED STABILIZATION OF 5145 Å ARGON LASER

9.1 General

In this chapter, a preliminary scheme is proposed for the stabilization of the 5145 Å argon laser that incorporates the molecular beam of iodine as a long term reference.

The major unknown, at present, is the short term stability of the free running argon ion laser. Very little information has appeared in the literature concerning the plasma noise and plasma oscillations in a constricted ionized argon discharge. Several causes of frequency fluctuations in the argon laser are briefly analyzed in a discussion on short term frequency stabilization.

The principal sources of line broadening and line shifts of the iodine resonance as observed in a molecular beam are examined.

Finally, several applications of long term stable lasers are suggested.

9.2 Outline of Proposed Stabilization Scheme

The proposed scheme to stabilize the frequency of the 5145 Å argon ion laser is shown in block diagram form in Figure 9.2-1. The scheme consists of two major feedback loops. The first is

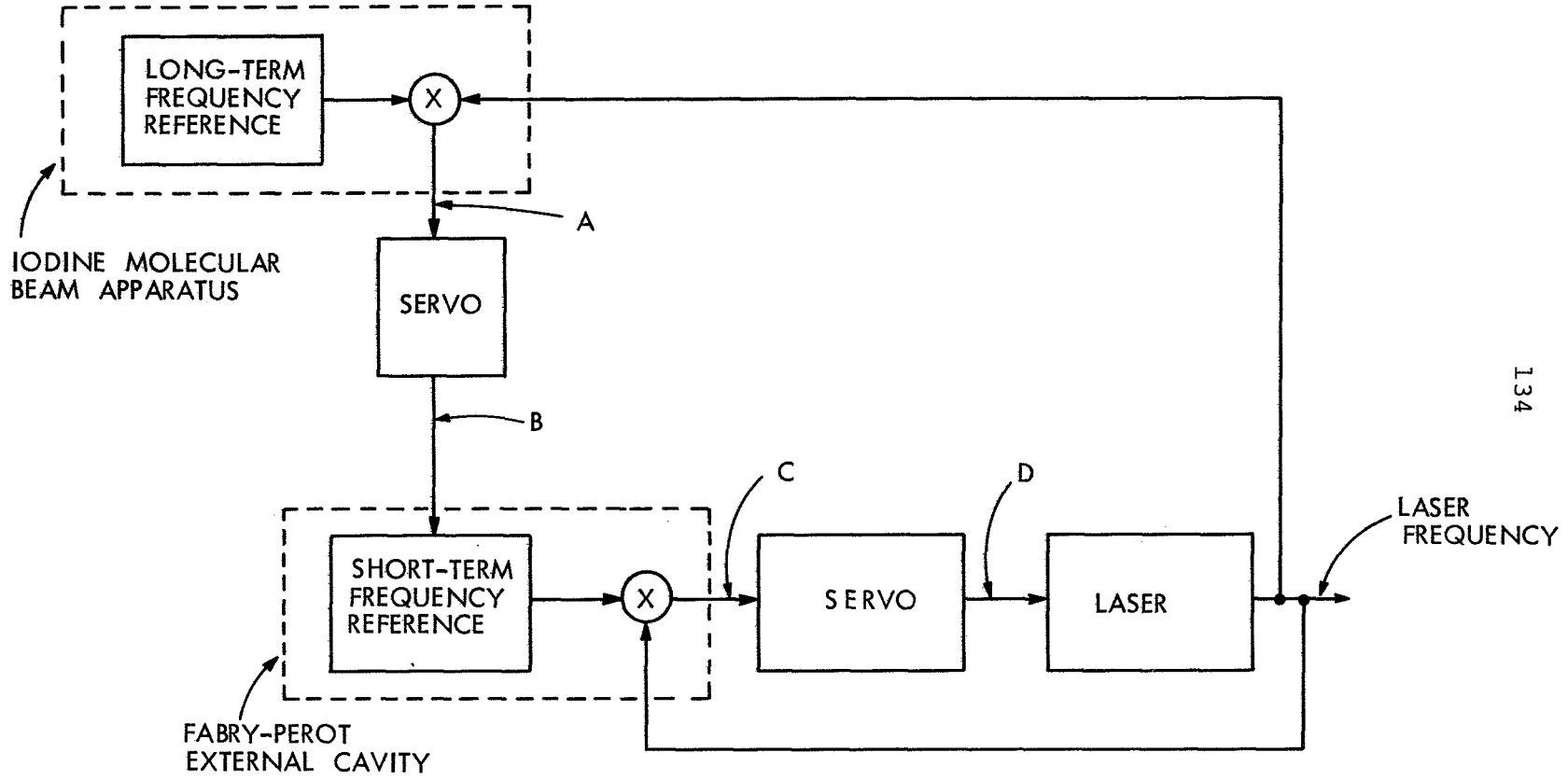

FIGURE 9.2-1 BLOCK DIAGRAM OF STABILIZATION SCHEME

(A) FREQUENCY DIFFERENCE BETWEEN LASER AND IODINE RESONANCE
(B) SIGNAL TO ADJUST THE LENGTH OF THE FABRY-PEROT CAVITY
(C) FREQUENCY DIFFERENCE BETWEEN LASER AND FABRY-PEROT TRANSMISSION RESONANCE
(D) SIGNAL TO ADJUST THE OPTICAL PATH LENGTH OF THE LASER CAVITY

a fast loop to compensate for the short term drifts of the laser frequency by using a transmission resonance of an external Fabry-Perot interferometer as a short term reference. The second is a comparatively slow loop, with a time constant of the order of a second, to control the long term drift of the short term reference. The center frequency of one of the iodine resonance lines observed in a molecular beam is used as the long term reference.

Since the molecular beam is a primary frequency reference, the resettability of the laser frequency should be approximately the same as the long term stability.

The slow response of the molecular beam reference is due to the small number of fluorescence photons that are available. The number of fluorescence photons is limited by the necessarily low density of molecules in the beam. At best an integration time of the order of a second is needed, for example, to obtain an adequate signal-to-noise ratio to detect a shift of about 300 Hz from the center of the 50 kHz wide molecular resonance, which corresponds to $\Delta\nu/\nu = 5 \times 10^{-13}$, as will be discussed in section 9.4. A fast response feedback loop that employs, for example, a Fabry-Perot interometer as a reference must therefore be incorporated to control the laser short term stability.

The signal to noise ratio that can be obtained with a stable Fabry-Perot interferometer depends on the intensity in

the laser beam. For a beam intensity of 10 mWatts and a Fabry-Perot resonance width of 3 MHz,[10] it should be possible to detect a shift of 300 Hz in less than 10^{-6} seconds. This estimate is based on Equation 9.4-3 in the section 9.4 and assumes a 10% peak transmission through the cavity, a 10% photodetector efficiency and that Pcisson noise is the dominant noise source. The cavity has to be carefully designed and well shielded from thermal, vibrational and acoustical disturbances.[10] Moreover, the fluctuation in the intensity of the laser light during a typical integration period must be less than the Poisson noise associated with light beam.

The basic operation of the two feedback loop stabilization scheme is shown in a schematic diagram in Figure 9.2-2. Light from a single longitudinal mode laser is passed through a stable Fabry-Perot interferometer that has an inherent width of less than 10 MHz and is detected on a photodetector. The resonance frequency of the Fabry-Perot interferometer is modulated and the output of the photodetector, after phase sensitive demodulation, is used in a fast feedback loop to adjust the length of the long laser cavity so as to maintain the laser frequency at the center of the Fabry-Perot resonance. In this way, the laser frequency is not subjected to any modulation which introduce undesirable sidebands at the laser frequency. The modulation of the resonance frequency of the

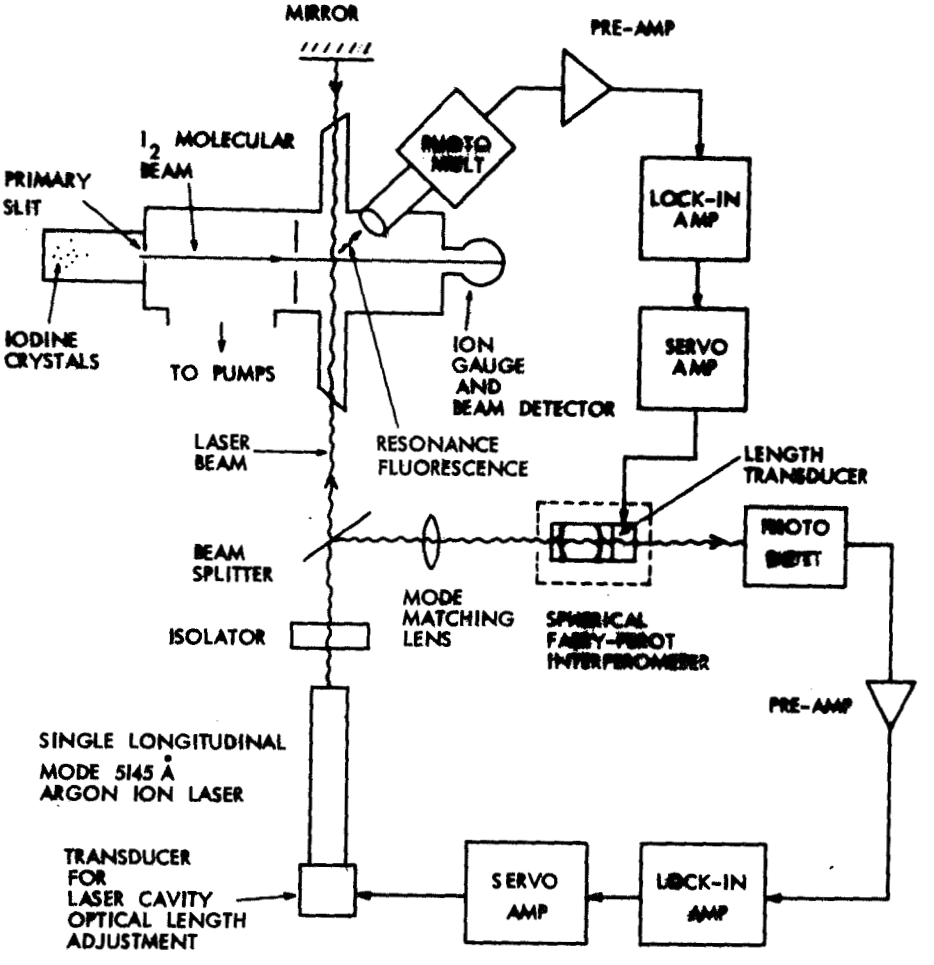

Figure 9.2-2 Schematic Diagram of Stabilization Scheme

Fabry-Perot cavity may be achieved by varying the length of the cavity piezo-electrically[10] or magneto-strictively. Alternatively, external FM modulation[50] of the laser frequency may be considered.

Drifts of the short cavity in the single-mode laser configuration cause amplitude variations in the laser output. Therefore, the length of the laser short cavity has to be controlled by an auxiliary feedback loop to ensure that the laser power output is always at its peak value. The phase sensitive signal may be obtained in this case by modulating the length of the short cavity which is not expected to have a first order effect on the laser frequency. However, the coupling effects in the single mode laser have not been examined in detail. For better stability, the three mirror short cavity can be made out of a solid quatrz prism which is coated on all sides, as described by Johnson and Rigrod.[42] The tuning of this short cavity can be carried out in this case by varying the temperature of the prism, since the response of this auxiliary loop need not be fast.

For the long-term stabilization and the setting of the laser frequency, a fraction of the laser light is passed through a molecular beam of iodine at right angles. The resonance fluorescence of the iodine, induced when the laser frequency falls within approximately the natural width of a selected iodine resonance line, is detected on a photomultiplier.

Maximum fluorescence is obtained when the laser frequency coincides with the peak of the iodine resonance line. Any deviation of the laser frequency from this reference is detected by a phase sensitive demodulation scheme. The resulting signal is used in a feedback loop to adjust the length of the Fabry-Perot cavity so that the center of the cavity resonance is tuned to the center of the iodine resonance. In this way, the laser frequency becomes the center frequency of the selected iodine resonance line. Again, to avoid modulating the laser frequency, direct modulation of the resonance frequency of the iodine transition by Stark or Zeeman effects may be considered. Another possibility, is the use of an external FM laser frequency modulator[50] which has been previously mentioned.

Feedback stabilization schemes are bandwidth limited. This implies that laser frequency fluctuations that are outside the bandwidth of the fast servo loop cannot be controlled. It is therefore essential to start off with a laser that is as stable as possible in free running operation, in particular, with regards to high frequency noise. The smaller the servo bandwidth required, the easier is the servo design.

The factors that generally influence the speed of response in the fast feedback loop are the signal to noise ratio in the frequency discriminator and the frequency response of the control elements.

The control element in the feedback loop that has the slowest response is the transducer that is used for tuning the length of the laser cavity. Normally, the length transducer is a piezo-electric crystal which holds one of the laser mirrors. The frequency response of such a mirror-piezo-electric crystal combination is typically several kHz. Smith[38] achieved 40 kHz with a 1/2 inch diameter by 1/2 inch long crystal and a 1/2 inch diameter by 1 mm thick mirror. Techniques for tuning the laser frequency more rapidly have to be investigated in order to extend the bandwidth of the servo. Based on the analysis in Section 9.3.1, it is perhaps worthwhile to exploit the variation of the refractive index of the discharge medium with discharge current as a means of achieving fast small changes in the optical length of the laser cavity.

An additional and perhaps a more significant restriction on the servo bandwidth is the fact that the modulation frequency discriminator must be at least 10 times greater than the servo bandwidth to allow for adequate filtering of the modulation frequency. If piezo-electric modulators are employed, the modulation frequency is limited to 50 kHz[10] which restricts the bandwidth of the servo to about 5 kHz. The investigation of other techniques for faster frequency modulation is very worthwhile.

A simplified version of the servo loop is shown in Figure

9.2-3, where the components with the dominant time constants are considered and those components with shorter time constants are left out. The laser itself is represented by a pure gain A_1 and the sources of laser frequency fluctuations are represented by the disturbance input $U_1(s)$; $G_2(s)$ is the transfer function of the laser length adjustment transducer which is a second order function for a piezo-electric crystal; $G_4(s)$ is a first order lag which corresponds to the integration time in the Fabry-Perot frequency discriminator. The Fabry-Perot interferometer, just like the laser, is represented by a pure gain A_5 with a disturbance input $U_2(s)$ due to thermal and mechanical sources. In the short term loop, the transfer functions that have been left out include those associated with the photodetector and the amplifiers. In addition, since the modulation frequency has to be higher than the bandwidth of the servo to achieve adequate filtering of the fundamental and harmonics of the modulation frequency, the modulation and subsequent demodulation processes are left out in this simplified representation.

In the long term loop, the dominant time constant is about one second which is associated with the integration time in the molecular beam frequency discriminator (G_7). The transfer functions of the Fabry-Perot length transducer, the photomultiplier, as well as the modulation and demodulation processes are ignored.

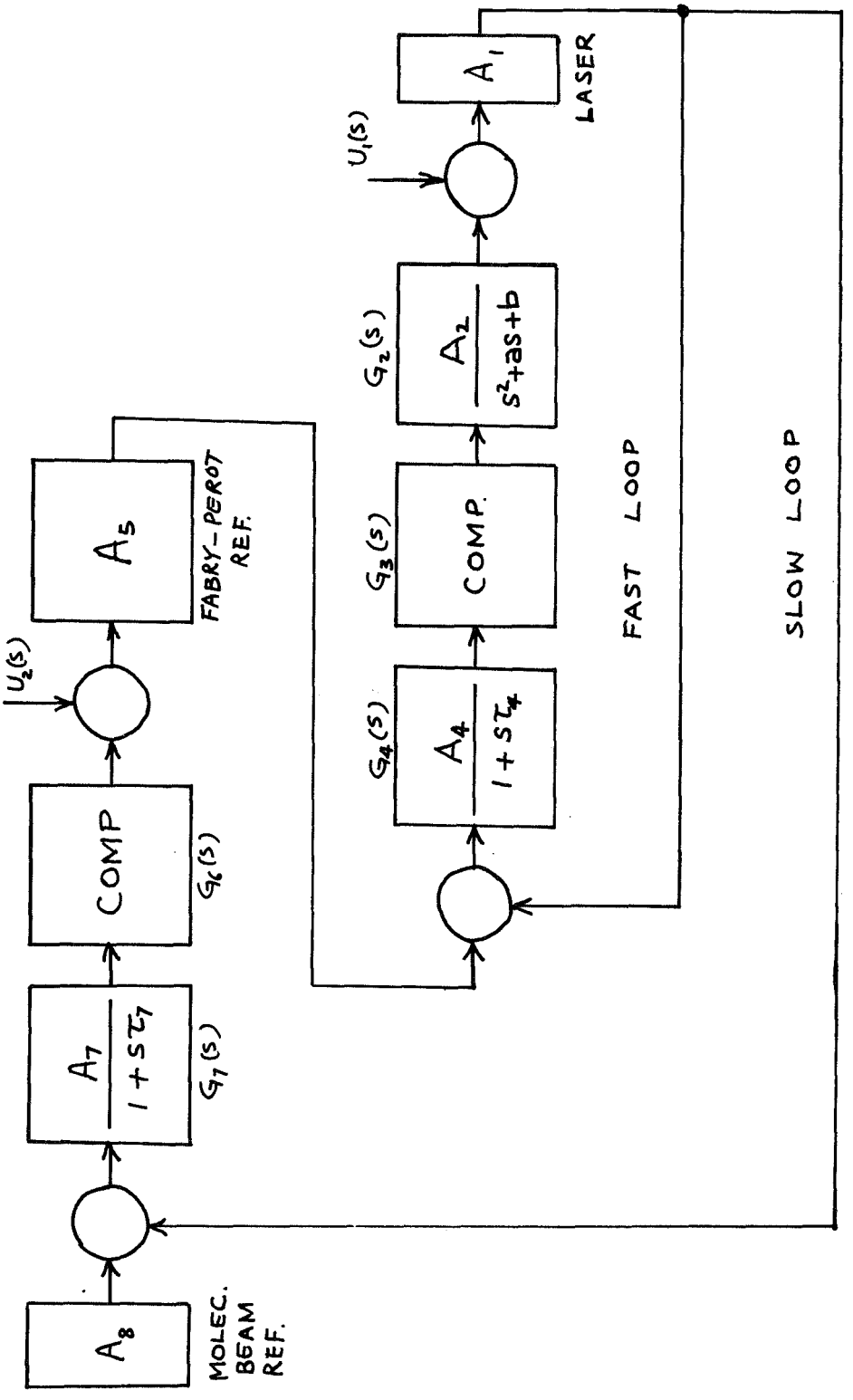

FIGURE 9.2-3 SIMPLIFIED LOOP DIAGRAM OF SERVO

Compensation networks $G_3(s)$ and $G_6(s)$ are needed to ensure that the loop remains stable with as wide a bandwidth as possible and also to boost the low frequency open loop gain to reduce static errors. The major unknowns at present are the magnitude and frequency range of $U_1(s)$ which can appreciably influence the performance requirements of the fast feedback loop. Sources of laser frequency fluctuation are discussed in the next section.

The design and performance of a control system for the He-Ne laser in which a Fabry-Perot cavity is used as a short term reference and an absorption line in a neon gas discharge is used as the long term reference has been discussed by White.[10] The bandwidth of the servo achieved by White was about 10 kHz and the open loop gain was 50 dB at 0.1 Hz and 25 dB from 1 to 10^3 Hz.

The proposed control system in this chapter is similar to that of White but offers the following advantages:

(a) the higher optical power of the argon ion laser increases the signal-to-noise ratio in the Fabry-Perot frequency discriminator

(b) the use of the discharge current to vary the refractive index of the lasing medium may prove to be an effective fast laser frequency control element

(c) the integration time associated with the molecular beam reference is about 100 times shorter than that associated

with the absorption cell reference used by White.

The proposed stabilization scheme should in principle be capable of holding the laser frequency to several parts in 10^{13} for an indefinite period of time. This is based on the capability of the molecular beam reference, as will be discussed in section 9.4 and on the assumption that the laser can be short-term stabilized to a few parts in 10^{13} for a period of the order of a second.

9.3 Discussion on the Short Term Frequency Stability of the Free Running Argon Ion Laser

The short term fluctuations and the short term drift of the laser frequency have been studied by Jaseja, Javan and Townes,[2] (1.15 μ He-Ne laser), by Siegman, Benedetto Daino and Manes,[51] (6328 Å He-Ne laser), and by Freed,[52] (CO_2 laser). The best frequency stability data was reported by Jaseja, et al, who claimed a short term laser spectral width of 8 parts in 10^{14} for less than a second and a short term drift of one part on 10^{13} per second.

Unfortunately, data concerning the short term frequency stability of the free running argon ion laser, which is of major concern in the proposed stabilization scheme, have not appeared in the literature; the investigation of the argon ion laser short term stability is considered outside the scope of this thesis.

9.3.1 Sources of Laser Frequency Fluctuations

The fluctuations in the frequency of the single longitudinal argon ion laser are generally caused by mechanical and thermal effects and also by the variation in the refractive index of the lasing medium. Most of these noise sources have been studied in connection with other types of gas lasers.

Techniques for vibration and acoustical isolation are discussed in references (2, 51, 52). In the case of the argon ion laser, additional sources of mechanical noise exist, such as the flow of water around the discharge tube and the forced air for cooling the cathode and anode. New discharge tube designs are becoming available where both the water and the forced air cooling may be dispensed with.

Because of the relatively high power dissipation in the ionized discharge, the argon laser tube runs hotter than in low current lasers. However, the variation of the length of the cavity due to thermal effects is expected to be slow with typical thermal time constants.

The variation in the refractive index of the laser gain medium changes the frequency of the laser according to the following relationship

$$\left|\frac{\Delta\nu}{\nu}\right| = \left|\frac{\Delta L_{opt}}{L_{opt}}\right| = \left|\frac{\Delta n}{n}\right| + \left|\frac{\Delta L}{L}\right| \quad \ldots\ldots 9.3.1\text{-}1$$

where ν is the laser frequency; L_{opt} is the optical length of the laser cavity; L is the physical length of the cavity and n is the refractive index of the laser medium which is assumed to fill the entire cavity. There are several effects that contribute to the value of n so that

$$n = 1 + n_1 + n_2 + n_3 + n_4 \ldots\ldots \quad 9.3.1\text{-}2$$

and the fractional change in n is then given by

$$\frac{\Delta n}{n} = \frac{\Delta n_1}{n} + \frac{\Delta n_2}{n} + \frac{\Delta n_3}{n} + \frac{\Delta n_4}{n}$$

where:

n_1 is the contribution from the anomalous dispersion of the gain medium. It is zero at the center of the atomic resonance and has opposite sign on either side of center. At any one frequency, the magnitude of n_1 is proportional to the population inversion. n_1 can have a range of values up to about 1×10^{-4} which depends on both the population inversion and the separation between the laser frequency and the center of the atomic resonance. Variations in n_1 are expected to be similar to those in other lasers that are operated at the same laser power and gas pressure.

n_2 is the contribution of the neutral gas which depends on the gas density. For an argon pressure of 1 mmHg, n_2 is about 3×10^{-7}. Again this effect is similar to that in other

lasers.

n_3 is the contribution due to the density of charged particles in the plasma. The magnitude of n_3 is approximately given by $n_3 \sim (\frac{f_e}{\nu_0})^2$ where f_e is the electron plasma frequency and ν_0 is the laser frequency. For typical electron densities of 10^{14} electrons per cm^3, $f_e = 3 \times 10^{11}$ Hz so that at the laser frequency of 5.9×10^{14} Hz, $n_3 \sim \frac{3 \times 10^{11}}{5.8 \times 10^{14}}$ i.e. $n_3 \simeq 2.5 \times 10^{-7}$. The effect of the ions is smaller by the ratio of the electron mass to the ion mass and this factor is $\sim 10^{-5}$ for the argon ion. The effect of n_3 is obviously larger in the argon ion laser than in low current discharge lasers. For example, for $n_3 = 3 \times 10^{-7}$, the discharge current must be held to one part in 10^6 in order that the effect of Δn_3 on the laser frequency is less than 5 parts in 10^{13}. The fractional fluctuation in the discharge current due to Poisson noise only should be smaller in the argon ion laser because of the higher discharge current.

n_4 is the contribution due to plasma acoustical oscillations which are cooperative phenomena that involve a large number of charged particles. The characteristics of these plasma oscillations have been studied in helium-neon lasers by Belisio, Freed and Haus[54] and, also, by Prescott and Van der Ziel.[55] In a d.c. operated He-Ne discharge, the threshold for the onset of plasma oscillations depends on the dimensions of the discharge tube, the gas pressure and the value of the discharge current. The frequency spectrum of the oscillations

appears to extend up to about 100 kHz.[56] In r-f discharges where the driving frequency is in the tens of megacycles, plasma oscillations seem to be absent. Although it has been indicated that plasma acoustical oscillations may not exist in d.c. operated ionized noble gas lasers due to the positive resistance characteristic of the discharge at high currents, quantitative data are not available. In addition it has also been claimed that rf operated argon ion discharges did not exhibit any plasma oscillations.[57]

Other types of plasma oscillations may be caused by plasma instabilities due to magnetic field effects associated with the high density of charged particles and also due to the external magnetic field.

The major contributions to the short term laser spectral width are expected to come from the rapid changes in the refractive index due to plasma oscillations and current density fluctuations. The other noise sources mentioned above tend to contribute to the short term wandering of the laser frequency rather than to the spectral width.

It is clear that a thorough study has to be made of the constricted argon ion discharge as to inherent instabilities, as well as the effects of external magnetic fields, the parameters in the external circuit, gas pressure, current density, etc., before a serious attempt is made at stabilizing the argon ion laser. This may involve trying out new discharge tube configurations as well as other methods of excitation such as

an r.f. or possibly a microwave discharge.

9.3.2 Fundamental Noise Sources in a Free Running Laser

A fundamental noise source in the laser medium is that due to the spontaneous emission of the inverted population which introduces a quantum phase fluctuation. This produces a frequency spread of the laser oscillation $\Delta\nu_f$ where [51]

$$\Delta\nu_f = \frac{\pi h\nu_0}{P} (\Delta\nu_{cav})^2 \quad \ldots\ldots 9.3.2\text{-}1$$

where $\Delta\nu_{cav}$ is the width of the "cold" laser cavity $= \frac{\nu_0}{Q} \quad \frac{\nu_0 \lambda \eta}{2\pi L}$; η is the cavity loss, and P is the laser power output. For a 5% cavity loss in a 100 cm long cavity with a power output of 1 mW, $\Delta\nu_f = 10^{-1}$ Hz or $\Delta\nu_f/\nu_0 = 2 \times 10^{-16}$.

The thermal vibration of the cavity provides another fundamental noise source. An estimate of the change in the length of the cavity which corresponds to a frequency shift $\Delta\nu = \nu_0 \frac{\Delta L}{L}$ caused by thermal vibrations at room temperature may be made as follows.

For a cavity consisting of a cylindrical rod, length L, area A, and mass M at room temperature T, the amplitude of the longitudinal thermal vibration x is given by

$$\frac{1}{2} kT = 2\pi^2 M f^2 n^2$$

where 1/2 kT is the equipartition energy and f is the frequency of the vibration, so that

$$n = \frac{1}{2\pi} \left(\frac{kT}{Mf^2}\right)^{1/2} \quad \ldots\ldots\ldots 9.3.2\text{-}2$$

For the longest x, f has the smallest frequency of vibration. The frequency of the lowest stretching mode is

$$f \sim \frac{1}{2L} \sqrt{\frac{Y}{\rho}}$$

where $\sqrt{\frac{Y}{\rho}}$ is the velocity of propagation of longitudinal waves in the rod, Y is the Young's modulus and ρ is the density. Substituting in Equation 9.3.2-2 for f we get

$$x \simeq \frac{L}{\pi} \left(\frac{kT\rho}{YM}\right)^{1/2}$$

Since $M = \rho V$ where V is the volume of the rod, x becomes

$$x = \frac{L}{\pi} \left(\frac{kT}{YV}\right)^{1/2}$$

This causes a change in the laser frequency of

$$\frac{\Delta\nu}{\nu} = \frac{x}{L} = \frac{1}{\pi} \left(\frac{kT}{YV}\right)^{1/2}$$

For $T = 3000°$ K, $Y \simeq 10^{12}$ dynes/cm^2, L = 100 cm, $V = 10^3$ cm^3, then $\Delta\nu/\nu \simeq 3 \times 10^{-15}$. The frequency f of the lowest stretching

mode is of the order of several kHz.

For the case in which the laser mirror is supported on a piezo-electric crystal, where the combined volume of mirror and crystal is 10 cm^3 and the combined length ℓ = 3 cm, then

$$\frac{\Delta\nu}{\nu} = \frac{x}{L} = \frac{\ell}{L} \frac{1}{\pi} \left(\frac{kT}{YV}\right)^{1/2} = 10^{-15}$$

The frequency of the vibration in this case is in the tens of kHz.

The narrowest laser spectral width that has been measured so far, namely, 8 parts in 10^{14} for the Helium-Neon laser,[2] is believed to be limited by external sources and not by fundamental limitations.

9.4 Discussion on the Use of the I_2 Molecular Beam as a Long Term Reference

In order to use one of the resonances in the molecular beam of I_2 as a long term frequency reference, we need to know (a) the signal to noise ratio expected in a specific integration time, (b) the effective width of the resonance and (c) the possible sources of shifts of the resonance frequency.

Again, it is assumed, for the purpose of this discussion, that the spectral width and the short term drift of the argon ion laser are adequate, i.e., similar to the Helium-Neon laser.[2]

9.4.1 Determination of the Resonance Peak

The signal to noise ratio dictates how well the peak of the resonance can be determined. In the case of a resonance line with a Lorentzian shape, the amplitude $V(\nu)$ as a function of frequency is described by

$$V(\nu) = \frac{V_0 \Gamma^2}{(\nu - \nu_0)^2 + \Gamma^2}$$

where V_0 is the peak amplitude that occurs at ν_0 and 2Γ is the width of the resonance line. The frequency discriminating ability at any frequency ν is given by the slope $\frac{dV}{d\nu}$. The points on the resonance curve that are most sensitive to frequency changes are the inflexion points where the slope $\frac{dV}{d\nu}$ is a maximum. The magnitude of the slope at the inflexion points located at $\nu - \nu_0 = \pm \frac{\Gamma}{3}$ is

$$\left.\frac{dV}{d\nu}\right|_{max} = \pm \frac{3\sqrt{3}}{8} \frac{V_0}{\Gamma} \quad \ldots\ldots\ldots \quad 9.4.1\text{-}1$$

If $d\nu$ is assumed to be the uncertainty in the frequency due to a noise signal dV, then Equation 9.4.1-1 may be re-written as

$$\frac{dV}{V_0} = \pm\ 0.65\ \frac{d\nu}{\Gamma}$$

or

$$d\nu \sim \frac{2\Gamma}{V_0/dV} \quad \ldots\ldots\ldots\ldots\ldots\ldots \quad 9.4.1\text{-}2$$

This relationship implies that the uncertainty in the frequency at the inflexion points of the resonance curve is given by the width of the resonance divided by the peak signal to noise ratio. For example, if the resonance width is 50 kHz, the signal to noise ratio needed to limit the frequency uncertainty to, say, 300 Hz, has to be $\frac{5 \times 10^4}{3 \times 10^2} \sim 150$.

Assuming only Poisson noise, the peak signal to noise ratio is given by $N_0\tau/(N_0\tau)^{1/2}$ where N_0 is the number of photons detected per second and τ is the integration time. Substituting in Equation 9.4.1-2 we get an expression for the frequency shift $d\nu$ that can be detected in terms of a Poisson noise limited signal which is

$$d\nu = \frac{\Delta\nu_\omega}{(N_0\tau)^{1/2}} \quad \ldots\ldots\ldots \quad 9.4.1\text{-}3$$

where $\Delta\nu_\omega = 2\Gamma$ is the width of the resonance.

The signal to noise ratio in the measured resonance fluorescence in the present experiments is about 20 to 1 in an integration time of 1/30 second and is close to the value estimated if Poisson noise is the dominant noise. The measured value of the signal to noise ratio is expected to remain the same when the effective doppler width of the

iodine resonance in the beam is finally reduced to 50 kHz, as will be shown in the next section. It should then be possible to detect a frequency shift of 300 Hz in an integration time of about 2 seconds.

9.4.2 The Effective Width of the I_2 Resonance in the Molecular Beam

In order that the effective doppler width of the I_2 resonance in the beam approach the natural width of 50 kHz, sources of line broadening have to be minimized.

The angular width of the molecular beam as defined by the geometry of the slits introduces a doppler broadening. If the molecular beam diverges by a small half angle θ, then a symmetrical doppler shift of the resonance line results due to the projection of the molecular velocity vector along the laser beam. The doppler width $\Delta\nu_{doppler}$ introduced by the slits is given by

$$\Delta\nu_{doppler} = 2 \frac{\bar{v}_b}{c} \theta \nu_0$$

where $\bar{v}_b$ is the average velocity of the molecules in the beam and ν_0 is the resonance frequency of the molecular transition. If the velocity distribution of the molecules is taken into account, the doppler width is further broadened to

$$\Delta\nu_{doppler} \simeq 4 \frac{\bar{v}_b}{c} \theta \nu_0 \quad \ldots\ldots 9.4.2\text{-}2$$

because the width of the velocity distribution curve is about $2 \bar{v}_b$.

Equation 9.4.2-1 applies, in the same way, to the laser beam with a half divergence angle θ.

For I_2 at room temperature $\bar{v}_b = 1.87 \times 10^4$ cm/sec, so that for $\Delta\nu_{doppler} \simeq \Delta\nu_{natural}$, the half angle θ should be 4×10^{-5} radians. This does not constitute much of a problem for the laser, since 4×10^{-5} radians is within the diffraction limit of a small lens where $\theta = 1.22 \frac{\lambda}{D}$; λ is the wavelength of the light and D is the diameter of the lens. In the case of the molecular beam with, say 15 cm between the oven and collimating slit, the restriction on θ implies that each slit cannot be wider than 10^{-3} cm. This reduces the present beam intensity by a factor of 40. To offset this loss, the oven pressure can be increased by a factor of 10 since the oven slit is narrower and a shorter mean free path can be tolerated. In addition, the interaction volume can be increased by at least a factor of 5 by enlarging the laser beam diameter to cover the entire height of the molecular beam at the interaction region.

Non-orthogonality between the laser and the molecular beam introduces a doppler shift $\delta\nu_d$ given by

$$\delta\nu_d = 2 \frac{\bar{v}_b}{c} \phi \nu_0$$

where ϕ is the misalignment angle. ϕ must be less than 4×10^{-7} radians or 0.07 seconds of arc for $\delta\nu_d$ to be less than 300 Hz. In order to eliminate the doppler shift due to non-orthogonality, the laser light is reflected back on itself through the I_2 beam. This converts the misalignment doppler shift to a symmetrical broadening of the resonance line. A ϕ of 10^{-4} radians or 10 seconds of arc contributes a broadening of about 50 kHz. A precision corner cube reflecter may be used to ensure that the reflected beam is superposed on the incident beam.

The interaction of the iodine molecule with static external fields can broaden the observed width of the resonance. The calculations in Section 8.4 indicate that the dominant effect comes from the interaction of an external magnetic field with the nuclear spin magnetic moment and also with the molecular rotation magnetic moment. In a field of one gauss, these interactions contribute a symmetrical broadening of the order of 1 kHz which is small compared with the 50 kHz natural linewidth of the molecular transition. In any case, magnetic shields may be used to reduce this effect if necessary.

9.4.3 Frequency Shifts of the I_2 Resonance in the Beam

If the iodine molecule is observed at an angle ϕ with respect to the normal to its direction of motion, the apparent frequency ν' of the transition is given by

$$\nu' = \frac{\nu_0}{\gamma(1 - \frac{\bar{v}_b}{c} \sin \phi)}$$

where ν_0 is the true frequency of the transition, $\bar{v}_b$ is the velocity of the molecule, c is the velocity of light and $\gamma = (1 - \frac{\bar{v}_b^2}{c^2})^{-1/2}$ is the special relativistic factor.

The shift due to the misalignment angle ϕ has been discussed in the previous section under a first order doppler shift.

The effect of the relativistic time dialation reduces the true frequency ν_0 by a factor of order $\bar{v}_b^2/c^2$, the so called second order doppler shift. The average velocity of the molecules in the beam is $\bar{v}_b = 1.87 \times 10^4$ cm/sec, so that the contribution of this relativistic effect is $\frac{\Delta\nu}{\nu} = \frac{\bar{v}_b^2}{c^2} = 3 \times 10^{-13}$, i.e. a shift of 200 Hz. The variation of this shift with the temperature in the oven is given by

$$\frac{\Delta\nu}{\nu} = 3 \times 10^{-13} \frac{\Delta T}{T}$$

where ΔT is the change in the oven temperature T. For $T = 300°$ K, $\Delta\nu/\nu = \frac{3 \times 10^{-13}}{300} \Delta T = 10^{-15} \Delta T$ and is clearly a small effect. The velocity distribution of the molecules in the beam contributes a slight broadening about the shifted center frequency of the resonance.

The frequency shift due to the recoil of the I_2 molecule in absorbing a photon $\delta\nu_{recoil}$ is obtained from conservation

of momentum and its maximum value is

$$\frac{\delta\nu_{\text{recoil}}\,|_{\,\max}}{\nu_0} = \frac{h\nu_0}{M_{I_2}c^2} = 8 \times 10^{-12}$$

where M_{I_2} is the mass of the I_2 molecule. This is not a shift in the true sense since it belongs to the natural excitation process. The center frequency of the resonance must obviously take this into consideration.

A possible source of frequency shift may be caused by the variation in the intensity of the laser field. This is termed "intensity shift" which is due to a perturbation of the energy levels in the molecule by the application of a resonant time-varying field. This has been observed in the case of the Cesium atomic beam clocks where the effect was of the order of cycles/mW of incident energy.[58] A study of such an effect has been made by Mizushima[59] who shows that there are two types of shifts in the frequency of the transition; an electric shift Ω_e and a magnetic shift Ω_m which are both dependent on the applied field. These are given by

$$\Omega_e = \frac{\zeta_0^2}{z}\left[\sum_\gamma |(\alpha|e_\lambda \cdot M_e|\gamma)|^2\left\{(\hbar w+W_\alpha-W_\gamma)^{-1}+(-\hbar w+W_\alpha-W_\gamma)^{-1}\right\}\right.$$

$$\left.-\sum_\gamma |(\beta|e_\lambda \cdot M_e|\gamma)|^2\left\{(\hbar w+W_\beta-W_\gamma)^{-1}+(-\hbar w+W_\beta-W_\gamma)^{-1}\right\}\right]$$

and 9.4.3-1

$$\Omega_m = \frac{B_0^2}{2}\left[\sum_\gamma |(\alpha|e_\lambda'\cdot M_m|\gamma)|^2\left\{(\hbar w+W_\alpha-W_\gamma)^{-1}+(-\hbar w+W_\alpha-W_\gamma)^{-1}\right\}\right.$$

$$\left. - \sum_\gamma |(\beta|e_\lambda'\cdot M_m|\gamma)|^2\left\{(\hbar w+W_\beta-W_\gamma)^{-1}+(-\hbar w+W_\beta-W_\gamma)^{-1}\right\}\right]$$

where α,β refer to the states associated with the transition having energies W_α, W_β; γ is a variable which refers to other states but does not include either α or β; w is the angular frequency of the incident radiation; ζ_0, B_0 are the electric and magnetic vectors of the applied field; $|(\alpha|e_\lambda\cdot M_e|\gamma)|$ is the electric dipole moment matrix element between states α and γ, and $|(\alpha|e_\lambda'\cdot M_m|\gamma)|$ is the magnetic dipole moment matrix element between states α and γ.

Equation 9.4.3-1 may be used to obtain an order of magnitude estimate of the shift in the I_2 transition by use of some simplifying assumptions. The dominant effect in our case, i.e. electric dipole transition, is the electric shift Ω_e, where α refers to the lower level and β refers to the upper level of the transition. The largest contribution comes from the term associated with the resonant denominator $(\hbar w+W_\alpha-W_\gamma)^{-1}$ when the level γ is closest to level β, i.e. when $W_\gamma \sim W_\beta$. If the level γ is assumed to be a close rotational level to the upper state β, where the separation is around 1000 MHz, then the value of the resonant denominator becomes $(10^9\ h)^{-1}$.

In addition, $(\alpha|e_\lambda \cdot M_e|\gamma)^2$ is approximately $(\alpha|e_\lambda \cdot M_e|\beta)^2$ which is μ_{12}^2. $(\beta|e_\lambda \cdot M_e|\gamma)^2$ is zero since pure rotational transitions are not allowed in a homonuclear molecule. Thus, Ω_e becomes

$$\Omega_e \simeq \frac{\zeta_0^2}{2} \frac{|(\alpha|e_\lambda \cdot M_e|\gamma)|^2}{\hbar w + W_\alpha - W_\gamma} = \frac{\zeta_0^2}{2} \frac{\mu_{12}^2}{10^9 h}$$

The measured μ_{12}^2 is 10^{-38} e.s.u. and $\zeta_0^2 = \frac{8\pi}{c} I$ where I is the laser intensity at saturation per cm^2 so that $\zeta_0^2 = 2 \times 10^{-6}$ $(\text{stat volts/cm})^2$ for $I = 2$ mW/cm^2. The frequency shift $\delta\nu_e$ due to the laser intensity becomes

$$\delta\nu_e = \frac{\Omega_e}{h} = 0.2 \text{ Hz}$$

and is a small shift.

Let us now consider the interactions between the molecules in the beam. The absence of a molecular dipole moment makes the molecular quadrupole moment interaction the dominant interaction between the molecules in the beam. A typical beam density at the interaction region is estimated in Section 5.2 as $\rho = 3 \times 10^{10}$ molecules/cm^3. This implies that the average spacing between molecules in the beam is $(\rho)^{-1/3}$ or 3×10^{-4} cm. This is larger than a molecular diameter by a factor of 3×10^4. Perturbation of the molecular energy levels due to the quadrupole-quadrupole interaction between the molecules is of order $\frac{e^2 a^4}{R^5}$ and is about 10^{-31} ergs where

a is the molecular diameter and R is the average spacing between the molecules. This perturbation contributes a shift in the energy levels of $\frac{\Delta\nu}{\nu} \sim 10^{-21}$.

9.5 Applications of Long Term Stable Lasers

There are several areas where a long term stabilized laser may be useful.

(a) Wavelength Standards. This is perhaps a natural application, where both long term stability and resettability of the laser frequency are important. The wavelength standard at present [60] is the $2p_{10} - 5d_5$ emission line of $Krypton^{86}$ and is defined to an accuracy of one part in 10^8. The gas laser, so far, has not been a strong rival to the Krypton lamp. A molecular beam stabilized laser, however, may eventually supersede the present wavelength standard. In the case of the I_2 - 5145 Å laser scheme, the wavelength of the chosen I_2 resonance would become the standard. Assuming adequate argon ion laser short term stability, the resettability of the laser frequency should be better than one part in 10^{12}.

(b) Geophysics. A laser that has good long term stability might make it possible to measure low frequency or DC strains in the earth.[61] In particular, the strains associated with continental drift, have been estimated to be of order $\Delta\ell/\ell \sim 10^{-10}$ per year.[1]

(c) Communication. A laser local oscillator with a narrow spectral width at a known frequency enhances the signal to noise power in heterodyne detection in optical communication. The ratio of the signal to noise power P_{sn} is given by

$$P_{sn} = k\frac{A_s}{\Delta B}$$

where A_s is the power in the received signal; ΔB is the bandwidth of the I.F. receiver and k is a constant. The above expression assumes the photodetector is dominated by Poisson noise of the local oscillator.

The I.F. bandwidth is, in principle, determined by the bandwidth of the information in the received signal. In addition, the I.F. bandwidth must also be wide enough to accomodate for drifts between the local oscillator and the transmitted carrier. In the case where signal to noise is more important than the bandwidth, it is advantageous to maintain a small bandwidth, thus necessitating the frequency stability of both the carrier and the local oscillator.

(d) Physics. A clear application of such a device would be in the study of the interaction between coherent radiation and individual unperturbed molecules; for example, intensity shifts,[59] resonance excitation in which the optical transition probability goes like $\sin^2 t$ rather than t, saturation

broadening phenomena, etc.

(e) Experimental Relativity. One experiment that is contemplated as soon as two stabilized lasers are available is the measurement of the anisotropy of mass in the I_2 molecule.[62, 63, 64] The laser should also find applications in "Ether drift" experiments, in particular, it may become possible to perform one way v/c measurements; for example, beating two independently stabilized lasers that are located at different distances from the detector.

CHAPTER 10

SUMMARY AND DIRECTIONS FOR FUTURE WORK

10.1 Summary of Work Accomplished

The principal objective in the thesis is to find a stable and sharp optical frequency reference that may be used, in a feedback loop, to stabilize the frequency of a laser.

Atomic or molecular resonances, observed in a molecular beam, are natural candidates for such an application. Molecular beam techniques provide a means for observing isolated particles where collisions are virtually absent. The effective doppler width of the transitions is very much reduced if the beam is well collimated and the particles are observed at right angles to their motion. Several techniques of using a molecular beam in laser frequency stabilization have been presented.

The major accomplishment has been the resonance excitation of molecular iodine in a beam by a 5145 Å single longitudinal mode argon ion laser. As far as is known, this is the first report of a laser induced transition in an atomic or molecular beam. The excitation of the I_2 molecules was detected by observing the resonance fluorescence of the molecules as a

result of laser excitation. Resonance fluorescence first appears when the laser frequency is about 600 MHz above that of the center of the laser gain curve and extends over approximately 1300 MHz. The structure of the observed resonances has not been completely resolved because the inherent width in the apparatus was of the order of 10 MHz, due to the spectral width of the single mode laser. Several of the resonances have a width of 22 MHz which is comparable to the limiting width in the apparatus. This implied that the ultimate width of these lines might be narrower than 22 MHz.

A measurement of the lifetime of the excited state in I_2 was then carried out to determine the natural width of the observed transitions. The lifetime measurement was performed by pulsing the laser light and then observing the decay of the induced fluorescence. The time constant of the exponential decay, i.e. the lifetime, was measured as 3 μ seconds. The natural width of the transitions is inferred to be 50 kHz from the measured lifetime.

Analysis of the data from the molecular beam experiments as well as absorption cell measurements showed that

(a) the iodine transitions saturated at a power spectral density of 4.0×10^{-10} Watts/cm^2-Hz;

(b) the dipole moment matrix element was 1.0×10^{-19} e.s.u. and

(c) the total population fraction of the molecules involved

in the observed transitions was 2×10^{-3}.

The electronic states in I_2 that are involved are the $X'\Sigma^+_{og}$ ground electronic state and the $B^3\Pi^+_{ou}$ electronic state. An attempt has been made to identify the vibrational and rotational quantum numbers associated with the observed resonances as well as to explain their structure. Estimates of the hyperfine structure in the I_2 molecule showed that the nuclear electric quadrupole interaction is the dominant one. The quadrupole splittings can extend from 200 - 800 MHz, depending on what the value of eqQ in the $B^3\Pi^+_{ou}$ state turns out to be. The values of eqQ in both the $X'\Sigma^+_{og}$ and the $B^3\Pi^+_{ou}$ state have been estimated by heuristic arguments. The hyperfine interactions due to nuclear spin-spin and nuclear spin-molecular rotation contributes a splitting of the order of 1 kHz. The external field dependence of the I_2 transitions is also small. The observed spectrum was then compared with the calculated I_2 spectrum, based on presently available molecular constants. With or without hyperfine structure, the calculated spectrum did in no way resemble the observed data. Since the upper vibrational level v' is high and the anharmonic vibration constants for such a high vibrational level in the $B^3\Pi^+_{ou}$ state are not well known, it is not surprising that the calculated spectrum was found inadequate.

The significance of the experiments performed lies in the possibility of using one of the iodine resonances as an

external frequency reference in the feedback stabilization of the argon laser. A proposed scheme for stabilizing the argon laser using an I_2 molecular beam has been briefly investigated. The short term instability of the argon laser due mainly to plasma oscillations is expected to be a problem. Based on

(a) the narrow width of such a reference,

(b) the fact that its center frequency is not Stark shifted by collisions in the molecular beam, and

(c) the large signal to noise ratio in the fluorescence data, a high frequency stability and resettability, of the order of several parts in 10^{13}, is anticipated.

Several applications of longterm stabilized lasers have been discussed in such areas as length standards, geophysics, communications, physics, and experimental relativity.

10.2 Directions for Future Work

The observed resonance interaction between the argon laser and a molecular beam of iodine marks only the beginning of an exciting research program. Several directions for the immediate future with different emphasis will be carried out.

One, is in the area of laser frequency stabilization where the immediate problem to be tackled is the short term stability of the free-running argon laser. This will be followed by the use of an external Fabry-Perot interferometer, in a fast feedback loop, as a short term reference and the I_2 beam

as a long term reference. The use of resonance fluorescence induced in a low pressure gas cell of I_2 will also be investigated for lasers where high frequency stability is not required.

Two, is a thorough analysis of the observed I_2 spectrum using a stabilized argon laser. This is of much interest because iodine, like other diatomic homonuclear molecules, can only be studied by optical spectroscopy.

Three, is the investigation of other laser-molecule interactions in molecular beams. In particular, a suitable scheme for the long term stabilization of the powerful CO_2, 10.6 micron, laser would be of much interest.

APPENDIX A

DETERMINATION OF TRANSITION PROBABILITY IN A TWO-LEVEL SYSTEM

Assume we have a two-level system in which the energy of the upper level is E_a and that of the lower level is E_b. In the presence of a time varying electric field $E = E_0 \cos wt$, the total Hamiltonian $\mathcal{H}$ along the x-direction becomes

$$\mathcal{H} = \mathcal{H}_0 - e x E_0 \cos wt$$

where $\mathcal{H}_0$ is the time independent unperturbed Hamiltonian of the system. A solution to the Schroedinger equation for $\mathcal{H}$ can be written

$$\psi = a(t)\ \psi_a\ e^{\frac{-E_a}{h}t} + b(t)\ \psi_b e^{\frac{-E_b}{h}t}$$

where ψ_a and ψ_b are the unperturbed eigenfunctions associated with levels E_a and E_b; and $a(t)$, $b(t)$ are time varying coefficients. After substituting in the Schroedinger equation $\frac{-h}{i}\frac{d\psi}{dt} = \mathcal{H}\psi$ for ψ and $\mathcal{H}$ we get

$$\frac{da}{dt} = \frac{i}{h}\mu_{ab_x} E_0\ b \cos wt\ e^{iw_0 t}$$

and

$$\frac{da}{dt} = \frac{i}{h}\mu_{ab_x} E_0\ a \cos wt\ e^{-iw_0 t}$$

where $w_0 = \frac{E_a - E_b}{\hbar}$; $\mu_{ab_x} = \int \psi_a \mid e\boldsymbol{x} \mid \psi_b \, d\tau$ is the off-diagonal dipole moment matrix element and it has been assumed that the diagonal matrix elements are zero, i.e. $\int \psi_a \mid e \mid \psi_a \, d\tau = \mu_{aa} = 0$ and $\int \psi_b \mid e\boldsymbol{x} \mid \psi_b \, d\tau = \mu_{bb} = 0$.

Now using $\cos wt = 1/2 \, (e^{iwt} + e^{-iwt})$, the above expressions become

$$\frac{da}{dt} = \frac{i}{2\hbar} \mu_{ab_x} b E_0 e^{i(w_0 - w)t}$$

and

$$\frac{db}{dt} = \frac{i}{2\hbar} \mu_{ab_x} a E_0 e^{-i(w_0 - w)t}$$

This is a pair of simultaneous differential equations and may be solved to give[65]

$$a(t) = - \frac{2i\beta \, e^{\frac{i(w_0 - w)t}{2}}}{\left[(w_0 - w)^2 + 4\beta^2\right]^{1/2}} \sin \frac{1}{2} \left[(w - w_0)^2 + 4\beta^2\right]^{1/2} t$$

where $\beta = \frac{\mu_{ab_x} E_0}{2\hbar}$.

If the atom is initially in state b, i.e., $|a|^2 = 0$, $|b|^2 = 1$, then the probability that the atom is in state a after application of the field for a time t, is given by

$$|a(t)|^2 = \frac{4\beta^2}{(w_0 - w)^2 + 4\beta^2} \sin^2 \frac{1}{2} \left[(w - w_0)^2 + 4\beta^2\right]^{1/2} t$$

$|a|^2$ is called the transition probability.

Here, Yariv's[66] treatment is followed to simplify this

relationship to

$$|a(t)|^2 = \beta^2 \, g(\nu-\nu_0)t$$

where $g(\nu-\nu_0)$ is the normalized lineshape of the transition. Substituting for β, we get

$$|a(t)|^2 = \frac{\mu_{ab_x}^2 E_0^2}{4\hbar^2} \, g(\nu-\nu_0)t$$

Now E_0^2 may be expressed in terms of the energy, P_0, in the laser beam so that

$$\frac{c}{8\pi} E_0^2 = P_0 = \int_{-\infty}^{\infty} I(\nu) \, d\nu$$

where $I(\nu)$ is the spectral intensity of the laser. Substituting for E_0^2, we get

$$|a(t)|^2 = \frac{8\pi\mu_{ab_x}^2}{4\hbar^2 c} \, t \int_{-\infty}^{\infty} I(\nu) \, g(\nu-\nu_0) \, d\nu$$

If the variation of $I(\nu)$ with ν is small compared with $g(\nu-\nu_0)$, then $I(\nu)$ may be taken outside the integral to give the following expression

$$|a(t)|^2 = \frac{2\pi\mu_{ab_x}^2}{\hbar^2 c} \, I(\nu)t$$

since

$$\int_{-\infty}^{\infty} g(\nu-\nu_0) \, d\nu = 1$$

The orientation of the I_2 molecules in our case in random so that the effective dipole moment matrix element μ_{12} is given by $\mu_{12}^2 = \frac{\mu_{12_x}^2 + \mu_{12_y}^2 + \mu_{12_z}^2}{3}$. The transition probability then becomes

$$|a(t)|^2 = \frac{8\pi^3}{3h^2c} \mu_{12}^2 \, I(\nu) t \, .$$

APPENDIX B

Computed I_2 Transitions Using Available Molecular Constants

The I_2 transitions between the $X'\Sigma^+_{0g}$ and the $B^3\Pi_{+0u}$ states that fall within ± 10 cm^{-1} of the 19430 cm^{-1} (5145 Å) laser line have been computed using the molecular constants given in references (26) and (27). The listing of the computed lines in numberical order is included below. The column headings from left to right are:

(a) wavenumbers away from 19429.79 cm^{-1} laser line

(b) ground state vibration number v"

(c) upper state vibration number v'

(d) ground state rotation number J"

(e) partition function of v", J" level

(f) indicates values of ΔJ computed; 1.0 for ΔJ = + 1 and -1.0 for ΔJ = - 1

(Note in columns (b), (c), (d), and (f) the computer output shows an extra factor of 10 which should be ignored. For example, 660.00 should be 66.00.)

-9.9367676E 00	20.0	630.0	270.0	7.1888254E-04	10.0
-9.8996582E 00	20.0	650.0	230.0	6.3703419E-04	10.0
-9.8994141E 00	20.0	600.0	100.0	3.0793087E-04	-10.0
-9.8437500E 00	20.0	640.0	240.0	6.5849209E-04	-10.0
-9.8432617E 00	10.0	780.0	240.0	1.8261259E-03	-10.0
-9.8083496E 00	20.0	600.0	120.0	3.6359485E-04	10.0
-9.7705078E 00	20.0	640.0	260.0	6.9943164E-04	10.0
-9.7382812E 00	10.0	770.0	430.0	2.5761828E-03	-10.0
-9.7341309E 00	10.0	490.0	330.0	2.2753943E-03	10.0
-9.7172852E 00	20.0	660.0	140.0	4.1773543E-04	-10.0
-9.7131348E 00	0.0	820.0	680.0	6.8344884E-03	-10.0
-9.7119141E 00	20.0	660.0	160.0	4.7013699E-04	10.0
-9.7050781E 00	0.0	840.0	360.0	6.6229440E-03	-10.0
-9.6035156E 00	20.0	610.0	190.0	5.4503698E-04	-10.0
-9.5668945E 00	10.0	500.0	510.0	2.6640561E-03	-10.0
-9.5625000E 00	0.0	830.0	560.0	7.3624179E-03	10.0
-9.5605469E 00	0.0	450.0	760.0	6.2067439E-03	-10.0
-9.5095215E 00	10.0	510.0	670.0	2.4880113E-03	10.0
-9.5092773E 00	20.0	600.0	90.0	2.7959771E-04	-10.0
-9.4895020E 00	20.0	620.0	230.0	6.3703419E-04	-10.0
-9.4685059E 00	20.0	610.0	210.0	5.9223059E-04	10.0
-9.4262695E 00	20.0	600.0	110.0	3.3593946E-04	10.0
-9.3930664E 00	10.0	530.0	850.0	1.9302722E-03	10.0
-9.3886719E 00	10.0	490.0	300.0	2.1436508E-03	-10.0
-9.3813477E 00	0.0	430.0	300.0	5.9447587E-03	10.0
-9.3581543E 00	10.0	540.0	890.0	1.7838662E-03	-10.0
-9.3579102E 00	20.0	620.0	250.0	6.7929621E-04	10.0
-9.3552246E 00	10.0	740.0	730.0	2.3304315E-03	-10.0
-9.3469238E 00	10.0	760.0	570.0	2.6475668E-03	10.0
-9.3244629E 00	10.0	520.0	770.0	2.2067814E-03	10.0
-9.3188477E 00	0.0	430.0	270.0	5.5286400E-03	-10.0
-9.2988281E 00	10.0	750.0	650.0	2.5313534E-03	-10.0
-9.1955566E 00	10.0	780.0	250.0	1.8838202E-03	10.0
-9.1633301E 00	20.0	660.0	130.0	3.9066933E-04	-10.0
-9.1579590E 00	20.0	660.0	150.0	4.4416660E-04	10.0
-9.1542969E 00	20.0	600.0	80.0	2.5096908E-04	-10.0
-9.1298828E 00	20.0	650.0	200.0	5.6892261E-04	-10.0
-9.1093750E 00	20.0	630.0	240.0	6.5849209E-04	-10.0
-9.0922852E 00	20.0	650.0	220.0	6.1494112E-04	10.0
-9.0791016E 00	20.0	600.0	100.0	3.0793087E-04	10.0
-9.0346680E 00	0.0	800.0	880.0	5.0492026E-03	-10.0
-9.0048828E 00	20.0	630.0	260.0	6.9943164E-04	10.0
-8.9638672E 00	0.0	840.0	370.0	6.7153536E-03	10.0
-8.9348145E 00	20.0	640.0	230.0	6.3703419E-04	-10.0
-8.8935547E 00	20.0	610.0	180.0	5.2059582E-04	-10.0
-8.8618164E 00	20.0	640.0	250.0	6.7929621E-04	10.0
-8.8342285E 00	20.0	600.0	70.0	2.2207499E-04	-10.0
-8.8266602E 00	10.0	780.0	230.0	1.7666195E-03	-10.0
-8.7670898E 00	20.0	600.0	90.0	2.7959771E-04	10.0
-8.7626953E 00	20.0	610.0	200.0	5.6892261E-04	10.0
-8.7231445E 00	10.0	490.0	320.0	2.2335579E-03	10.0
-8.6442871E 00	20.0	660.0	120.0	3.6359485E-04	-10.0
-8.6391602E 00	20.0	660.0	140.0	4.1773543E-04	10.0
-8.6342773E 00	10.0	760.0	550.0	2.6603756E-03	-10.0
-8.6313477E 00	20.0	620.0	220.0	6.1494112E-04	-10.0
-8.5917969E 00	10.0	510.0	640.0	2.5510613E-03	-10.0
-8.5585937E 00	10.0	770.0	440.0	2.5944465E-03	10.0
-8.5493164E 00	20.0	600.0	60.0	1.9294520E-04	-10.0
-8.5251465E 00	10.0	500.0	530.0	2.6659744E-03	10.0
-8.5170898E 00	0.0	430.0	290.0	5.8115870E-03	10.0
-8.5039062E 00	20.0	620.0	240.0	6.5849209E-04	10.0
-8.4919434E 00	0.0	790.0	960.0	4.2305440E-03	-10.0
-8.4902344E 00	20.0	600.0	80.0	2.5096908E-04	10.0
-8.4738770E 00	0.0	440.0	600.0	7.2535202E-03	10.0
-8.4567871E 00	0.0	430.0	260.0	5.3790510E-03	-10.0
-8.3886719E 00	10.0	480.0	280.0	2.0856207E-03	-10.0

-8.37011726 00	10.0	550.0	940.0	1.5990091E-03	-10.0
-8.3574219E 00	20.0	650.0	190.0	5.4503698E-04	-10.0
-8.3508301E 00	0.0	830.0	540.0	7.3880553E-03	-10.0
-8.3239746E 00	20.0	650.0	210.0	5.9223059E-04	10.0
-8.2998047E 00	20.0	600.0	50.0	1.6361043E-04	-10.0
-8.2521973E 00	0.0	440.0	570.0	7.3422156E-03	-10.0
-8.2482910E 00	20.0	600.0	70.0	2.2207499E-04	10.0
-8.2407227E 00	0.0	810.0	800.0	5.8423951E-03	10.0
-8.2199707E 00	10.0	720.0	870.0	1.8574332E-03	10.0
-8.2148437E 00	20.0	610.0	170.0	4.9562147E-04	-10.0
-8.2075195E 00	0.0	820.0	690.0	6.7660026E-03	10.0
-8.2048340E 00	10.0	780.0	240.0	1.8261259E-03	10.0
-8.2043457E 00	20.0	630.0	230.0	6.3703419E-04	-10.0
-8.1645508E 00	20.0	660.0	110.0	3.3593946E-04	-10.0
-8.1594238E 00	20.0	660.0	130.0	3.9066933E-04	10.0
-8.1435547E 00	10.0	520.0	740.0	2.3007228E-03	-10.0
-8.1228027E 00	0.0	840.0	350.0	6.5245777E-03	-10.0
-8.1130371E 00	0.0	460.0	920.0	4.6353052E-03	10.0
-8.1049805E 00	10.0	710.0	920.0	1.6729105E-03	10.0
-8.1040039E 00	20.0	630.0	250.0	6.7929621E-04	10.0
-8.0917969E 00	20.0	610.0	190.0	5.4503698E-04	10.0
-8.0852051E 00	20.0	600.0	40.0	1.3410153E-04	-10.0
-8.0610352E 00	20.0	640.0	220.0	6.1494112E-04	-10.0
-8.0415039E 00	20.0	600.0	60.0	1.9294520E-04	10.0
-8.0268555E 00	10.0	540.0	910.0	1.7059218E-03	10.0
-7.9921875E 00	20.0	640.0	240.0	6.5849209E-04	10.0
-7.9565430E 00	10.0	770.0	420.0	2.5557871E-03	-10.0
-7.9541016E 00	10.0	530.0	820.0	2.0373606E-03	-10.0
-7.9055176E 00	20.0	600.0	30.0	1.0444982E-04	-10.0
-7.8813477E 00	10.0	500.0	500.0	2.6601902E-03	-10.0
-7.8701172E 00	20.0	600.0	50.0	1.6361043E-04	10.0
-7.8510742E 00	10.0	780.0	220.0	1.7053506E-03	-10.0
-7.8044434E 00	20.0	620.0	210.0	5.9223059E-04	-10.0
-7.7612305E 00	20.0	600.0	20.0	7.4686701E-05	-10.0
-7.7443848E 00	10.0	490.0	310.0	2.1896367E-03	10.0
-7.7336426E 00	20.0	600.0	40.0	1.3410153E-04	10.0
-7.7197266E 00	20.0	660.0	100.0	3.0793087E-04	-10.0
-7.7145996E 00	20.0	660.0	120.0	3.6359485E-04	10.0
-7.6982422E 00	10.0	730.0	810.0	2.0722842E-03	10.0
-7.6848145E 00	20.0	620.0	230.0	6.3703419E-04	10.0
-7.6831055E 00	0.0	430.0	280.0	5.6728497E-03	10.0
-7.6479492E 00	20.0	600.0	10.0	4.4843939E-05	-10.0
-7.6320801E 00	20.0	600.0	30.0	1.0444982E-04	10.0
-7.6250000E 00	0.0	430.0	250.0	5.2241981E-03	-10.0
-7.6240234E 00	20.0	650.0	180.0	5.2059582E-04	-10.0
-7.5908703E 00	20.0	650.0	200.0	5.6852261E-04	10.0
-7.5815430E 00	0.0	450.0	780.0	6.0290359E-03	10.0
-7.5751953E 00	20.0	610.0	160.0	4.7013699E-04	-10.0
-7.5659180E 00	20.0	600.0	20.0	7.4686701E-05	10.0
-7.5532227E 00	10.0	720.0	850.0	1.9302722E-03	-10.0
-7.5385742E 00	20.0	600.0	0.0	1.4953315E-05	10.0
-7.5346680E 00	20.0	600.0	10.0	4.4843939E-05	10.0
-7.5112305E 00	10.0	710.0	900.0	1.7469209E-03	-10.0
-7.4807129E 00	0.0	460.0	890.0	4.9470067E-03	-10.0
-7.4599609E 00	20.0	610.0	180.0	5.2059582E-04	10.0
-7.4350586E 00	10.0	690.0	980.0	1.4527014E-03	-10.0
-7.4208984E 00	10.0	490.0	280.0	2.0456018E-03	-10.0
-7.4082031E 00	10.0	750.0	660.0	2.5103197E-03	10.0
-7.4016113E 00	0.0	840.0	360.0	6.6229440E-03	10.0
-7.3730469E 00	10.0	510.0	660.0	2.5103197E-03	10.0
-7.3383789E 00	20.0	630.0	220.0	6.1494112E-04	-10.0
-7.3139648E 00	20.0	660.0	90.0	2.7959771E-04	-10.0
-7.3090820E 00	20.0	660.0	110.0	3.3593946E-04	10.0
-7.2551270E 00	10.0	780.0	230.0	1.7666195E-03	10.0
-7.2421875E 00	20.0	630.0	240.0	6.5849209E-04	10.0
-7.2224121E 00	20.0	640.0	210.0	5.9223059E-04	-10.0

-7.2124023E 00	10.0	560.0	980.0	1.4527014E-03	-10.0
-7.1997070E 00	0.0	830.0	550.0	7.3777363E-03	10.0
-7.1691895E 00	0.0	450.0	750.0	6.2956363E-03	-10.0
-7.1669922E 00	10.0	740.0	740.0	2.3007228E-03	10.0
-7.1574707E 00	20.0	640.0	230.0	6.3703419E-04	10.0
-7.0827637E 00	10.0	550.0	960.0	1.5255134E-03	10.0
-7.0820312E 00	10.0	760.0	560.0	2.6548516E-03	10.0
-7.0166016E 00	20.0	620.0	200.0	5.6852261E-04	-10.0
-6.9785156E 00	10.0	730.0	790.0	2.1406766E-03	-10.0
-6.9704590E 00	20.0	610.0	150.0	4.4416660E-04	-10.0
-6.9433594E 00	20.0	660.0	80.0	2.5056908E-04	-10.0
-6.9384766E 00	20.0	660.0	100.0	3.0753087E-04	10.0
-6.9323730E 00	0.0	800.0	890.0	4.9470067E-03	10.0
-6.9257812E 00	20.0	650.0	170.0	4.9562147E-04	-10.0
-6.9162598E 00	10.0	780.0	210.0	1.6423701E-03	-10.0
-6.9008789E 00	20.0	620.0	220.0	6.1454112E-04	10.0
-6.8964844E 00	20.0	650.0	190.0	5.4503698E-04	10.0
-6.8791504E 00	0.0	430.0	270.0	5.5286400E-03	10.0
-6.8593750E 00	20.0	610.0	170.0	4.9562147E-04	10.0
-6.8591309E 00	10.0	500.0	520.0	2.6659730E-03	10.0
-6.8371582E 00	10.0	520.0	760.0	2.2388427E-03	10.0
-6.8327637E 00	10.0	700.0	960.0	1.5255134E-03	10.0
-6.8232422E 00	0.0	430.0	240.0	5.0642006E-03	-10.0
-6.8037109E 00	10.0	770.0	430.0	2.5761828E-03	10.0
-6.7973633E 00	10.0	490.0	300.0	2.1436508E-03	10.0
-6.7951660E 00	0.0	820.0	670.0	6.8997368E-03	-10.0
-6.6984863E 00	0.0	810.0	780.0	6.0290359E-03	-10.0
-6.6826172E 00	0.0	440.0	590.0	7.2876438E-03	10.0
-6.6621094E 00	10.0	750.0	640.0	2.5510613E-03	-10.0
-6.6140137E 00	10.0	530.0	840.0	1.9663055E-03	10.0
-6.6115723E 00	20.0	660.0	70.0	2.2207499E-04	-10.0
-6.6069336E 00	20.0	660.0	90.0	2.7959771E-04	10.0
-6.5834961E 00	0.0	840.0	340.0	6.4202882E-03	-10.0
-6.5075684E 00	20.0	630.0	210.0	5.9223059E-04	-10.0
-6.4846191E 00	10.0	490.0	270.0	1.9936005E-03	-10.0
-6.4667969E 00	10.0	510.0	630.0	2.5693895E-03	-10.0
-6.4648437E 00	0.0	440.0	560.0	7.3624179E-03	-10.0
-6.4221191E 00	10.0	740.0	720.0	2.3592471E-03	-10.0
-6.4189453E 00	20.0	640.0	200.0	5.6852261E-04	-10.0
-6.4152832E 00	20.0	630.0	230.0	6.3703419E-04	10.0
-6.4008789E 00	20.0	610.0	140.0	4.1773543E-04	-10.0
-6.3820801E 00	10.0	760.0	540.0	2.6640964E-03	-10.0
-6.3579102E 00	20.0	640.0	220.0	6.1454112E-04	10.0
-6.3461914E 00	10.0	780.0	220.0	1.7053506E-03	10.0
-6.3420410E 00	10.0	540.0	880.0	1.8207177E-03	-10.0
-6.3349609E 00	10.0	700.0	940.0	1.5990091E-03	-10.0
-6.3149414E 00	20.0	660.0	60.0	1.9294520E-04	-10.0
-6.3105469E 00	20.0	660.0	80.0	2.5056908E-04	10.0
-6.2978516E 00	20.0	610.0	160.0	4.7013699E-04	10.0
-6.2636719E 00	20.0	620.0	190.0	5.4503698E-04	-10.0
-6.2626953E 00	20.0	650.0	160.0	4.7013699E-04	-10.0
-6.2373047E 00	20.0	650.0	180.0	5.2059582E-04	10.0
-6.2282715E 00	10.0	500.0	490.0	2.6543427E-03	-10.0
-6.2155762E 00	10.0	770.0	410.0	2.5332463E-03	-10.0
-6.1520996E 00	20.0	620.0	210.0	5.9223059E-04	10.0
-6.1154785E 00	0.0	790.0	970.0	4.1293018E-03	10.0
-6.1057129E 00	0.0	430.0	260.0	5.3790510E-03	10.0
-6.0537109E 00	20.0	660.0	50.0	1.6361043E-04	-10.0
-6.0529785E 00	20.0	660.0	70.0	2.2207499E-04	10.0
-6.0520020E 00	0.0	430.0	230.0	4.8991777E-03	-10.0
-6.0227051E 00	10.0	780.0	200.0	1.5777324E-03	-10.0
-6.0102539E 00	0.0	830.0	530.0	7.3932633E-03	-10.0
-5.8823242E 00	0.0	840.0	350.0	6.5245777E-03	10.0
-5.8823242E 00	10.0	490.0	290.0	2.0956297E-03	10.0
-5.8664551E 00	20.0	610.0	130.0	3.9086933E-04	-10.0
-5.8312988E 00	20.0	660.0	40.0	1.2410153E-04	-10.0

-5.8305664E 00	20.0	660.0	60.0	1.9294520E-04	10.0
-5.7673340E 00	20.0	610.0	150.0	4.4416660E-04	10.0
-5.7119141E 00	20.0	630.0	200.0	5.6892261E-04	-10.0
-5.6716309E 00	10.0	520.0	730.0	2.3304315E-03	-10.0
-5.6542969E 00	20.0	640.0	190.0	5.4503698E-04	-10.0
-5.6477051E 00	20.0	660.0	30.0	1.0444982E-04	-10.0
-5.6474609E 00	20.0	660.0	50.0	1.6361043E-04	10.0
-5.6384277E 00	20.0	650.0	150.0	4.4416660E-04	-10.0
-5.6235352E 00	20.0	630.0	220.0	6.1494112E-04	10.0
-5.6132812E 00	20.0	650.0	170.0	4.9562147E-04	10.0
-5.5974121E 00	20.0	640.0	210.0	5.9223059E-04	10.0
-5.5805664E 00	10.0	490.0	260.0	1.9356592E-03	-10.0
-5.5458984E 00	20.0	620.0	180.0	5.2059582E-04	-10.0
-5.4995117E 00	20.0	660.0	20.0	7.4666701E-05	-10.0
-5.4992676E 00	20.0	660.0	40.0	1.3410153E-04	10.0
-5.4782715E 00	10.0	780.0	210.0	1.6423701E-03	10.0
-5.4423828E 00	20.0	620.0	200.0	5.6892261E-04	10.0
-5.3862305E 00	20.0	660.0	10.0	4.4843939E-05	-10.0
-5.3859863E 00	20.0	660.0	30.0	1.0444982E-04	10.0
-5.3669434E 00	20.0	610.0	120.0	3.6359485E-04	-10.0
-5.3627930E 00	0.0	430.0	250.0	5.2241981E-03	10.0
-5.3234863E 00	0.0	800.0	970.0	5.1510222E-03	-10.0
-5.3120117E 00	20.0	660.0	20.0	7.4666701E-05	10.0
-5.3112793E 00	0.0	430.0	220.0	4.7292672E-03	-10.0
-5.3110352E 00	0.0	820.0	680.0	6.8344884E-03	10.0
-5.2866211E 00	0.0	460.0	910.0	4.7419444E-03	10.0
-5.2768555E 00	20.0	660.0	10.0	4.4843939E-05	10.0
-5.2768555E 00	20.0	660.0	0.0	1.4953315E-05	10.0
-5.2758789E 00	20.0	610.0	140.0	4.1773543E-04	10.0
-5.2675781E 00	10.0	510.0	650.0	2.5313534E-03	10.0
-5.2258301E 00	10.0	500.0	510.0	2.6640561E-03	10.0
-5.2155762E 00	0.0	450.0	770.0	6.1198324E-03	10.0
-5.1943359E 00	10.0	530.0	810.0	2.0722842E-03	-10.0
-5.1699219E 00	10.0	780.0	190.0	1.5114930E-03	-10.0
-5.1555176E 00	10.0	550.0	930.0	1.6359277E-03	-10.0
-5.0893555E 00	10.0	770.0	420.0	2.5557871E-03	10.0
-5.0874023E 00	0.0	840.0	330.0	6.3101090E-03	-10.0
-5.0532227E 00	20.0	650.0	140.0	4.1773543E-04	-10.0
-5.0283203E 00	20.0	650.0	180.0	4.7013699E-04	10.0
-5.0229492E 00	10.0	540.0	900.0	1.7469209E-03	10.0
-4.9992676E 00	10.0	490.0	280.0	2.0456018E-03	10.0
-4.9550781E 00	20.0	630.0	190.0	5.4503698E-04	-10.0
-4.9248047E 00	20.0	640.0	180.0	5.2059582E-04	-10.0
-4.9216309E 00	0.0	440.0	580.0	7.3172487E-03	10.0
-4.9033203E 00	0.0	810.0	790.0	5.9365109E-03	10.0
-4.9028320E 00	20.0	610.0	110.0	3.3593946E-04	-10.0
-4.8798828E 00	0.0	830.0	540.0	7.3860553E-03	10.0
-4.8720703E 00	20.0	640.0	200.0	5.6892261E-04	10.0
-4.8669434E 00	20.0	630.0	210.0	5.9223059E-04	10.0
-4.8632812E 00	20.0	620.0	170.0	4.9562147E-04	-10.0
-4.8593750E 00	10.0	720.0	860.0	1.8939676E-03	10.0
-4.8574219E 00	10.0	760.0	550.0	2.6663756E-03	10.0
-4.8195801E 00	20.0	610.0	130.0	3.9066933E-04	10.0
-4.8088379E 00	0.0	450.0	740.0	6.3803494E-03	-10.0
-4.8027344E 00	10.0	750.0	650.0	2.5313534E-03	10.0
-4.7636719E 00	20.0	620.0	190.0	5.4503698E-04	10.0
-4.7080078E 00	10.0	490.0	250.0	1.8838202E-03	-10.0
-4.7077637E 00	0.0	440.0	550.0	7.3777363E-03	-10.0
-4.6613770E 00	0.0	460.0	880.0	5.0492026E-03	-10.0
-4.6516113E 00	10.0	780.0	200.0	1.5777324E-03	10.0
-4.6499023E 00	0.0	430.0	240.0	5.0642006E-03	10.0
-4.6071777E 00	10.0	500.0	480.0	2.6464842E-03	-10.0
-4.6003418E 00	0.0	430.0	210.0	4.5546107E-03	-10.0
-4.5737305E 00	10.0	710.0	910.0	1.7099218E-03	10.0
-4.5434570E 00	10.0	730.0	800.0	2.1067390E-03	10.0
-4.5153809E 00	10.0	770.0	400.0	2.5065532E-03	-10.0

-4.5031738E 00	20.0	650.0	130.0	3.5066933E-04	-10.0
-4.4782715E 00	20.0	650.0	150.0	4.4416660E-04	10.0
-4.4777832E 00	0.0	790.0	950.0	4.3322630E-03	-10.0
-4.4736328E 00	20.0	610.0	100.0	3.0793087E-04	-10.0
-4.4060059E 00	0.0	840.0	340.0	6.4202882E-03	10.0
-4.3981934E 00	20.0	610.0	120.0	3.6359485E-04	10.0
-4.3811035E 00	10.0	520.0	750.0	2.2701756E-03	10.0
-4.3769531E 00	10.0	510.0	620.0	2.5862858E-03	-10.0
-4.3581543E 00	10.0	780.0	180.0	1.4427132E-03	-10.0
-4.2653809E 00	10.0	740.0	730.0	2.3304315E-03	10.0
-4.2343750E 00	20.0	640.0	170.0	4.9562147E-04	-10.0
-4.2294922E 00	20.0	630.0	180.0	5.2059582E-04	-10.0
-4.2197266E 00	20.0	620.0	160.0	4.7013699E-04	-10.0
-4.1999512E 00	10.0	720.0	840.0	1.9663055E-03	-10.0
-4.1816406E 00	20.0	640.0	190.0	5.4503698E-04	10.0
-4.1704102E 00	10.0	760.0	530.0	2.6659744E-03	-10.0
-4.1494141E 00	20.0	630.0	200.0	5.6852261E-04	10.0
-4.1479492E 00	10.0	490.0	270.0	1.9936005E-03	10.0
-4.1240234E 00	20.0	620.0	180.0	5.2059582E-04	10.0
-4.0795898E 00	20.0	610.0	90.0	2.7959771E-04	-10.0
-4.0683594E 00	10.0	750.0	630.0	2.5693895E-03	-10.0
-4.0581055E 00	10.0	690.0	990.0	1.4166317E-03	10.0
-4.0122070E 00	20.0	610.0	110.0	3.3593946E-04	10.0
-3.9909668E 00	10.0	710.0	890.0	1.7838662E-03	-10.0
-3.9880371E 00	20.0	650.0	120.0	3.6359485E-04	-10.0
-3.9672852E 00	0.0	430.0	230.0	4.8951777E-03	10.0
-3.9633789E 00	20.0	650.0	140.0	4.1773543E-04	10.0
-3.9199219E 00	0.0	430.0	200.0	4.3753572E-03	-10.0
-3.9196777E 00	0.0	820.0	660.0	6.9616027E-03	-10.0
-3.9808594E 00	10.0	550.0	950.0	1.5621928E-03	10.0
-3.8740234E 00	10.0	530.0	830.0	2.0020164E-03	10.0
-3.8676758E 00	10.0	490.0	240.0	1.8261259E-03	-10.0
-3.8664551E 00	0.0	470.0	990.0	3.9265943E-03	-10.0
-3.8657227E 00	10.0	780.0	190.0	1.5114930E-03	10.0
-3.8315430E 00	10.0	560.0	970.0	1.4890060E-03	-10.0
-3.8312988E 00	10.0	730.0	780.0	2.1740408E-03	-10.0
-3.7246094E 00	20.0	610.0	80.0	2.5056908E-04	-10.0
-3.7121582E 00	0.0	830.0	520.0	7.3932596E-03	-10.0
-3.6635742E 00	10.0	690.0	970.0	1.4890060E-03	-10.0
-3.6611328E 00	20.0	610.0	100.0	3.0793087E-04	10.0
-3.6340332E 00	0.0	840.0	320.0	6.1940886E-03	-10.0
-3.6247559E 00	10.0	500.0	500.0	2.6601902E-03	10.0
-3.6071777E 00	20.0	620.0	150.0	4.4416660E-04	-10.0
-3.5871582E 00	10.0	780.0	170.0	1.3744540E-03	-10.0
-3.5791016E 00	20.0	640.0	160.0	4.7013699E-04	-10.0
-3.5429688E 00	20.0	630.0	170.0	4.9562147E-04	-10.0
-3.5280762E 00	10.0	740.0	710.0	2.3871143E-03	-10.0
-3.5263672E 00	20.0	640.0	180.0	5.2059582E-04	10.0
-3.5195312E 00	20.0	620.0	170.0	4.9562147E-04	10.0
-3.5083008E 00	20.0	650.0	110.0	3.3593946E-04	-10.0
-3.4875488E 00	20.0	650.0	130.0	3.5066933E-04	10.0
-3.4667969E 00	20.0	630.0	190.0	5.4503698E-04	10.0
-3.4157715E 00	10.0	770.0	410.0	2.5332463E-03	10.0
-3.4006348E 00	20.0	610.0	70.0	2.2207499E-04	-10.0
-3.3808594E 00	0.0	810.0	770.0	6.1198324E-03	-10.0
-3.3566895E 00	10.0	540.0	870.0	1.8574332E-03	-10.0
-3.3452148E 00	20.0	610.0	90.0	2.7959771E-04	10.0
-3.3288574E 00	10.0	490.0	260.0	1.9396592E-03	10.0
-3.3149414E 00	0.0	430.0	220.0	4.7292672E-03	10.0
-3.2700195E 00	0.0	430.0	190.0	4.1916631E-03	-10.0
-3.2446289E 00	0.0	800.0	880.0	5.0492026E-03	10.0
-3.2346191E 00	10.0	520.0	720.0	2.3592471E-03	-10.0
-3.1972656E 00	10.0	510.0	640.0	2.5510613E-03	10.0
-3.1914063E 00	0.0	440.0	570.0	7.3422156E-03	10.0
-3.1816406E 00	10.0	700.0	950.0	1.5621928E-03	10.0
-3.1208496E 00	10.0	780.0	180.0	1.4427132E-03	10.0

-3.1157227E 00	20.0	610.0	60.0	1.9294520E-04	-10.0
-3.0673828E 00	20.0	650.0	100.0	3.0793087E-04	-10.0
-3.0644531E 00	20.0	610.0	80.0	2.5096908E-04	10.0
-3.0590820E 00	10.0	490.0	230.0	1.7666195E-03	-10.0
-3.0505371E 00	20.0	650.0	120.0	3.6359485E-04	10.0
-3.0336914E 00	20.0	620.0	140.0	4.1773543E-04	-10.0
-3.0183105E 00	10.0	500.0	470.0	2.6365893E-03	-10.0
-2.9814453E 00	0.0	440.0	540.0	7.3880553E-03	-10.0
-2.9729004E 00	0.0	840.0	330.0	6.3101090E-03	10.0
-2.9587402E 00	20.0	640.0	150.0	4.4416660E-04	-10.0
-2.9501953E 00	20.0	620.0	160.0	4.7013699E-04	10.0
-2.9101562E 00	20.0	640.0	170.0	4.9562147E-04	10.0
-2.8916016E 00	20.0	630.0	160.0	4.7013699E-04	-10.0
-2.8803711E 00	0.0	450.0	760.0	6.2087439E-03	10.0
-2.8623047E 00	20.0	610.0	50.0	1.6361043E-04	-10.0
-2.8571777E 00	10.0	780.0	160.0	1.3037813E-03	-10.0
-2.8554687E 00	10.0	770.0	390.0	2.4817016E-03	-10.0
-2.8193359E 00	20.0	630.0	180.0	5.2059582E-04	10.0
-2.8186035E 00	20.0	610.0	70.0	2.2207499E-04	10.0
-2.6928711E 00	0.0	430.0	210.0	4.5546107E-03	10.0
-2.6867676E 00	10.0	700.0	930.0	1.6359277E-03	-10.0
-2.6728516E 00	10.0	760.0	540.0	2.6640964E-03	10.0
-2.6655273E 00	20.0	650.0	90.0	2.7959771E-04	-10.0
-2.6499023E 00	0.0	430.0	180.0	4.0036961E-03	-10.0
-2.6489258E 00	20.0	650.0	110.0	3.3593946E-04	10.0
-2.6477051E 00	20.0	610.0	40.0	1.3410153E-04	-10.0
-2.6284180E 00	10.0	560.0	990.0	1.4166317E-03	10.0
-2.6118164E 00	20.0	610.0	60.0	1.9294520E-04	10.0
-2.6027832E 00	0.0	830.0	530.0	7.3932633E-03	10.0
-2.5412598E 00	10.0	490.0	250.0	1.8838202E-03	10.0
-2.4953613E 00	20.0	620.0	130.0	3.9086933E-04	-10.0
-2.4909668E 00	0.0	460.0	900.0	4.8445500E-03	10.0
-2.4792480E 00	0.0	450.0	730.0	6.4627379E-03	-10.0
-2.4692383E 00	10.0	530.0	900.0	2.1067390E-03	-10.0
-2.4680176E 00	20.0	610.0	30.0	1.0444982E-04	-10.0
-2.4570312E 00	0.0	820.0	670.0	6.8997368E-03	10.0
-2.4365234E 00	20.0	610.0	50.0	1.6361043E-04	10.0
-2.4167480E 00	10.0	780.0	170.0	1.3744540E-03	10.0
-2.4157715E 00	20.0	620.0	150.0	4.4416660E-04	10.0
-2.3774414E 00	20.0	640.0	140.0	4.1773543E-04	-10.0
-2.3291016E 00	20.0	640.0	160.0	4.7013699E-04	10.0
-2.3237305E 00	20.0	610.0	20.0	7.4686701E-05	-10.0
-2.3183594E 00	10.0	510.0	610.0	2.6017006E-03	-10.0
-2.3000488E 00	20.0	610.0	40.0	1.3410153E-04	10.0
-2.2988281E 00	20.0	650.0	80.0	2.5096908E-04	-10.0
-2.2824707E 00	10.0	490.0	220.0	1.7053506E-03	-10.0
-2.2822266E 00	20.0	650.0	100.0	3.0793087E-04	10.0
-2.2790527E 00	20.0	630.0	150.0	4.4416660E-04	-10.0
-2.2363281E 00	10.0	750.0	640.0	2.5510613E-03	10.0
-2.2241211E 00	0.0	840.0	310.0	6.0722865E-03	-10.0
-2.2109375E 00	20.0	630.0	170.0	4.9562147E-04	10.0
-2.2104492E 00	20.0	610.0	10.0	4.4843939E-05	-10.0
-2.1945801E 00	20.0	610.0	30.0	1.0444982E-04	10.0
-2.1684570E 00	10.0	780.0	150.0	1.2317603E-03	-10.0
-2.1284180E 00	20.0	610.0	20.0	7.4686701E-05	10.0
-2.1247559E 00	0.0	790.0	960.0	4.2305440E-03	10.0
-2.1013184E 00	0.0	430.0	200.0	4.3753572E-03	10.0
-2.1010742E 00	20.0	610.0	0.0	1.4953315E-05	10.0
-2.0971680E 00	20.0	610.0	10.0	4.4843939E-05	10.0
-2.0603027E 00	0.0	430.0	170.0	3.8116274E-03	-10.0
-2.0556641E 00	10.0	500.0	490.0	2.6543427E-03	10.0
-2.0534668E 00	10.0	540.0	890.0	1.7838662E-03	10.0
-1.9985352E 00	10.0	760.0	520.0	2.6659730E-03	-10.0
-1.9919434E 00	20.0	620.0	120.0	3.6359485E-04	-10.0
-1.9760742E 00	10.0	550.0	920.0	1.6729105E-03	-10.0
-1.9670410E 00	20.0	650.0	70.0	2.2207499E-04	-10.0

-1.9599609E 00	10.0	520.0	740.0	2.3007228E-03	10.0
-1.9506836E 00	20.0	650.0	90.0	2.7959771E-04	10.0
-1.9204102E 00	20.0	620.0	140.0	4.1773543E-04	10.0
-1.8730469E 00	0.0	460.0	870.0	5.1510222E-03	-10.0
-1.8273926E 00	20.0	640.0	130.0	3.9086933E-04	-10.0
-1.7868652E 00	20.0	640.0	150.0	4.4416660E-04	10.0
-1.7858887E 00	10.0	490.0	240.0	1.8261259E-03	10.0
-1.7827148E 00	10.0	770.0	400.0	2.5085532E-03	10.0
-1.7536621E 00	10.0	780.0	160.0	1.3037813E-03	10.0
-1.6977539E 00	20.0	630.0	140.0	4.1773543E-04	-10.0
-1.6704102E 00	20.0	650.0	60.0	1.9254520E-04	-10.0
-1.6582031E 00	20.0	650.0	80.0	2.5096908E-04	10.0
-1.6540527E 00	0.0	800.0	860.0	5.2523389E-03	-10.0
-1.6337891E 00	20.0	630.0	160.0	4.7013699E-04	10.0
-1.6081543E 00	0.0	810.0	780.0	6.0250359E-03	10.0
-1.5827637E 00	0.0	840.0	320.0	6.1940886E-03	10.0
-1.5397949E 00	0.0	430.0	190.0	4.1916631E-03	10.0
-1.5375977E 00	10.0	490.0	210.0	1.6423701E-03	-10.0
-1.5336914E 00	10.0	720.0	850.0	1.9302722E-03	10.0
-1.5239258E 00	20.0	620.0	110.0	3.3593546E-04	-10.0
-1.5202637E 00	10.0	780.0	140.0	1.1584614E-03	-10.0
-1.5136719E 00	10.0	750.0	620.0	2.5862858E-03	-10.0
-1.5012207E 00	0.0	430.0	160.0	3.6156378E-03	-10.0
-1.4916992E 00	0.0	440.0	560.0	7.3624179E-03	10.0
-1.4616699E 00	10.0	500.0	460.0	2.6246309E-03	-10.0
-1.4567871E 00	0.0	830.0	510.0	7.3879436E-03	-10.0
-1.4562988E 00	20.0	620.0	130.0	3.9086933E-04	10.0
-1.4277344E 00	10.0	730.0	790.0	2.1406766E-03	10.0
-1.4130859E 00	20.0	650.0	50.0	1.6361043E-04	-10.0
-1.4045410E 00	20.0	650.0	70.0	2.2207499E-04	10.0
-1.4025879E 00	10.0	740.0	720.0	2.3592471E-03	10.0
-1.3200684E 00	20.0	640.0	120.0	3.8359485E-04	-10.0
-1.2856445E 00	0.0	440.0	530.0	7.3932633E-03	-10.0
-1.2797852E 00	20.0	640.0	140.0	4.1773543E-04	10.0
-1.2363281E 00	10.0	770.0	380.0	2.4526913E-03	-10.0
-1.1945801E 00	20.0	650.0	40.0	1.3410153E-04	-10.0
-1.1860352E 00	20.0	650.0	60.0	1.9254520E-04	10.0
-1.1650391E 00	10.0	530.0	820.0	2.0373606E-03	10.0
-1.1555176E 00	20.0	630.0	130.0	3.9086933E-04	-10.0
-1.1542969E 00	10.0	510.0	630.0	2.5693855E-03	10.0
-1.1315918E 00	10.0	780.0	150.0	1.2317603E-03	10.0
-1.0954590E 00	20.0	630.0	150.0	4.4416660E-04	10.0
-1.0947266E 00	20.0	620.0	100.0	3.0793087E-04	-10.0
-1.0866699E 00	0.0	820.0	650.0	7.0199333E-03	-10.0
-1.0854492E 00	10.0	710.0	900.0	1.7469209E-03	10.0
-1.0622559E 00	10.0	490.0	230.0	1.7666195E-03	10.0
-1.0310059E 00	20.0	620.0	120.0	3.6359485E-04	10.0
-1.0109863E 00	20.0	650.0	30.0	1.0444982E-04	-10.0
-1.0085449E 00	0.0	430.0	180.0	4.0036961E-03	10.0
-1.0029297E 00	20.0	650.0	50.0	1.6361043E-04	10.0
-9.7216797E-01	0.0	430.0	150.0	3.4159098E-03	-10.0
-9.1333008E-01	10.0	780.0	130.0	1.0839568E-03	-10.0
-8.9183594E-01	10.0	720.0	830.0	2.0020164E-03	-10.0
-8.6279297E-01	20.0	650.0	20.0	7.4666701E-05	-10.0
-8.5717773E-01	0.0	840.0	300.0	5.9447587E-03	-10.0
-8.5473633E-01	20.0	650.0	40.0	1.3410153E-04	10.0
-8.4423828E-01	20.0	640.0	110.0	3.3593946E-04	-10.0
-8.2885742E-01	10.0	520.0	710.0	2.3871143E-03	-10.0
-8.2495117E-01	10.0	490.0	200.0	1.5777324E-03	-10.0
-8.0786133E-01	20.0	640.0	130.0	3.9086933E-04	10.0
-7.4951172E-01	20.0	650.0	10.0	4.4843939E-05	-10.0
-7.4536133E-01	20.0	650.0	30.0	1.0444982E-04	10.0
-7.2680664E-01	10.0	730.0	770.0	2.2067814E-03	-10.0
-7.1777344E-01	10.0	550.0	940.0	1.5950091E-03	10.0
-7.0385742E-01	0.0	470.0	980.0	4.0266221E-03	-10.0
-6.9677734E-01	20.0	620.0	90.0	2.7959771E-04	-10.0

-6.7675781E-01	10.0	740.0	700.0	2.4139807E-03	-10.0
-6.7529297E-01	20.0	650.0	20.0	7.4686701E-05	10.0
-6.4819336E-01	20.0	630.0	120.0	3.6359485E-04	-10.0
-6.4111328E-01	20.0	620.0	110.0	3.3593946E-04	10.0
-6.4013672E-01	20.0	650.0	10.0	4.4843939E-05	10.0
-6.4013672E-01	20.0	650.0	0.0	1.4953315E-05	10.0
-5.9228516E-01	20.0	630.0	140.0	4.1773543E-04	10.0
-5.7617188E-01	0.0	450.0	750.0	6.2956363E-03	10.0
-5.5053711E-01	10.0	780.0	140.0	1.1584614E-03	10.0
-5.2905273E-01	10.0	760.0	530.0	2.6659744E-03	10.0
-5.1855469E-01	10.0	500.0	480.0	2.6464842E-03	10.0
-5.0781250E-01	0.0	430.0	170.0	3.8116274E-03	10.0
-5.0610352E-01	10.0	710.0	880.0	1.8207177E-03	-10.0
-5.0244141E-01	0.0	790.0	940.0	4.4343621E-03	-10.0
-4.8901367E-01	10.0	560.0	960.0	1.5255134E-03	-10.0
-4.7338867E-01	0.0	430.0	140.0	3.2126382E-03	-10.0
-4.0722656E-01	20.0	640.0	100.0	3.0793087E-04	-10.0
-4.0625000E-01	10.0	540.0	860.0	1.8939676E-03	-10.0
-3.7475586E-01	20.0	640.0	120.0	3.6359485E-04	10.0
-3.7060547E-01	10.0	490.0	220.0	1.7053506E-03	10.0
-3.6816406E-01	0.0	830.0	520.0	7.3932596E-03	10.0
-3.4741211E-01	10.0	780.0	120.0	1.0083192E-03	-10.0
-3.3789063E-01	20.0	620.0	80.0	2.5096908E-04	-10.0
-3.1787109E-01	10.0	690.0	980.0	1.4527014E-03	10.0
-2.9101563E-01	10.0	510.0	600.0	2.6155838E-03	-10.0
-2.8613281E-01	20.0	620.0	100.0	3.0793087E-04	10.0
-2.3583984E-01	0.0	840.0	310.0	6.0722865E-03	10.0
-1.9018555E-01	10.0	770.0	390.0	2.4817016E-03	10.0
-1.8066406E-01	0.0	450.0	720.0	6.5426491E-03	-10.0
-1.8017578E-01	20.0	630.0	110.0	3.3593946E-04	-10.0
-1.4428711E-01	10.0	490.0	190.0	1.5114930E-03	-10.0
-1.2817383E-01	20.0	630.0	130.0	3.9086933E-04	10.0
-1.0522461E-01	0.0	810.0	760.0	6.2087439E-03	-10.0
-3.7109375E-02	0.0	430.0	160.0	3.6456378E-03	10.0
-1.3916016E-02	20.0	620.0	70.0	2.2207499E-04	-10.0
-1.0498047E-02	10.0	780.0	130.0	1.0839568E-03	10.0
-5.3710937E-03	20.0	640.0	90.0	2.7959771E-04	-10.0
-4.8828125E-03	0.0	430.0	130.0	3.0060220E-03	-10.0
2.6855469E-02	20.0	640.0	110.0	3.3593946E-04	10.0
3.3691406E-02	20.0	620.0	90.0	2.7959771E-04	10.0
6.2744141E-02	10.0	500.0	450.0	2.6107905E-03	-10.0
6.5580078E-02	10.0	690.0	960.0	1.5255134E-03	-10.0
1.3256836E-01	10.0	760.0	510.0	2.6640561E-03	-10.0
1.7749023E-01	0.0	440.0	550.0	7.3777363E-03	10.0
1.7773438E-01	10.0	780.0	110.0	9.3162502E-04	-10.0
2.2460938E-01	10.0	530.0	790.0	2.1406766E-03	-10.0
2.5683594E-01	20.0	630.0	100.0	3.0793087E-04	-10.0
2.7319336E-01	0.0	460.0	890.0	4.9470067E-03	10.0
2.7490234E-01	20.0	620.0	60.0	1.9294520E-04	-10.0
2.8930664E-01	10.0	490.0	210.0	1.6423701E-03	10.0
2.9101563E-01	10.0	750.0	630.0	2.5693895E-03	10.0
3.0493164E-01	20.0	630.0	120.0	3.6359485E-04	10.0
3.1445313E-01	20.0	620.0	80.0	2.5096908E-04	10.0
3.4204102E-01	10.0	770.0	370.0	2.4215234E-03	-10.0
3.5424805E-01	0.0	820.0	660.0	6.9616027E-03	10.0
3.6132813E-01	20.0	640.0	80.0	2.5096908E-04	-10.0
3.7963867E-01	0.0	440.0	520.0	7.3932596E-03	-10.0
3.8574219E-01	20.0	640.0	100.0	3.0793087E-04	10.0
4.0161133E-01	0.0	800.0	870.0	5.1510222E-03	10.0
4.0307617E-01	0.0	430.0	150.0	3.4159098E-03	10.0
4.2602539E-01	10.0	520.0	730.0	2.3304315E-03	10.0
4.3310547E-01	0.0	430.0	120.0	2.7962646E-03	-10.0
4.3457031E-01	10.0	700.0	940.0	1.5990091E-03	10.0
4.6679688E-01	0.0	840.0	290.0	5.8115870E-03	-10.0
4.8876953E-01	10.0	780.0	120.0	1.0083192E-03	10.0
5.0488281E-01	10.0	490.0	180.0	1.4437132E-03	-10.0

5.2832031E-01	20.0	620.0	50.0	1.6361043E-04	-10.0
5.6420898E-01	20.0	620.0	70.0	2.2267499E-04	10.0
6.5478516E-01	20.0	630.0	90.0	2.7959771E-04	-10.0
6.6186523E-01	10.0	780.0	100.0	8.5395179E-04	-10.0
6.8920898E-01	20.0	640.0	70.0	2.2267499E-04	-10.0
6.9873047E-01	20.0	630.0	110.0	3.3553946E-04	10.0
7.0166016E-01	10.0	560.0	980.0	1.4527014E-03	10.0
7.1337891E-01	20.0	640.0	90.0	2.7959771E-04	10.0
7.4682617E-01	20.0	620.0	40.0	1.3410153E-04	-10.0
7.5048828E-01	10.0	680.0	950.0	1.4166317E-03	-10.0
7.5585938E-01	0.0	830.0	500.0	7.3772222E-03	-10.0
7.7490234E-01	20.0	620.0	60.0	1.9294520E-04	10.0
8.1298828E-01	0.0	430.0	140.0	3.2126382E-03	10.0
8.4082031E-01	0.0	430.0	110.0	2.5835771E-03	-10.0
8.4960938E-01	10.0	510.0	620.0	2.5862858E-03	10.0
8.8403320E-01	0.0	460.0	860.0	5.2523389E-03	-10.0
8.8452148E-01	10.0	540.0	880.0	1.8207177E-03	10.0
9.1699219E-01	10.0	490.0	200.0	1.5777324E-03	10.0
9.2626953E-01	10.0	700.0	920.0	1.6729105E-03	-10.0
9.2651367E-01	20.0	620.0	30.0	1.0444982E-04	-10.0
9.4702148E-01	10.0	780.0	110.0	9.3162502E-04	10.0
9.5019531E-01	20.0	620.0	50.0	1.6361043E-04	10.0
9.8193359E-01	20.0	640.0	60.0	1.9294520E-04	-10.0
9.8583984E-01	10.0	500.0	470.0	2.6365893E-03	10.0
1.0019531E 00	10.0	750.0	610.0	2.6017006E-03	-10.0
1.0019531E 00	20.0	640.0	80.0	2.5056908E-04	10.0
1.0175781E 00	20.0	630.0	80.0	2.5056908E-04	-10.0
1.0576172E 00	20.0	630.0	100.0	3.0763087E-04	10.0
1.0681152E 00	0.0	840.0	300.0	5.9447587E-03	10.0
1.0708008E 00	20.0	620.0	20.0	7.4686701E-05	-10.0
1.0905762E 00	20.0	620.0	40.0	1.3410153E-04	10.0
1.1049805E 00	10.0	780.0	90.0	7.7527843E-04	-10.0
1.1218262E 00	10.0	490.0	170.0	1.3744540E-03	-10.0
1.1684570E 00	10.0	550.0	910.0	1.7059218E-03	-10.0
1.1840820E 00	20.0	620.0	10.0	4.4843939E-05	-10.0
1.1928711E 00	0.0	430.0	130.0	3.0060220E-03	10.0
1.1960449E 00	20.0	620.0	30.0	1.0444982E-04	10.0
1.2185059E 00	0.0	430.0	100.0	2.3681736E-03	-10.0
1.2353516E 00	20.0	640.0	50.0	1.6361043E-04	-10.0
1.2556152E 00	20.0	640.0	70.0	2.2267499E-04	10.0
1.2661133E 00	20.0	620.0	20.0	7.4686701E-05	10.0
1.2934570E 00	20.0	620.0	0.0	1.4953315E-05	10.0
1.2973633E 00	20.0	620.0	10.0	4.4843939E-05	10.0
1.3415527E 00	20.0	630.0	70.0	2.2267499E-04	-10.0
1.3613281E 00	10.0	770.0	380.0	2.4526913E-03	10.0
1.3642578E 00	10.0	780.0	100.0	8.5395179E-04	10.0
1.3774414E 00	20.0	630.0	90.0	2.7959771E-04	10.0
1.4211426E 00	10.0	740.0	710.0	2.3871143E-03	10.0
1.4577637E 00	20.0	640.0	40.0	1.3410153E-04	-10.0
1.4741211E 00	20.0	640.0	60.0	1.9294520E-04	10.0
1.5070801E 00	10.0	780.0	80.0	6.9598597E-04	-10.0
1.5126953E 00	10.0	530.0	810.0	2.0722842E-03	10.0
1.5129395E 00	10.0	490.0	190.0	1.5114930E-03	10.0
1.5422363E 00	0.0	430.0	120.0	2.7962646E-03	10.0
1.5458984E 00	10.0	520.0	700.0	2.4139807E-03	-10.0
1.5549316E 00	10.0	500.0	440.0	2.5944465E-03	-10.0
1.5656738E 00	0.0	430.0	90.0	2.1502748E-03	-10.0
1.5747070E 00	10.0	760.0	520.0	2.6659730E-03	10.0
1.5903320E 00	10.0	570.0	990.0	1.4166317E-03	-10.0
1.6342773E 00	20.0	630.0	60.0	1.9294520E-04	-10.0
1.6413574E 00	20.0	640.0	30.0	1.0444982E-04	-10.0
1.6452637E 00	0.0	810.0	770.0	6.1198324E-03	10.0
1.6491699E 00	10.0	730.0	780.0	2.1740408E-03	10.0
1.6533203E 00	20.0	640.0	50.0	1.6361043E-04	10.0
1.6660156E 00	20.0	630.0	80.0	2.5056908E-04	10.0
1.6970215E 00	0.0	450.0	740.0	6.3803494E-03	10.0

1.7011719E 00	10.0	510.0	590.0	2.6278887E-03	-10.0
1.7041016E 00	0.0	820.0	640.0	7.0745870E-03	-10.0
1.7070313E 00	10.0	490.0	160.0	1.3037813E-03	-10.0
1.7404785E 00	10.0	780.0	90.0	7.7537843E-04	10.0
1.7475586E 00	0.0	840.0	280.0	5.6728497E-03	-10.0
1.7531738E 00	10.0	720.0	840.0	1.9663055E-03	10.0
1.7856445E 00	20.0	640.0	20.0	7.4686701E-05	-10.0
1.7976074E 00	20.0	640.0	40.0	1.3410153E-04	10.0
1.8159180E 00	0.0	440.0	540.0	7.3880553E-03	10.0
1.8234863E 00	0.0	830.0	510.0	7.3879436E-03	10.0
1.8269043E 00	0.0	790.0	950.0	4.3322630E-03	10.0
1.8613281E 00	0.0	430.0	110.0	2.5835771E-03	10.0
1.8681641E 00	10.0	780.0	70.0	6.1585684E-04	-10.0
1.8798828E 00	10.0	770.0	360.0	2.3882012E-03	-10.0
1.8828125E 00	0.0	430.0	80.0	1.9301041E-03	-10.0
1.8876953E 00	20.0	630.0	50.0	1.6361043E-04	-10.0
1.8989258E 00	20.0	640.0	10.0	4.4843939E-05	-10.0
1.9030762E 00	20.0	640.0	30.0	1.0444982E-04	10.0
1.9157715E 00	20.0	630.0	70.0	2.2207499E-04	10.0
1.9736328E 00	0.0	800.0	850.0	5.3530186E-03	-10.0
1.9770508E 00	20.0	640.0	20.0	7.4686701E-05	10.0
2.0083008E 00	20.0	640.0	0.0	1.4953315E-05	10.0
2.0122070E 00	20.0	640.0	10.0	4.4843939E-05	10.0
2.0144043E 00	0.0	440.0	510.0	7.3879436E-03	-10.0
2.0756836E 00	10.0	780.0	80.0	6.9598597E-04	10.0
2.0769043E 00	10.0	490.0	180.0	1.4427132E-03	10.0
2.0874023E 00	0.0	450.0	710.0	6.6159303E-03	-10.0
2.1062012E 00	20.0	630.0	40.0	1.3410153E-04	-10.0
2.1303711E 00	20.0	630.0	60.0	1.9254520E-04	10.0
2.1391602E 00	10.0	740.0	650.0	2.4397874E-03	-10.0
2.1501465E 00	0.0	430.0	100.0	2.3681736E-03	10.0
2.1694336E 00	0.0	430.0	70.0	1.7078903E-03	-10.0
2.1884766E 00	10.0	780.0	60.0	5.3507416E-04	-10.0
2.2236328E 00	10.0	760.0	500.0	2.6661502E-03	-10.0
2.2602539E 00	10.0	490.0	150.0	1.2317603E-03	-10.0
2.2897949E 00	20.0	630.0	30.0	1.0444982E-04	-10.0
2.3056641E 00	20.0	630.0	50.0	1.6361043E-04	10.0
2.3288574E 00	0.0	840.0	290.0	5.8115870E-03	10.0
2.3425293E 00	10.0	730.0	760.0	2.2388427E-03	-10.0
2.3684082E 00	10.0	710.0	850.0	1.7838662E-03	10.0
2.3698730E 00	10.0	780.0	70.0	6.1585684E-04	10.0
2.3935547E 00	10.0	720.0	820.0	2.0373606E-03	-10.0
2.4086914E 00	0.0	430.0	90.0	2.1502748E-03	10.0
2.4187012E 00	10.0	550.0	930.0	1.6359277E-03	10.0
2.4235840E 00	0.0	470.0	970.0	4.1293018E-03	-10.0
2.4257812E 00	0.0	430.0	60.0	1.4838646E-03	-10.0
2.4340820E 00	20.0	630.0	20.0	7.4686701E-05	-10.0
2.4499512E 00	20.0	630.0	40.0	1.3410153E-04	10.0
2.4582520E 00	10.0	500.0	460.0	2.6246309E-03	10.0
2.4677734E 00	10.0	780.0	50.0	4.5372313E-04	-10.0
2.5092773E 00	10.0	540.0	850.0	1.9302722E-03	-10.0
2.5473633E 00	20.0	630.0	10.0	4.4843939E-05	-10.0
2.5554199E 00	20.0	630.0	30.0	1.0444982E-04	10.0
2.6088867E 00	10.0	490.0	170.0	1.3746540E-03	10.0
2.6232910E 00	10.0	780.0	60.0	5.3507416E-04	10.0
2.6254883E 00	20.0	630.0	20.0	7.4686701E-05	10.0
2.6369629E 00	0.0	430.0	80.0	1.9301041E-03	10.0
2.6520996E 00	0.0	430.0	50.0	1.2582627E-03	-10.0
2.6567383E 00	20.0	630.0	0.0	1.4953315E-05	10.0
2.6606445E 00	20.0	630.0	10.0	4.4843939E-05	10.0
2.7060547E 00	10.0	780.0	40.0	3.7188944E-04	-10.0
2.7792969E 00	10.0	750.0	620.0	2.5862858E-03	10.0
2.7810059E 00	10.0	520.0	720.0	2.3592471E-03	10.0
2.7814941E 00	10.0	490.0	140.0	1.1584614E-03	-10.0
2.8222656E 00	10.0	560.0	950.0	1.5621928E-03	-10.0
2.8261719E 00	10.0	510.0	610.0	2.6017006E-03	10.0

2.8347168E 00	0.0	430.0	70.0	1.7078903E-03	10.0
2.8356934E 00	10.0	780.0	50.0	4.5372313E-04	10.0
2.8479004E 00	0.0	430.0	40.0	1.0313215E-03	-10.0
2.8723145E 00	10.0	770.0	370.0	2.4215234E-03	10.0
2.8835449E 00	10.0	530.0	780.0	2.1740408E-03	-10.0
2.9033203E 00	10.0	780.0	30.0	2.8965948E-04	-10.0
2.9255371E 00	0.0	830.0	490.0	7.3610060E-03	-10.0
2.9401855E 00	10.0	710.0	870.0	1.8574332E-03	-10.0
2.9853516E 00	0.0	840.0	270.0	5.5286400E-03	-10.0
3.0026855E 00	0.0	430.0	60.0	1.4838646E-03	10.0
3.0063477E 00	0.0	460.0	880.0	5.0492026E-03	10.0
3.0070801E 00	10.0	780.0	40.0	3.7188944E-04	10.0
3.0134277E 00	0.0	430.0	30.0	8.0328202E-04	-10.0
3.0148926E 00	10.0	500.0	430.0	2.5761828E-03	-10.0
3.0595703E 00	10.0	780.0	20.0	2.0712068E-04	-10.0
3.1093750E 00	10.0	490.0	160.0	1.3037813E-03	10.0
3.1232910E 00	0.0	820.0	650.0	7.0199333E-03	10.0
3.1284180E 00	0.0	810.0	750.0	6.2956363E-03	-10.0
3.1374512E 00	10.0	780.0	30.0	2.8965948E-04	10.0
3.1401367E 00	0.0	430.0	50.0	1.2582627E-03	10.0
3.1484375E 00	0.0	430.0	20.0	5.7438575E-04	-10.0
3.1752930E 00	10.0	780.0	10.0	1.2436091E-04	-10.0
3.2268066E 00	10.0	780.0	20.0	2.0712068E-04	10.0
3.2470703E 00	0.0	430.0	40.0	1.0313215E-03	10.0
3.2536621E 00	0.0	430.0	10.0	3.4487690E-04	-10.0
3.2707520E 00	10.0	490.0	130.0	1.0839568E-03	-10.0
3.2753906E 00	10.0	780.0	10.0	1.2436091E-04	10.0
3.2829590E 00	10.0	780.0	0.0	4.1468433E-05	10.0
3.3239746E 00	0.0	430.0	30.0	8.0328202E-04	10.0
3.3703613E 00	0.0	430.0	20.0	5.7438575E-04	10.0
3.3725586E 00	0.0	430.0	0.0	1.1499999E-04	10.0
3.3769531E 00	10.0	770.0	350.0	2.3527306E-03	-10.0
3.3793945E 00	10.0	690.0	970.0	1.4890060E-03	10.0
3.3867188E 00	0.0	430.0	10.0	3.4487690E-04	10.0
3.4238281E 00	0.0	440.0	530.0	7.3932633E-03	10.0
3.4296875E 00	0.0	790.0	930.0	4.5367442E-03	-10.0
3.4785156E 00	10.0	750.0	600.0	2.6155838E-03	-10.0
3.5466309E 00	0.0	840.0	280.0	5.6728497E-03	10.0
3.5773926E 00	10.0	490.0	150.0	1.2317603E-03	10.0
3.6101074E 00	0.0	460.0	850.0	5.3530186E-03	-10.0
3.6186523E 00	0.0	440.0	500.0	7.3772222E-03	-10.0
3.6379395E 00	10.0	760.0	510.0	2.6640561E-03	10.0
3.6621094E 00	10.0	510.0	580.0	2.6385640E-03	-10.0
3.7282715E 00	10.0	490.0	120.0	1.0083192E-03	-10.0
3.7675781E 00	10.0	690.0	950.0	1.5621928E-03	-10.0
3.7878418E 00	10.0	540.0	870.0	1.8574332E-03	10.0
3.8852539E 00	10.0	520.0	690.0	2.4397874E-03	-10.0
3.8986816E 00	10.0	500.0	450.0	2.6105905E-03	10.0
3.9396973E 00	0.0	450.0	730.0	6.4627379E-03	10.0
3.9726563E 00	0.0	830.0	500.0	7.3772222E-03	10.0
4.0004883E 00	10.0	560.0	970.0	1.4890060E-03	10.0
4.0058594E 00	0.0	800.0	860.0	5.2523389E-03	10.0
4.0124512E 00	10.0	700.0	930.0	1.6359277E-03	10.0
4.0136719E 00	10.0	490.0	140.0	1.1584614E-03	10.0
4.1538086E 00	10.0	490.0	110.0	9.3162502E-04	-10.0
4.1557617E 00	10.0	530.0	800.0	2.1067390E-03	10.0
4.1801758E 00	0.0	840.0	260.0	5.3790510E-03	-10.0
4.2060547E 00	10.0	740.0	700.0	2.4139807E-03	10.0
4.2744141E 00	10.0	760.0	490.0	2.6543427E-03	-10.0
4.2817383E 00	10.0	550.0	900.0	1.7465209E-03	-10.0
4.3242188E 00	0.0	450.0	700.0	6.6944361E-03	-10.0
4.3427734E 00	10.0	770.0	360.0	2.3882012E-03	10.0
4.4182129E 00	10.0	490.0	130.0	1.0839568E-03	10.0
4.4426270E 00	10.0	500.0	420.0	2.5557871E-03	-10.0
4.4523926E 00	0.0	820.0	630.0	7.1254149E-03	-10.0
4.4965820E 00	10.0	700.0	910.0	1.7099218E-03	-10.0

4.5297852E 00	10.0	680.0	980.0	1.4527014E-03	-10.0
4.5476074E 00	10.0	490.0	100.0	8.5355179E-04	-10.0
4.6872559E 00	10.0	730.0	770.0	2.2067814E-03	10.0
4.6882324E 00	0.0	470.0	990.0	3.9265943E-03	10.0
4.7214355E 00	0.0	840.0	270.0	5.5286400E-03	10.0
4.7675781E 00	10.0	510.0	600.0	2.6155838E-03	10.0
4.7905273E 00	10.0	490.0	120.0	1.0083192E-03	10.0
4.8334961E 00	10.0	770.0	340.0	2.3151245E-03	-10.0
4.8564453E 00	0.0	810.0	760.0	6.2087439E-03	10.0
4.9091797E 00	10.0	490.0	90.0	7.7537843E-04	-10.0
4.9125977E 00	10.0	740.0	680.0	2.4644830E-03	-10.0
5.0009766E 00	10.0	720.0	830.0	2.0020164E-03	10.0
5.0012207E 00	0.0	440.0	520.0	7.3932596E-03	10.0
5.0336914E 00	10.0	570.0	980.0	1.4527014E-03	-10.0
5.0527344E 00	0.0	830.0	480.0	7.3952130E-03	-10.0
5.1047363E 00	10.0	520.0	710.0	2.3811143E-03	10.0
5.1311035E 00	10.0	490.0	110.0	9.3162502E-04	10.0
5.1921387E 00	0.0	440.0	450.0	7.3610060E-03	-10.0
5.2246094E 00	10.0	750.0	610.0	2.6017006E-03	10.0
5.2390137E 00	10.0	490.0	80.0	6.9558597E-04	-10.0
5.3066406E 00	10.0	500.0	440.0	2.5944465E-03	10.0
5.3315430E 00	0.0	840.0	250.0	5.2241981E-03	-10.0
5.3688965E 00	10.0	730.0	750.0	2.2701756E-03	-10.0
5.3937988E 00	10.0	540.0	840.0	1.9663055E-03	-10.0
5.4399414E 00	10.0	490.0	100.0	8.5355179E-04	10.0
5.5075684E 00	10.0	530.0	770.0	2.2067814E-03	-10.0
5.5161133E 00	10.0	550.0	920.0	1.6729105E-03	10.0
5.5236816E 00	0.0	470.0	960.0	4.2305440E-03	-10.0
5.5368652E 00	10.0	490.0	70.0	6.1585684E-04	-10.0
5.5593262E 00	0.0	800.0	840.0	5.4529458E-03	-10.0
5.5920410E 00	10.0	510.0	570.0	2.6475668E-03	-10.0
5.6337891E 00	10.0	720.0	810.0	2.0722842E-03	-10.0
5.6611328E 00	10.0	760.0	500.0	2.6601902E-03	10.0
5.7082520E 00	0.0	460.0	870.0	5.1510222E-03	10.0
5.7165527E 00	10.0	490.0	90.0	7.7537843E-04	10.0
5.7358398E 00	0.0	790.0	940.0	4.4343621E-03	10.0
5.7727051E 00	10.0	770.0	350.0	2.3527306E-03	10.0
5.7829590E 00	10.0	710.0	880.0	1.8207177E-03	10.0
5.8027344E 00	10.0	490.0	60.0	5.3507416E-04	-10.0
5.8381348E 00	10.0	500.0	410.0	2.5332463E-03	-10.0
5.8503418E 00	0.0	820.0	640.0	7.0745870E-03	10.0
5.8530273E 00	0.0	840.0	260.0	5.3750510E-03	10.0
5.9121094E 00	10.0	750.0	590.0	2.6278887E-03	-10.0
5.9614258E 00	10.0	490.0	80.0	6.9598597E-04	10.0
6.0368652E 00	10.0	490.0	50.0	4.5372313E-04	-10.0
6.0788574E 00	0.0	830.0	490.0	7.3610060E-03	10.0
6.0986328E 00	10.0	560.0	940.0	1.5990091E-03	-10.0
6.1513672E 00	0.0	450.0	720.0	6.5426491E-03	10.0
6.1740723E 00	10.0	490.0	70.0	6.1585684E-04	10.0
6.1938477E 00	10.0	520.0	680.0	2.4644830E-03	-10.0
6.2390137E 00	10.0	490.0	40.0	3.7188944E-04	-10.0
6.2495117E 00	10.0	770.0	330.0	2.2753943E-03	-10.0
6.2849121E 00	10.0	760.0	480.0	2.6464842E-03	-10.0
6.3046875E 00	0.0	460.0	840.0	5.4529458E-03	-10.0
6.3200684E 00	0.0	810.0	740.0	6.3803494E-03	-10.0
6.3476562E 00	10.0	710.0	860.0	1.8939676E-03	-10.0
6.3552246E 00	10.0	490.0	60.0	5.3507416E-04	10.0
6.4091797E 00	10.0	490.0	30.0	2.8965948E-04	-10.0
6.4401855E 00	0.0	840.0	240.0	5.0642006E-03	-10.0
6.5043945E 00	10.0	490.0	50.0	4.5372313E-04	10.0
6.5302734E 00	0.0	450.0	690.0	6.7660026E-03	-10.0
6.5473633E 00	10.0	490.0	20.0	2.0712068E-04	-10.0
6.5480957E 00	0.0	440.0	510.0	7.3879436E-03	10.0
6.6213379E 00	10.0	490.0	40.0	3.7188944E-04	10.0
6.6538086E 00	10.0	490.0	10.0	1.2436091E-04	-10.0
6.6562500E 00	10.0	540.0	860.0	1.8939676E-03	10.0

6.6777344E 00	10.0	510.0	590.0	2.6278887E-03	10.0
6.6823730E 00	10.0	500.0	430.0	2.5761828E-03	10.0
6.7065430E 00	10.0	490.0	30.0	2.8965948E-04	10.0
6.7353516E 00	0.0	440.0	480.0	7.3352130E-03	-10.0
6.7597656E 00	10.0	490.0	20.0	2.0712068E-04	10.0
6.7675781E 00	10.0	530.0	790.0	2.1406766E-03	10.0
6.7707520E 00	10.0	490.0	0.0	4.1468433E-05	10.0
6.7812500E 00	10.0	490.0	10.0	1.2436091E-04	10.0
6.9414062E 00	0.0	840.0	250.0	5.2241981E-03	10.0
6.9516602E 00	10.0	740.0	690.0	2.4357874E-03	10.0
7.0422363E 00	10.0	690.0	960.0	1.5255134E-03	10.0
7.1367187E 00	0.0	830.0	470.0	7.3117726E-03	-10.0
7.1584473E 00	0.0	820.0	620.0	7.1722716E-03	-10.0
7.1618652E 00	10.0	770.0	340.0	2.3151245E-03	10.0
7.2016602E 00	10.0	500.0	400.0	2.5085532E-03	-10.0
7.2648926E 00	10.0	560.0	960.0	1.5255134E-03	10.0
7.3208008E 00	0.0	790.0	920.0	4.6353052E-03	-10.0
7.3605957E 00	10.0	550.0	890.0	1.7838662E-03	-10.0
7.3935547E 00	10.0	520.0	700.0	2.4139807E-03	10.0
7.4228516E 00	10.0	690.0	940.0	1.5550091E-03	-10.0
7.4865723E 00	10.0	510.0	560.0	2.6548516E-03	-10.0
7.5058594E 00	0.0	840.0	230.0	4.8551777E-03	-10.0
7.5512695E 00	10.0	700.0	920.0	1.6729105E-03	10.0
7.5688477E 00	0.0	800.0	850.0	5.3530186E-03	10.0
7.6247559E 00	10.0	770.0	320.0	2.2325579E-03	-10.0
7.6308594E 00	10.0	750.0	600.0	2.6155838E-03	10.0
7.6437988E 00	10.0	760.0	490.0	2.6543427E-03	10.0
7.6467285E 00	10.0	740.0	670.0	2.4880113E-03	-10.0
7.6862793E 00	10.0	730.0	760.0	2.2388427E-03	10.0
7.7609863E 00	0.0	470.0	980.0	4.0286221E-03	10.0
7.9870605E 00	0.0	840.0	240.0	5.0642006E-03	10.0
8.0004883E 00	10.0	680.0	990.0	1.4166317E-03	10.0
8.0253906E 00	0.0	810.0	750.0	6.2956363E-03	10.0
8.0261230E 00	10.0	500.0	420.0	2.5557871E-03	10.0
8.0317383E 00	10.0	700.0	900.0	1.7469209E-03	-10.0
8.0644531E 00	0.0	440.0	500.0	7.3772222E-03	10.0
8.1003418E 00	10.0	530.0	760.0	2.2388427E-03	-10.0
8.1425781E 00	0.0	830.0	480.0	7.3352130E-03	10.0
8.2060547E 00	10.0	720.0	920.0	2.0373606E-03	10.0
8.2431641E 00	10.0	540.0	830.0	2.0020164E-03	-10.0
8.2475586E 00	0.0	440.0	470.0	7.3117726E-03	-10.0
8.2548828E 00	10.0	760.0	470.0	2.6365893E-03	-10.0
8.2700195E 00	10.0	680.0	970.0	1.4890060E-03	-10.0
8.3066406E 00	10.0	750.0	580.0	2.6385640E-03	-10.0
8.3322754E 00	0.0	450.0	710.0	6.6199303E-03	10.0
8.3564453E 00	10.0	730.0	740.0	2.3007228E-03	-10.0
8.3791504E 00	0.0	460.0	860.0	5.2523389E-03	10.0
8.4418945E 00	10.0	570.0	970.0	1.4890060E-03	-10.0
8.4670410E 00	10.0	520.0	670.0	2.4880113E-03	-10.0
8.5100098E 00	10.0	770.0	330.0	2.2753943E-03	10.0
8.5280762E 00	0.0	840.0	220.0	4.7292672E-03	-10.0
8.5329590E 00	10.0	500.0	390.0	2.4817016E-03	-10.0
8.5344238E 00	0.0	820.0	630.0	7.1254149E-03	10.0
8.5566406E 00	10.0	510.0	580.0	2.6385640E-03	10.0
8.5825195E 00	10.0	550.0	910.0	1.7099218E-03	10.0
8.5886230E 00	0.0	470.0	950.0	4.3322630E-03	-10.0
8.7058105E 00	0.0	450.0	680.0	6.8344884E-03	-10.0
8.8354492E 00	10.0	720.0	800.0	2.1067390E-03	-10.0
8.9592285E 00	10.0	770.0	310.0	2.1896367E-03	-10.0
8.9685059E 00	0.0	460.0	830.0	5.5519789E-03	-10.0
8.9892578E 00	0.0	840.0	230.0	4.8951777E-03	10.0
9.1037598E 00	0.0	800.0	830.0	5.5519789E-03	-10.0
9.1550293E 00	10.0	710.0	870.0	1.8574332E-03	10.0
9.1784668E 00	0.0	830.0	460.0	7.2786100E-03	-10.0
9.3374023E 00	10.0	500.0	410.0	2.5332463E-03	10.0
9.3405762E 00	10.0	560.0	930.0	1.6359277E-03	-10.0

9.3444824E	00	10.0	530.0	780.0	2.17404C8E-03	10.0
9.3537598E	00	10.0	510.0	550.0	2.66C3756E-03	-10.0
9.3562012E	00	0.0	780.0	990.0	3.9285943E-03	-10.0
9.4694824E	00	0.0	810.0	730.0	6.4627379E-03	-10.0
9.4936523E	00	10.0	540.0	850.0	1.93C2722E-03	10.0
9.5075684E	00	0.0	840.0	210.0	4.5546107E-03	-10.0
9.5239258E	00	10.0	570.0	990.0	1.4166317E-03	10.0
9.5500488E	00	0.0	440.0	490.0	7.3610060E-03	10.0
9.5864258E	00	10.0	760.0	480.0	2.6464842E-03	10.0
9.6018066E	00	0.0	790.0	930.0	4.5367442E-03	10.0
9.6508789E	00	10.0	520.0	690.0	2.4357874E-03	10.0
9.6547852E	00	10.0	740.0	680.0	2.4644830E-03	10.0
9.7163086E	00	10.0	710.0	850.0	1.93C2722E-03	-10.0
9.7294922E	00	0.0	440.0	460.0	7.2786100E-03	-10.0
9.8178711E	00	10.0	770.0	320.0	2.2335579E-03	10.0
9.8217773E	00	0.0	820.0	610.0	7.2150193E-03	-10.0
9.8320312E	00	10.0	500.0	380.0	2.4526913E-03	-10.0
9.9484863E	00	0.0	840.0	220.0	4.7252672E-03	10.0
9.9980469E	00	10.0	750.0	590.0	2.6278887E-03	10.0

REFERENCES

1. W. Honig,"Measurement of Continental Drift and Earth Movement with Lasers", Proc. IEEE, Vol. 52, p. 430, April 1964.

2. T. S. Jaseja, A. Javan and C. H. Townes,"Frequency Stability of He-Ne Masers and Measurements of Length", Physical Review Letters, Vol. 10, p. 165, 1 March 1963.

3. R. D. Moekler,"Atomic Beam Frequency Standards", Advances in Electronics and Electron Physics, Academic Press, 1961.

4. A. D. White,"Frequency Stabilization of Gas Lasers", IEEE J. of Quantum Electronics, November 1965.

5. K. Shimoda and A. Javan,"Stabilization of the He-Ne Maser on the Atomic Line Center", J. Of Applied Physics, Vol. 36, No. 3, p. 718, March 1965.

6. W. R. Bennett, Jr., S. F. Jacobs, J. T. Latourette and P. Rabinowitz,"Dispersion Characteristics and Frequency Stabilization of a Gas Laser", Applied Physics Letters, Vol. 5, p. 56, August 1964.

7. I. Tobias, M. Skolnick, R. A. Wallace and T. Polanyi, "Derivation of a Frequency-Sensitive Signal from a Gas Laser in an Axial Magnetic Field", Applied Physics Letters, Vol. 6, p. 198, May 15, 1965.

8. A. L. Bloom and D. L. Wright,"Pressure Shifts in a Stabilized Single Wavelength Helium-Neon Laser", Applied Optics, Vol. 5, No. 10, October 1966.

9. A. D. White,"Pressure- and Current-Dependent Shifts in the Center Frequency of the Doppler-Broadened ($2p_4 \rightarrow 3s_2$) 6328-A^{20} Ne Transition", Applied Physics Letters, Vol. 10, No. 1, 1 January 1967.

10. A. D. White,"Control System for Frequency Stabilizing a 6328 A Gas Laser", Review of Scientific Instruments, Vol. 38, No. 8, p. 1079, August 1967.

11. M. S. Lipsett and P. H. Lee,"Laser Wavelength Stabilization with a Passive Interferometer", Applied Optics, Vol. 5, No. 5, p. 823, May 1966.

12. A. D. White, E. I. Gordon, and E. G. Labuda,"Frequency Stabilization of Single Mode Gas Lasers", Applied Physics Letters, Vol. 5, p. 97, September 1964.

13. P. H. Lee and M. L. Skolnick,"Saturated Neon Absorption Inside a 6328 Å Laser", Applied Physics Letters, Vol. 10, No. 11, p. 303, 1 June 1967.

14. P. H. Lee, private communication.

15. N. F. Ramsey,"Molecular Beams", Oxford University Press, 1963; J. G. King and J. R. Zacharias,"Some New Applications and Techniques of Molecular Beams," Advances in Electronics and Electron Physics, Vol. 9, Academic Press, 1956.

16. N. G. Basov and V. S. Letokhov,"Atomic Beam Lasers", J. of Experimental and Theoretical Physics (JETP), p. 3, July 1965 (in English).

17. V. S. Letokhov and B. D. Pavlik,"Production of Coherent Light by Atomic or Molecular Beams", (JETP), 53, 1107, 1967 (in Russian).

18. S. Ezekiel and R. Weiss,"Long-Term Frequency Stabilization of a Laser Employing a Molecular or Atomic Beam as Primary Frequency Reference", Quarterly Progress Report No. 80, Research Laboratory of Electronics, M.I.T., p. 22, 15 January 1966.

19. C. E. Moore,"Atomic Energy Levels", Vols. 1, 2, and 3, National Bureau of Standards, Washington, Circular 467.

20. A listing of these transitions, in wavenumbers, vacuum wavelength and air wavelength, in numerical order, giving the atomic number of the atom and the energy level of the lower and upper states, will be deposited in the R.L.E. Document Room, M.I.T.

21. Further investigation showed that the energy level of the 6s state in Rubidium given in Moore's tables was in error by 1.1 cm^{-1}. This makes the match within 2.6 cm^{-1} and requires a Zeeman field of about 27kgauss.

22. O. S. Heavens,"Radiating Transition Probabilities of the Lower Excited States of the Alkali Metals", J. Optical Society of America, Vol. 51, No. 10, p. 1058, October 1961.

23. S. Ezekiel and R. Weiss,"Laser Excitation of the 5s-6s Forbidden Transition in an Atomic Beam of Rubidium", M.I.T., Research Laboratory of Electronics, Quarterly Progress Report No. 88, January 1968 (to be published).

24. J. I. Steinfeld,"Molecular Energy Transfer and Spectroscopy", M.I.T., Research Laboratory of Electronics, Quarterly Progress Report No. 86, p. 9, 15 July 1967.

25. R. Mecke,"Das Bandenspektrum des Jod", Ann. Physik, 71, 104 (1923).

26. D. H. Rank and B. S. Rao,"Molecular Constants of the Ground State of I_2", J. of Molecular Spectroscopy, 13, 34 (1964).

27. J. I. Steinfeld, R. N. Zare, L. Jones, M. Lesk, and W. Klemperer,"Spectroscopic Constants and Vibrational Assignment for the $B^3\pi_{ou}^+$ State of Iodine", J. of Chemical Physics, 42, 25 (1965).

28. L. Mathieson and A. L. G. Rees,"Electronic States and Potential Energy Diagram of the Iodine Molecule", J. of Chemical Physics, 25, p. 753 (1956).

29. G. Herzberg,"Spectra of Diatomic Molecules," Van Nostrand, 1950.

30. N. F. Ramsey,"Molecular Beams," Oxford University Press, 1963.

31. E. I. Gordon, E. F. Labuda and W. B. Bridges,"Continuous Visible Laser Action in Singly Ionized Argon, Krypton and Zenon," Applied Physics Letters, Vol. 4, p. 178, 15 May 1964.

32. W. R. Bennett, Jr., G. N. Mercer, P. J. Kindlmann, B. Wexler, and H. Hyman,"Direct Electron Excitation Cross Sections Pertinent to the Argon Ion Laser," Physical Review Letters, Vol. 17, p. 987, 7 November 1966.

33. E. F. Labuda, E. I. Gordon and R. C. Miller,"Continuous-Duty Argon Ion Lasers," IEEE J. of Quantum Electronics, Vol. QE-1, No. 6, p. 273, September 1965.

34. E. A. Ballik, W. R. Bennett, Jr., and G. N. Mercer, "Temperatures, Lorentzian Widths, and Drift Velocities in the Argon-Ion Laser," Applied Physics Letters, Vol. 8, No. 8, P. 214, April 15, 1966.

35. R. A. Paananen,"Progress in Ionized-Argon Lasers," IEEE Spectrum, June 1966.

36. K. G. Hernqvist and T. R. Fendley, Jr.,"Construction of Long Life Argon Lasers," IEEE J. of Quantum Electronics, Vol. QE-3, No. 2, p. 66, February 1967.

37. H. Manger and H. Rothe,"Selection of Axial Modes of Optical Masers," Physics Letters, Vol. 7, No. 5, p. 330, 15 December 1963.

38. P. W. Smith,"Stabilized, Single Frequency Output from a Long Laser Cavity," IEEE J. of Quantum Electronics, Vol. QE-1, p. 343, November 1965.

39. M. DiDomenico, Jr.,"Characteristics of a Single-Frequency Michelson Type He-Ne Gas Laser," IEEE J. of Quantum Electronics, Vol. QE-2, No. 8, August 1966.

40. G. A. Massey, M. K. Oshman and R. Targ,"Generation of Single-Frequency Light Using the FM Laser," Applied Physics Letters, Vol. 6, p. 10, January 1965.

41. P. W. Smith,"On the Stabilization of a High-Power Single-Frequency Laser," IEEE J. Quantum Electronics, Vol. QE-2, No. 9, p. 666, September 1966.

42. W. W. Rigrod and A. M. Johnson,"Resonant Prism Mode Selector for Gas Lasers," IEEE J. of Quantum Electronics, Vol. QE-3, No. 11, p. 644, November 1967.

43. P. Zory,"Single-Frequency Operation of Argon Ion Lasers," IEEE J. of Quantum Electronics, Vol. QE-3, No. 10, October 1967.

44. H. Kogelnik and T. Li,"Laser Beams and Resonators," Applied Optics, Vol. 5, No. 10, p. 1550, October 1966.

45. S. Ezekiel,"Determination of Auxiliary Mirror Curvature in a Michelson-Type Single Longitudinal Mode Resonator," IEEE J. Quantum Electronics, Vol. QE-3, No. 10, p. 418, October 1967.

46. M. Born and E. Wolf,"Principles of Optics," Macmillan, 1964.

47. R. L. Fork, D. R. Herriot and H. Kogelnik,"A Scanning Spherical Mirror Interferometer for Spectral Analysis of Laser Radiation," Applied Optics, Vol. 3, No. 12, p. 1471, December 1964.

48. J. H. Stern and N. W. Gregory,"The Condensation Coefficient of Iodine," J. of Physical Chemistry, Vol. 61, p. 1226, 1957.

49. C. H. Townes and A. L. Schawlow,"Microwave Spectroscopy," McGraw-Hill, 1955.

50. A. E. Siegman,"Absolute Frequency Stabilization of a Laser Oscillator Against a Laser Amplifier," IEEE J. of Quantum Electronics, p. 337, July 1967.

51. A. E. Siegman, Benedetto Daino and K. R. Manes,"Preliminary Measurements of Laser Short-Term Frequency Fluctuations," IEEE J. Quantum Electronics, Vol. QE-3, No. 5, p. 180, May 1967.

52. C. Freed,"Stability Measurements of CO_2-N_2-H_2 Lasers at 10.6 m Wavelength," IEEE J. of Quantum Electronics, Vol. QE-3, No. 5, p. 203, May 1967.

53. J. D. Jackson,"Classical Electrodynamics," Wiley, 1962.

54. J. A. Bellisio, C. Freed and H. A. Haus,"Noise Measurements on He-Ne Laser Oscillators," Applied Physics Letters, Vol. 4, No. 1, p. 5, 1 January 1964.

55. L. J. Prescott and Van der Ziel,"Detection of Spontaneous Emission Noise in He-Ne Lasers," Physics Letters, Vol. 12, pp. 317-319, October 15, 1964.

56. A. L. Bloom,"Noise in Lasers and Laser Detectors," Spectra-Physics Laser Technical Bulletin Number 4, March 1965.

57. A. L. Bloom,"Gas Lasers," Applied Optics, Vol. 5, No. 10, p. 1500, October 1966.

58. R. D. Haun, Jr., and J. R. Zacharias, Physical Review, 107, 107 (1957).

59. M. Mizushima,"Theory of Resonance Frequency Shift Due to Radiation Field," Physical Review, Vol. 133, No. 2A, p. A414, 20 January 1964.

60. K. M. Baird and D. S. Smith,"Primary Standard of Length," J. of Optical Society of America, Vol. 52, No. 5, pp. 507-514, May 1962.

61. W. Honig,"Laser Benioff Strain Seismometers," Proc. IEEE, p. 101, January 1965.

62. G. Cocconi and E. E. Salpeter,"A Search for Anisotropy of Inertia," Nuovo Cimento, 10, 646 (1958).

63. V. W. Hughes,"Mach's Principle and Experiments on Mass Anisotropy," in Gravitation and Relativity, Edited by Chiu and Hoffmann, Benjamin, Inc., 1964.

64. R. W. P. Drever, Phil. Mag., 6, 683 (1961).

65. Class Notes, Prof. A. Javan's Course on Quantum Electronics, M.I.T., Fall 1966.

66. A. Yariv, Quantum Electronics, Wiley, 1967, p. 123.

67. J. I. Steinfeld, Private Communication.

68. V. Jaccarino, J. G. King, R. A. Satten, and H. H. Stroke, "Hyperfine Structure of I^{127}. Nuclear Magnetic Octupole Moment," Physical Review, Vol. 94, No. 6, pp. 1798-1799, June 15, 1954.

69. A. D. White,"Gas Laser Frequency Stabilization", Microwaves, pp. 51-61, January 1967.

70. D. A. MacLennan,"Electron Ejection from Atomically Clean Tungsten Surface by Helium and Neon Metastable Atoms," Physical Review, Vol. 148, No. 1, 5 August 1966.

71. I. I. Rabi, S. Millman, P. Kusch and J. R. Zacharias, Physical Review, 55, 526, 1939.

BIOGRAPHICAL SKETCH

Shaoul Ezekiel was born on July 20, 1935, in Baghdad, Iraq. His secondary education was at Hasmonean Grammar School, London, England, where he was appointed 'Head Pupil' during the last year of school. He was awarded a Major County Scholarship to study electrical engineering at the Imperial College of Science and Technology, University of London, England, and graduated with a Bachelor of Science degree with Honours in June 1957.

After graduation, he joined the General Electric Co., Coventry, England, where he worked on the design and test of co-axial cable transmission and receiving systems, logical design and data handling. In September 1959, he emigrated to Montreal, Canada, where he joined Canadian Aviation Electronics Ltd. as a research and development engineer with responsibility in the development of components and sub-systems for Flight and Tactical Simulators and later for Visual Simulators.

In June 1962, he was appointed research assistant in the Department of Aeronautics and Astronautics at M.I.T. His research at the Experimental Astronomy Laboratory, under the direction of Prof. Winston R. Markey, included the design of a 2-axis star tracker for project Stargazer - a stabilized manned balloon-borne telescope, and the development

of a very sensitive accelerometer (below 10^{-6} g) which employed a superconducting suspension and interferometric displacement detection. During the Spring of 1965, he was teaching assistant to Prof. Walter Wrigley in a course on Inertial Guidance. Since August 1965, he has been investigating the feasibility of a molecular beam reference for laser frequency stabilization. He was appointed Instructor in the Department of Physics at M.I.T. in January 1968.

He received the degree of Master of Science from M.I.T. in June 1964.

He is married to the former Susan Kovnat of New York City.

Publications, etc.

"MITROS: A Feasibility Study of an Equatorial Weather Satellite System", (with others) paper delivered by invitation at the National Weather Satellite Center, U.S. Weather Bureau, Suitland, Maryland, June, 1963.

"Towards a Low Level Accelerometer", Experimental Astronomy Laboratory Report TE-11, June, 1964. (S.M. Thesis)

"A Sensitive Cryogenic Accelerometer", (with P.K. Chapman) paper presented at the Symposium on Unconventional Inertial Sensors, Polytechnic Institute of Brooklyn, Farmingdale, New York, October, 1964.

"An Unconventional Inertial Measurement Technique", (with P.K. Chapman) paper presented at the Colloque sur les Gyroscopes Avances, Centre National D'Etudes Spatiales, Paris, November, 1964.

"A Superconduction Suspension for a Sensitive Accelerometer", (with P.K. Chapman) Review of Scientific Instruments, January, 1965.

"Analytical and Experimental Investigations of Low-Level Acceleration Measurement Techniques", (with P.K. Chapman and J.T. Egan) EAL Report RE-23, April, 1966.

"Determination of Auxiliary Mirror Curvature in a Michelson-Type Single Longitudinal Mode Resonator", IEEE J. of Quantum Electronics, October, 1967.

"Laser Induced Fluorescence in a Molecular Beam of Iodine", (with R. Weiss) Physical Review Letters, 15 January 1968.

"A Molecular Beam Reference for Laser Frequency Stabilization", (with R. Weiss), paper presented at the International Quantum Electronics Conference, Miami, May, 1968.